Characterizing Stress Granule Assembly and Disassembly through the Lens of Translation Initiation Machinery

By

JESSICA BOLIVAR
DISSERTATION

Submitted in partial satisfaction of the requirements for the degree of

DOCTOR OF PHILOSOPHY

in

Biochemistry, Molecular, Cell, and Developmental Biology

in the

OFFICE OF GRADUATE STUDIES

of the

UNIVERSITY of CALIFORNIA

DAVIS

Approved:

_____

Christopher Fraser, Chair

_____

John Albeck

_____

Priya Shah

Committee in Charge

2024

Abstract

This dissertation investigates the role of the translation initiation machinery in the dynamics of stress granules (SGs). Stress granules are cytoplasmic, non-membrane bound organelles composed of mRNA transcripts, RNA-binding proteins, 40S ribosomal subunits, and eukaryotic initiation factors (eIFs). They form in response to environmental stress to promote cell survival and recovery. A major gap in knowledge addressed in this work is the need to measure real- time kinetics of SG assembly and disassembly. Furthermore, the involvement of translation initiation factors in SG assembly remains unclear. My research addresses these gaps by developing a system to monitor SG dynamics using a stable inducible Flp-In™ T-REx™-HeLa Cell Line system, enabling real-time tracking and modeling.

Chapter 1 reviews the mechanisms of SG formation, their interplay with the translation initiation machinery, and their regulation under stress conditions. In Chapter 2, I describe the protocols developed to characterize the HeLa Fl-In cell line used throughout this study. Chapter 3 focuses on the role of the RNA Recognition Motif (RRM) of the initiation factor eIF4B in regulating SG assembly. Using single-cell live-imaging, I quantified the kinetics of SG formation and discovered that overexpression of GFP-tagged eIF4B with a point mutation in the RRM domain results in a decreased rate of SG formation, fewer total SGs, and a delayed stress response compared to wild type eIF4B. Furthermore, I demonstrated that eIF4B directly binds to G3BP1, a known SG nucleator, suggesting a mechanism by which eIF4B influences SG assembly. Chapter 4 examines the mechanisms of SG disassembly, a process poorly understood but linked to neurodegenerative disorders due to the inability to disassemble SGs, leaving cells in a constant state of stress. I developed a method to measure the rate of SG disassembly

accurately, addressing the challenge of focal drift in time-lapse imaging. Future work will explore overcoming focal drift using microfluidics devices or environmental chambers. Chapter 5 presents preliminary data on the interaction of GFP-tagged eIF4G with SGs. Unexpectedly, modest overexpression of eIF4G in HeLa cells results in hypersensitivity to oxidative stress, even though SGs still form. Proposed future experiments aim to confirm and extend understanding of this phenomenon.

Overall, this dissertation provides novel insights into the dynamic interplay between translation initiation machinery and SGs, with potential therapeutic implications for targeting SG dynamics in diseases such as cancer and neurodegeneration.

ACKNOWLEDGEMENTS

First and foremost, I would like to thank the Lord, Jesus Christ, for being my savior. I would like to thank my advisor, Chris Fraser, for being an amazing mentor. Coming into his lab, I was worried and intimidated about studying Biochemistry because I did not have any prior experience in this field. Chris and the Fraser Lab gave me the confidence I needed to succeed in my PhD. Chris taught me how to think like a scientist and really push my boundaries on the subject that I was not comfortable with. I would like to thank the Fraser Lab members: Nancy and Masa. Both have taught me a great deal regarding Biochemistry and gave so much amazing advice and help. During my time here, I have learned so much and felt extremely supported in the Fraser Lab. I would like to thank my dissertation committee: Dr. John Albeck and Dr. Priya Shah for helping me be a better scientist. I would like to dedicate my dissertation to my parents. My dad, Ben Bolivar, passed away in 2006. My dad inspired me to pursue a college education and before he passed, he wanted me to pursue my dreams. Dad, thank you so much for always believing in me. My mom, Tina Bolivar, has always encouraged me to follow my dreams. Mom, thank you so much for giving me confidence to continue with my education and encouraging me to always ask questions. I would like to thank my sister, Angela Bolivar- Strickland. Thank you so much for being my person. I would also like to thank my friends from BMCDB, especially Nick DeCuzzi, Hannah Morris Little and Zoe Estrada, thank you for supporting me throughout this program and beyond. I couldn't do this without you. I would also like to thank my church family, TFH Natomas, thank you for all your help and spiritual guidance.

Table of Contents

Chapter One

Exploring the roles between stress granules and translation initiation machinery

This chapter is an unpublished literature review, discussing the link between the translation initiation machinery and stress granules. This chapter was written by me and edited by Dr. Christopher Fraser.

Abstract

Cells form stress granules (SGs) in response to various stress stimuli, such as heat shock, oxidative stress, osmotic shock, and proteasome inhibition. SGs are non-membrane bound organelles composed of non-translating RNAs, RNA-binding proteins, and stalled translation pre-initiation complexes, including translation initiation factors and the 40S ribosomal subunit. The formation of SGs is primarily regulated by the phosphorylation of eIF2α, a key event in the integrative stress response (ISR) pathway. However, recent studies have revealed an alternative SG assembly pathway independent of eIF2α phosphorylation, highlighting the dual role of the translation machinery in SG dynamics.

To overcome many different stress stimuli such as heat stock, oxidative stress, osmotic shock and proteasome inhibition (Lee & Namkoong, 2022; Mahboubi & Stochaj, 2017), cells form structures called Stress Granules (SGs) (Wang et al., 2022). SGs are non-membrane bound organelles that are composed of non-translating RNAs, RNA binding proteins, and stalled translation pre-initiation complexes which consist of translation initiation factors and the 40S ribosomal subunit (Marcelo et al., 2021). The formation of these SGs is tightly regulated by cellular stress responses. One key mechanism is the phosphorylation of the eukaryotic initiation factor 2α (eIF2α) mainly occurs upon activation of the integrative stress response (ISR) pathway (Taniuchi et al., 2016) **(Figure 1).** Until recently, it was thought that phosphorylation of eIF2α was the only pathway to assemble stress granules, however, a new pathway independent of phosphorylation of eIF2α has been discovered, which suggests the translation machinery has a dual role in SG assembly (Mazroui et al., 2006). For the focus of this dissertation, I will dive deeply into the following questions: How do stress granules and translation communicate with each other? Do stress granules serve as non-membrane bound organelles to protect important proteins such as translation machinery or does the translation machinery play an active role in assembling stress granules? Before looking at these questions, I will review the emerging research on stress granules and disease pathology.

Stress Granules: Cancer and Neurological Diseases

Stress granules have been studied in the context of cancer and neurodegenerative disorders due to their involvement in the progression of different stages of tumorigenesis and the aggregation of proteins linked to neurodegenerative disorders (Wolozin & Ivanov, 2019; Zhou et al., 2023). In the context of cancer, studies have linked dysregulated SG dynamics to cancer progression, cell death repression, metastasis and invasion, and chemotherapy resistance (Asadi et al., 2021; Lee & Namkoong, 2022). It is important to note that to survive cancer cells have to adapt to high-stress tumor microenvironments (Song & Grabocka, 2023). Several studies have shown that SGs and cancer use a variety of pro-tumorigenic signaling pathways. In addition, *in vitro* studies in which chemotherapeutics induced SG assembly in cells to become chemo-resistant have shown that cancer employs SGs as a mechanism to survive (Gao et al., 2019; Grabocka & Bar-Sagi, 2016; Zhan et al., 2020). Thus, it has become increasingly important to understand the mechanism of SG assembly and how cancer can use this mechanism to protect and promote growth.

Chronic cell stress occurs when SGs are prevented from disassembling, which can be caused by mutated or misfolded proteins. (Wang et al. 2022; Brown et al. 2020). An example of a mutation that leads to aggregation is found in RNA-binding proteins such as Tar DNA-binding protein 43 (TDP-43), which is a SG nucleator (Aulas et al., 2012) that shares a genetic link with amyotrophic lateral sclerosis (ALS) (Maziuk et al., 2017). Thus, it is important to study SG dynamics and how the different components of SGs are able to dissolve when stress no longer occurs in the cell.

Mechanisms of Stress Granule Assembly

The general process of SG assembly occurs in three steps: 1. The ISR pathway is activated resulting in global translation shutdown through phosphorylation of eIF2α, 2. SG nucleators initiate assembly (Hofmann et al., 2021; N. Kedersha & Anderson, 2002), and 3. organization of the components of the stress granule (Wheeler et al., 2016)**(Figure 1).**

Integrative Stress Response Pathway

The goal of this pathway is to restore and maintain cellular homeostasis, particularly in response to various stressors that can disrupt normal cellular function. Cells can experience a range of stress conditions, including oxidative stress, hypoxia, glucose deprivation, and endoplasmic reticulum (ER) stress (Fulda et al., 2010). Each type of stress activates specific kinases that initiate adaptive responses to mitigate damage. For example, in response to ER stress, the Protein Kinase R (PKR)-like Endoplasmic Reticulum Kinase (PERK) is activated, leading to the phosphorylation of eIF2α, which subsequently reduces global protein synthesis to alleviate the burden on the ER (Saito et al., 2011). Similarly, dsRNA Protein Kinase R (PKR) is activated under conditions such as viral infection, triggering a similar response to halt protein synthesis and prevent viral replication (Rojas Margarito et al., 2010).

During amino acid (AA) deprivation, general control nonderepressible 2 (GCN2) is activated, which also phosphorylates eIF2α, thereby adjusting protein synthesis to conserve resources (She et al., 2013). Heme deficiency triggers the activation of Heme-regulated eIF2α kinase (HRI), which not only reduces global protein synthesis but also helps in maintaining redox balance and iron homeostasis (Chen, 2007).

The formation of stress granules (SGs) is initiated by the phosphorylation of eIF2α, a key component of the eIF2-GTP-tRNAiMet ternary complex, which then inhibits protein synthesis by preventing the assembly of the 43S pre-initiation complex (Pakos-Zebrucka et al., 2016). This phosphorylation is a central event in the integrated stress response (ISR), allowing cells to prioritize the translation of specific mRNAs that encode stress-response proteins while globally reducing protein synthesis to conserve energy and resources. Please refer to **(Figure 1)** for a visual summary of this pathway. The overarching goal of this pathway is to enable cells to adapt to stress conditions, ensure survival, and maintain cellular homeostasis by tightly regulating protein synthesis and other stress responses.

Stress Granule Nucleators

Stress granule nucleators are proteins that are involved with initiating and regulating stress granule assembly. In the absence of stress, overexpression of nucleators can induce SG formation, suggesting that their concentration alone is an important factor in the stress response (Hofmann et al., 2021). A mechanism to explain how the concentration of SG nucleators can regulate SG formation is that they are prone to self-aggregate and contain an intrinsically disordered region or prion-like domains (PrLD) (Gilks et al., 2004; March et al., 2016). The following nucleators contain an intrinsically disordered region, which likely allow RNA and other proteins to be able to bind to this region: G3BP (Ras-GAP SH3-domain Binding Protein) (N. Kedersha et al., 2005), TIA-1 (T-cell Intracellular Antigen-1) (Gilks et al., 2004; N. L. Kedersha et al.,

1999), TIAR (TIA-1 related protein)(Anderson & Kedersha, 2002), FUS (Fused in Sarcoma) (Dormann et al., 2010; Vance et al., 2009), and TDP-43 (TAR DNA-binding Protein 43,(Neumann et al., 2006)). After the nucleation event, there are two models that arrange the order of the SG assembly.

Models for stress granule assembly and formation

There are two models that support the arrangement of SGs. In the first model, a large pool of untranslated mRNA ribonucleoproteins gather and create the nucleation event through liquid-liquid phase separation of weak interactions and grow into the mature stress granule (Lin et al., 2015; Molliex et al., 2015). In the second model, nucleators form the core which then forms into a mature biphasic SG with a dynamic outer shell consisting of mRNA ribonucleoproteins (Wheeler et al., 2016). One recent study has supported the second model whereby eIF4A, a helicase protein, can bind mRNAs to limit the size of SGs using *in vitro* assays (Tauber et al., 2020). Because this model provides an alternative way to assemble SGs, it is important to determine how the availability and activity of translation initiation factors can affect SG dynamics. Please refer to **(Figure 1),** which summarizes the pathway.

Noncanonical SG Assembly Pathway- Translation Initiation Factors

Previous studies have suggested that SG assembly is initiated by shutting down global translation in response to eIF2α phosphorylation (N. Kedersha et al., 2002). However, other studies have suggested that SG assembly can be uncoupled from this

phosphorylation event and potentially involve other translation initiation factors (Mokas et al., 2009). For example, eIF4G, a scaffold protein that is part of the m7G cap binding complex, interacts with one of the primary SG nucleators, Ras GTPase-activating protein-binding protein 1 (G3BP1) to form SGs (X. Yang et al., 2019). Additionally, the eIF4A helicase protein was shown to limit SG assembly by reducing RNA-RNA interactions and thereby limiting the amount of mRNA recruitment to SGs (Tauber et al., 2020). This is an important finding, because it supports the SG arrangement model whereby RNAs form a dynamic outer shell (Wheeler et al., 2016), which allows eIF4A to function in disassembly of SGs. In addition, the eIF4A accessory factor eIF4B, stimulates eIF4A helicase activity to increase the unwinding rate of mRNA secondary structure in the 5′ UTR (Andreou et al., 2017). This raises the possibility that this activity may regulate the helicase activity of eIF4A in order to regulate SG formation. Consistent with this, RNAi knockdown of eIF4B leads to spontaneous SG assembly, as monitored by immunofluorescence staining in fixed cells (Mokas et al., 2009). Given the recent finding that eIF4A limits SG assembly by disrupting RNA-RNA interactions (Tauber et al., 2020), I wanted to further investigate the role of eIF4B in stress granule assembly and disassembly.

The goal of my dissertation is to 1) characterize how eIF4B and eIF4G function in SG formation and 2) to optimize a live cell imaging assay to monitor SG assembly and disassembly in real time. Currently, a limitation in the field is the inability to precisely track the kinetics of different SG markers in live cells. To characterize SGs, researchers have mainly relied on fixed time point assays like Immunofluorescence (IF). The benefits of IF include 1) that it can identify which proteins are present in a particular time frame and location (spatial), and 2) the antibodies are specific to protein, and one is

able to visualize individual protein levels. However, some of the limitations for IF include photobleaching (loss of signal) and the inability to observe real-time changes in protein expression levels. Thus, there has been a need to establish live single-cell analysis to determine the mechanism of SG behavior that can overcome these limitations. For my dissertation, I therefore focused on moving the field forward by analyzing real-time data for SG and translation at the single cell level. One of the previous limitations was the lack of a link between SG formation and translation rate at the single cell-level. With the accomplishments of my collaborator, Nick DeCuzzi, we were able to achieve this goal. We can now link live cell data (formation of SGs) and translation activity in the same pipeline.

Figure and Legend

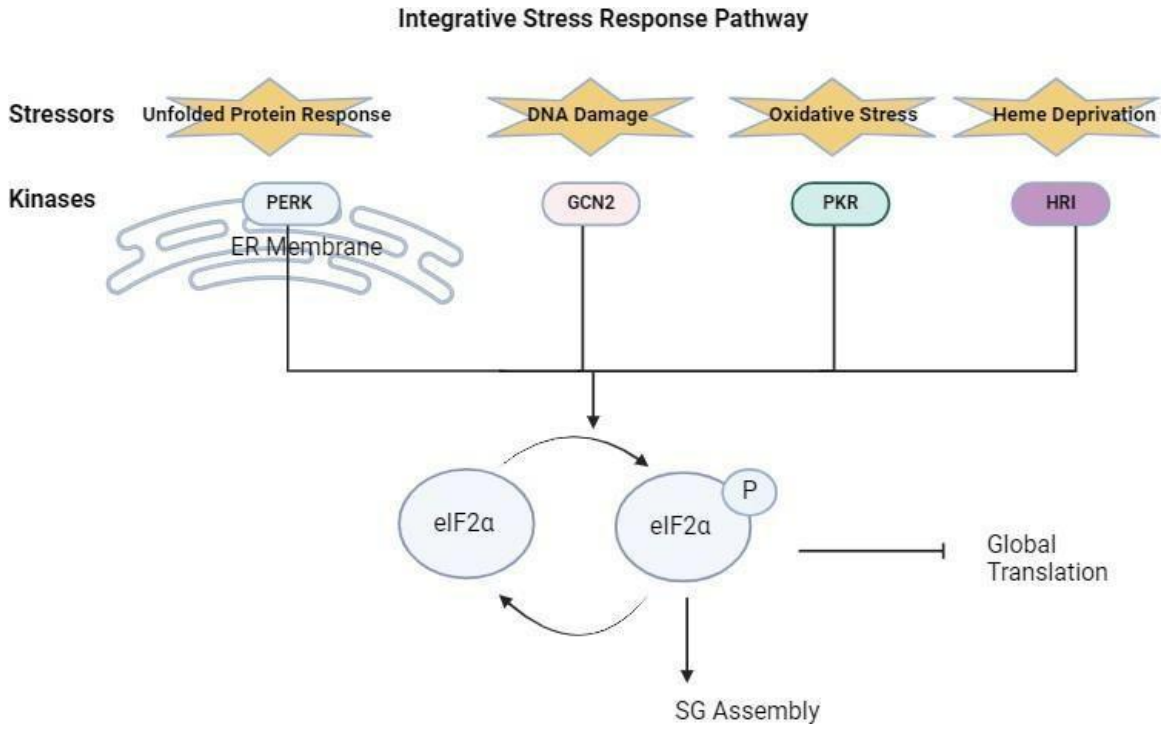

Model 1

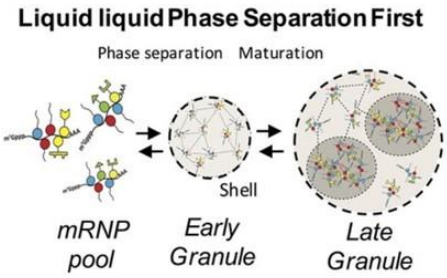

Model 2

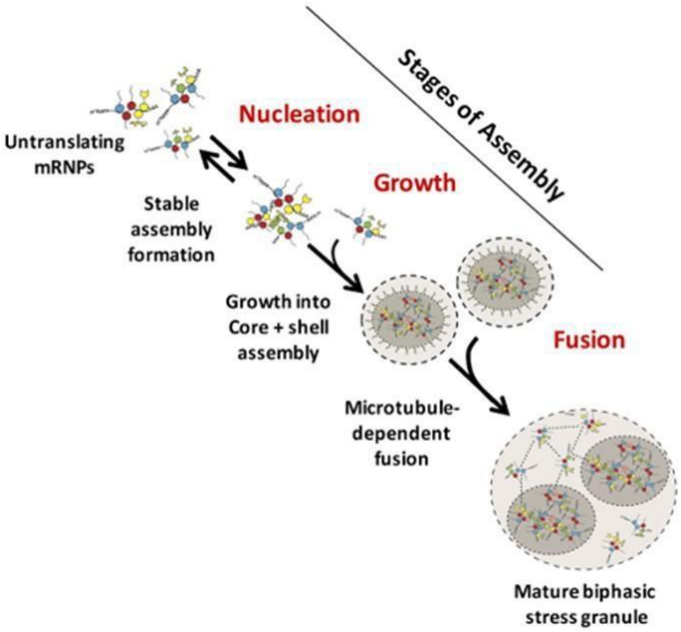

Stages of Assembly Image was adapted from (Wheeler et al. 2016) Figure was also made with BioRender

Figure 1. Activation of the Integrative Stress Response Pathway and SG assembly Pathway. Depending on the different stress responses, the following four kinases: PERK, GNC2, PKR, HRI can phosphorylate eIF2α. Once this phosphorylation event occurs, global translation is shut down and SGs assemble. The SG model indicates a nucleation event that favors the beginning of the core and then growth of the shell (composed of mRNAs) that forms the mature SG.

References

Anderson, Paul, and Nancy Kedersha. 2002. “Stressful Initiations.” *Journal of Cell Science* 115 (Pt 16): 3227–34.

Andreou, Alexandra Zoi, Ulf Harms, and Dagmar Klostermeier. 2017. “eIF4B Stimulates eIF4A ATPase and Unwinding Activities by Direct Interaction through Its 7-Repeats Region.” *RNA Biology* 14 (1): 113–23.

Asadi, Mohammad Reza, Dara Rahmanpour, Marziyeh Sadat Moslehian, Hani Sabaie, Mehdi Hassani, Soudeh Ghafouri-Fard, Mohammad Taheri, and Maryam Rezazadeh. 2021. “Stress Granules Involved in Formation, Progression and Metastasis of Cancer: A Scoping Review.” *Frontiers in Cell and Developmental Biology* 9 (September): 745394.

Aulas, Anaïs, Stéphanie Stabile, and Christine Vande Velde. 2012. “Endogenous TDP-43, but Not FUS, Contributes to Stress Granule Assembly via G3BP.” *Molecular Neurodegeneration* 7 (October): 54.

Brown, Dean G., James Shorter, and Heike J. Wobst. 2020. “Emerging Small-Molecule Therapeutic Approaches for Amyotrophic Lateral Sclerosis and Frontotemporal Dementia.” *Bioorganic & Medicinal Chemistry Letters* 30 (4): 126942.

Chen, Jane-Jane. 2007. “Regulation of Protein Synthesis by the Heme-Regulated eIF2alpha Kinase: Relevance to Anemias.” *Blood* 109 (7): 2693–99.

Dormann, Dorothee, Ramona Rodde, Dieter Edbauer, Eva Bentmann, Ingeborg Fischer, Alexander Hruscha, Manuel E. Than, et al. 2010. “ALS-Associated Fused in Sarcoma (FUS) Mutations Disrupt Transportin-Mediated Nuclear Import.” *The EMBO Journal* 29 (16): 2841–57.

Fulda, Simone, Adrienne M. Gorman, Osamu Hori, and Afshin Samali. 2010. “Cellular Stress Responses: Cell Survival and Cell Death.” *International Journal of Cell Biology* 2010 (February): 214074.

Gao, Xiaomeng, Li Jiang, Yanling Gong, Xiaobing Chen, Meidan Ying, Hong Zhu, Qiaojun He, Bo Yang, and Ji Cao. 2019. “Stress Granule: A Promising Target for Cancer Treatment.” *British Journal of Pharmacology* 176 (23): 4421–33.

Gilks, Natalie, Nancy Kedersha, Maranatha Ayodele, Lily Shen, Georg Stoecklin, Laura M. Dember, and Paul Anderson. 2004. “Stress Granule Assembly Is Mediated by Prion-like Aggregation of TIA-1.” *Molecular Biology of the Cell* 15 (12): 5383–98.

Grabocka, Elda, and Dafna Bar-Sagi. 2016. “Mutant KRAS Enhances Tumor Cell Fitness by Upregulating Stress Granules.” *Cell* 167 (7): 1803–13.e12.

Hofmann, Sarah, Nancy Kedersha, Paul Anderson, and Pavel Ivanov. 2021. “Molecular Mechanisms of Stress Granule Assembly and Disassembly.” *Biochimica et Biophysica Acta, Molecular Cell Research* 1868 (1): 118876.

Kedersha, Nancy, Samantha Chen, Natalie Gilks, Wei Li, Ira J. Miller, Joachim Stahl, and Paul Anderson. 2002. “Evidence That Ternary Complex (eIF2-GTP-tRNA(i)(Met))-Deficient Preinitiation Complexes Are Core Constituents of Mammalian Stress Granules.” *Molecular Biology of the Cell* 13 (1): 195–210.

Kedersha, Nancy, Georg Stoecklin, Maranatha Ayodele, Patrick Yacono, Jens Lykke-Andersen, Marvin J. Fritzler, Donalyn Scheuner, Randal J. Kaufman, David E. Golan, and Paul Anderson. 2005. “Stress Granules and Processing Bodies Are Dynamically Linked Sites of mRNP Remodeling.” *The Journal of Cell Biology* 169 (6): 871–84.

Kedersha, N., and P. Anderson. 2002. “Stress Granules: Sites of mRNA Triage That Regulate mRNA Stability and Translatability.” *Biochemical Society Transactions* 30 (Pt 6): 963–69.

Kedersha, N. L., M. Gupta, W. Li, I. Miller, and P. Anderson. 1999. “RNA-Binding Proteins TIA-1 and TIAR Link the Phosphorylation of eIF-2 Alpha to the Assembly of Mammalian Stress Granules.” *The Journal of Cell Biology* 147 (7): 1431–42.

Lee, Jeong In, and Sim Namkoong. 2022. “Stress Granules Dynamics: Benefits in Cancer.” *BMB Reports* 55 (12): 577–86.

Lin, Yuan, David S. W. Protter, Michael K. Rosen, and Roy Parker. 2015. “Formation and Maturation of Phase-Separated Liquid Droplets by RNA-Binding Proteins.” *Molecular Cell* 60 (2): 208–19.

Mahboubi, Hicham, and Ursula Stochaj. 2017. “Cytoplasmic Stress Granules: Dynamic Modulators of Cell Signaling and Disease.” *Biochimica et Biophysica Acta, Molecular Basis of Disease* 1863 (4): 884–95.

Marcelo, Adriana, Rebekah Koppenol, Luís Pereira de Almeida, Carlos A. Matos, and Clévio Nóbrega. 2021. “Stress Granules, RNA-Binding Proteins and Polyglutamine Diseases: Too Much Aggregation?” *Cell Death & Disease* 12 (6): 592.

March, Zachary M., Oliver D. King, and James Shorter. 2016. “Prion-like Domains as Epigenetic Regulators, Scaffolds for Subcellular Organization, and Drivers of Neurodegenerative Disease.” *Brain Research* 1647 (September): 9–18.

Maziuk, Brandon, Heather I. Ballance, and Benjamin Wolozin. 2017. “Dysregulation of RNA Binding Protein Aggregation in Neurodegenerative Disorders.” *Frontiers in Molecular Neuroscience* 10 (April): 89.

Mazroui, Rachid, Rami Sukarieh, Marie-Eve Bordeleau, Randal J. Kaufman, Peter Northcote, Junichi Tanaka, Imed Gallouzi, and Jerry Pelletier. 2006. “Inhibition of Ribosome Recruitment Induces Stress Granule Formation Independently of Eukaryotic Initiation Factor 2alpha Phosphorylation.” *Molecular Biology of the Cell* 17 (10): 4212–19.

Mokas, Sophie, John R. Mills, Cristina Garreau, Marie-Josée Fournier, Francis Robert, Prabhat Arya, Randal J. Kaufman, Jerry Pelletier, and Rachid Mazroui. 2009. “Uncoupling Stress Granule Assembly and Translation Initiation Inhibition.” *Molecular Biology of the Cell* 20 (11): 2673–83.

Molliex, Amandine, Jamshid Temirov, Jihun Lee, Maura Coughlin, Anderson P. Kanagaraj, Hong Joo Kim, Tanja Mittag, and J. Paul Taylor. 2015. “Phase Separation by Low Complexity Domains Promotes Stress Granule Assembly and Drives Pathological Fibrillization.” *Cell* 163 (1): 123–33.

Neumann, Manuela, Deepak M. Sampathu, Linda K. Kwong, Adam C. Truax, Matthew C. Micsenyi, Thomas T. Chou, Jennifer Bruce, et al. 2006. “Ubiquitinated TDP-43 in Frontotemporal Lobar Degeneration and Amyotrophic Lateral Sclerosis.” *Science* 314 (5796): 130–33.

Pakos-Zebrucka, Karolina, Izabela Koryga, Katarzyna Mnich, Mila Ljujic, Afshin Samali, and Adrienne M. Gorman. 2016. “The Integrated Stress Response.” *EMBO Reports* 17 (10): 1374–95.

Rojas Margarito, Arias Carlos F., and López Susana. 2010. “Protein Kinase R Is Responsible for the Phosphorylation of eIF2α in Rotavirus Infection.” *Journal of Virology* 84 (20): 10457–66.

Saito, Atsushi, Kimiko Ochiai, Shinichi Kondo, Kenji Tsumagari, Tomohiko Murakami, Douglas R. Cavener, and Kazunori Imaizumi. 2011. “Endoplasmic Reticulum Stress Response Mediated by the PERK-eIF2(alpha)-ATF4 Pathway Is Involved in Osteoblast Differentiation Induced by BMP2.” *The Journal of Biological Chemistry* 286 (6): 4809–18.

She, Pengxiang, Piyawan Bunpo, Judy K. Cundiff, Ronald C. Wek, Robert A. Harris, and Tracy G. Anthony. 2013. “General Control Nonderepressible 2 (GCN2) Kinase Protects Oligodendrocytes and White Matter during Branched-Chain Amino Acid Deficiency in Mice*.” *The Journal of Biological Chemistry* 288 (43): 31250–60.

Song, Min-Seok, and Elda Grabocka. 2023. “Stress Granules in Cancer.” In *Organelles in Disease*, edited by Stine Helene Falsig Pedersen and Diane L. Barber, 25–52. Cham: Springer International Publishing.

Taniuchi, Shusuke, Masato Miyake, Kazue Tsugawa, Miho Oyadomari, and Seiichi Oyadomari. 2016. “Integrated Stress Response of Vertebrates Is Regulated by Four eIF2α Kinases.” *Scientific Reports* 6 (September): 32886.

Tauber, Devin, Gabriel Tauber, Anthony Khong, Briana Van Treeck, Jerry Pelletier, and Roy Parker. 2020. “Modulation of RNA Condensation by the DEAD-Box Protein eIF4A.” *Cell* 180 (3): 411–26.e16.

Vance, Caroline, Boris Rogelj, Tibor Hortobágyi, Kurt J. De Vos, Agnes Lumi Nishimura, Jemeen Sreedharan, Xun Hu, et al. 2009. “Mutations in FUS, an RNA Processing Protein, Cause Familial Amyotrophic Lateral Sclerosis Type 6.” *Science* 323 (5918): 1208–11.

Wang, Jihui, Yixia Gan, Jian Cao, Xuefen Dong, and Wei Ouyang. 2022. “Pathophysiology of Stress Granules: An Emerging Link to Diseases (Review).” *International Journal of Molecular Medicine* 49 (4). https://doi.org/10.3892/ijmm.2022.5099.

Wheeler, Joshua R., Tyler Matheny, Saumya Jain, Robert Abrisch, and Roy Parker. 2016. “Distinct Stages in Stress Granule Assembly and Disassembly.” *eLife* 5 (September). https://doi.org/10.7554/eLife.18413.

Wolozin, Benjamin, and Pavel Ivanov. 2019. “Stress Granules and Neurodegeneration.” *Nature Reviews. Neuroscience* 20 (11): 649–66.

Yang, Xiaodan, Zhulong Hu, Qiang Zhang, Shanshan Fan, Yi Zhong, Dong Guo, Yali Qin, and Mingzhou Chen. 2019. “SG Formation Relies on eIF4GI-G3BP Interaction Which Is Targeted by Picornavirus Stress Antagonists.” *Cell Discovery* 5 (January): 1.

Zhan, Yuting, Haihua Wang, Yue Ning, Hongmei Zheng, Sile Liu, Yang Yang, Ming Zhou, and Songqing Fan. 2020. “Understanding the Roles of Stress Granule during Chemotherapy for Patients with Malignant Tumors.” *American Journal of Cancer Research* 10 (8): 2226–41.

Zhou, Huan, Jing Luo, Kelin Mou, Lin Peng, Xiaoyue Li, Yulin Lei, Jianmei Wang, Sheng Lin, Yuhao Luo, and Li Xiang. 2023. “Stress Granules: Functions and Mechanisms in Cancer.” *Cell & Bioscience* 13 (1): 86.

Chapter Two

Characterization of Stress Granule Dynamics in a stable inducible Flp-In™ T-REx™ HeLa Cell Line system using fluorescence microscopy

This chapter contains unpublished work and was written by me with editing by Dr. Christopher Fraser. Experiments were conducted by me and Katie Beglinger made the Flp-In T-REx HeLa line overexpressing GFP-eIF4B. I collaborated with Nick DeCuzzi and John Albeck for the Image Analysis pipeline.

Abstract

Cells must respond to environmental stress to ensure survival and recovery. A mechanism used by cells to respond to stress involves forming cytoplasmic structures called stress granules (SGs). SGs are non-membrane bound organelles composed of mRNA transcripts, RNA binding proteins, and 40S ribosomal subunits bound by eukaryotic initiation factors (eIFs). During the stress response, the rapid formation of SGs (within ~30 minutes) serves to protect mRNAs and the translation initiation machinery for survival and recovery. However, the precise mechanism by which SGs assemble during stress and disassemble after stress is poorly defined. Specifically, we do not understand how interactions between the translation machinery and other SG components regulate the kinetics of SG assembly and disassembly. This gap in our knowledge exists because few studies of SG dynamics have monitored these events in real-time. Previous studies have characterized SG dynamics using assays like immunofluorescent time series or software packages that track particles and calculate the percentages of stress granules in a given frame. Obtaining real-time kinetics of SGs can reveal fundamental information about how translation initiation factors have an effect on SG assembly and disassembly. Here, I have developed a system to monitor SG assembly and disassembly over time using a stable inducible Flp-In™ T-REx™-HeLa Cell Line system. This system was used throughout my dissertation.

Introduction

Fluorescence microscopy is a powerful tool for characterizing a process in real-time. Using this tool, significant progress has been made in studying SG dynamics. For example, Fluorescence Recovery After Photobleaching (FRAP) (Streit et al., 2022) measures the exchange rate and recovery of a population of proteins that are fluorescently tagged and photobleached over time. Photoactivatable GFP Fluorescence Decay After Photoactivation (FDAP) is used to study the mobility and transport processes within the cell (Niewidok et al., 2018). Collecting individual single time frames using immunofluorescence microscopy provides further information on spatial resolution between multiple fluorescently labeled proteins (Vonaesch et al., 2017). These various assays enable one to measure and monitor SGs at a single cell level. Nevertheless, improvements in modeling and developing a tool to automate and compare the entire population of SGs per cell without introducing bias is still needed.

Here, I have developed an assay and tool to monitor SGs in real time using a GFP-labeled eukaryotic initiation factor that is inducibly expressed in a stable cell line. To better understand the mechanism of SG assembly, my assay is able to image SG formation and disassembly and can successfully track SGs in single cells in real time. For my assay, I have used a widefield microscope. One advantage of using a widefield microscope is that it enables one to obtain accurate temporal resolution, whereas a confocal microscope provides high-resolution structures for better spatial resolution (N. Kedersha et al., 2008). Using this assay, I have been able to obtain real-time kinetics of SG assembly. In this chapter, I outline the methods I developed to achieve this goal.

Stress Granule Assembly and Disassembly Measurement in Real Time

Materials

- 96 Well Glass Bottom Plate (In Vitro Scientific P96-1.5H-N)
- FluoroBrite™ DMEM (Gibco, Catalog Number: A1896701)
- Fetal Bovine Serum (Gibco, Catalog Number: 16000069)
- Sodium (meta) Arsenite (Sigma Aldrich, Catalog Number: 7784-46-5): Prepare Stock Solution 500mM in sterile water
- Corning™ DMEM (Dulbecco's Modified Eagle's Medium) (Thermofisher, Cat# MT15017CV)
- Hoescht Stain (Thermofisher, Catalog 33342)
- P Vac Portable Vacuum System (Argos Technology, Cat: 04397-07)
- Ti2 Widefield Microscope (Nikon)

******Important Note before starting experiment for Cell Culture**

Thaw cell lines at least two weeks before beginning experiments to allow cells to establish good growth behavior. The SG assay is composed of three days as described below:

Day 1:

1. Seed cells in 200 µL of DMEM media with appropriate antibiotics depending on cell line: 0.01x 10^6^ cells into each well (Use 96 well plate)

Day 2:

1. Induce expression of EGFP-eIF4B in cells with 0.1 µg/mL (final concentration) of tetracycline into each well (Use DMEM as the base). Carefully pipette tetracycline into the wells (no need for media change) and allow for cells to be induced for 24 hours (but see time course to determine appropriate expression time).

Day 3:

1. Warm up Fluorobrite and FBS in a 37 °C bath for 30 mins.
2. Prepare 125 µM of Sodium Arsenite from a stock solution of 500 mM with Fluorobrite media. If you are using a 96 well plate, calculate the concentration for the final volume to be 50 µL per well. Set this solution aside until it is time to image the plate.
3. Prepare FluoroBrite™ DMEM imaging media with a supplement of 2% FBS, and 1:10,000 concentration of Hoechst stain for a final concentration of 1 µg/mL. Make sure media is covered in foil (Light sensitive)
4. Once you have prepared your materials, while working with your cells, you need to take less than 30 seconds to complete steps 5–7. Be sure not to dry out the wells. Use the multichannel pipette, while pipetting be sure to pick up and wash cells from a corner of the well so that cells do not get displaced during this process.
5. Remove all of the media from each well by pipetting.
6. Wash cells by adding 200 µL of fluorobrite (1x) and remove wash from each well

with a pipette.

7. Add 150 µL of Fluorobrite that is supplemented with 2% FBS, and Hoechst Stain.
8. Place the plate back into the 37 °C with 5% CO_2 incubator. Allow 30 mins for the Hoescht to stain the nucleus.
9. Image Cells as described below.

Imaging Cells:

Materials:

- Your Glass Bottom Cell Plate (from previous step) (In Vitro Scientific P96-1.5H-N)
- 200 µL Pipette Tips
- Beaker (Waste) with bleach solution (10 % final after adding cell media)
- Multichannel Pipette (20–200 µL)
- Gloves
- PVac System pump (Argos Technology, Cat: 04397-07)
- 25 mL Reservoir for sodium arsenite (toxic waste to be collected by EH&S)
- A rolling cart- To bring in all of your materials to the scope room

1. While the cells are incubating, turn on the microscope. Allow at least 1 hour for the microscope to warm up.

2. I use the “downstairs microscope” Ti2 Widefield Microscope from the Albeck Lab, so be sure to get permission to add your timeslot to the Albeck Calendar and training from his lab.

Directions to turn on Microscope and NIS Elements Software

***** Before using the microscope, the lens, camera, and filter cubes are very expensive. Please do not break and report to the Albeck Lab if you have any problems with the microscope.*

Turn on the microscope in the following order:

1. CO_2 Tank
2. O_2 and CO_2 pump
3. Camera on the scope
4. Turn on Lasers
5. Turn on Computer
6. Turn on NIS Elements Software

NIS Elements Acquisition Setting details

1. Once you have started the software, change the following settings
2. Change the lens settings to 40X.
3. Be sure you have the proper filter cubes since they coordinate with the settings from the NIS Element software. I use the GFP, BFP, and Cy5 filter cubes.
4. Settings for the following cubes:

1. 200 ms with 14% Laser, Binning 2x2- GFP
2. 75 ms with 20% Laser, Binning 2x2- BFP
3. 200 ms with 14% Laser, Binning 2x2- Cy5

5. Make sure you check the following sections: Time, Color and to pick XYs.

SG Assembly Assay

1. Allow at least 30 mins for the cells to acclimate in the chamber of the microscope.
2. Once you have set up the setting in NIS Elements, locate your cells by using the perfect focus option *** It is extremely important that you do not crash your sample into the lens. When you use the knobs to raise up the lens, be sure to do it slowly until you hear the beep. Then use the fine adjustment knob to sharpen the image.
3. Once you locate your cells, be sure to select XYs that are at least 60-70 confluent and use cells that are flat and not clumped on top of each other.
4. Each well = 1 XY in a 96 well plate.
5. Before starting your experiment, be sure to time how long it will take for the microscope to image your entire plate.
6. Once you get this recording, you can go to the “Time” section and add this information in.

7. Begin your experiment with two rounds of images and then pause the experiment.
8. Press the Escape Z and remove the lid
9. Add 50 µL of 125 µM of sodium arsenite to each of the wells and gently mix using a P1000.
10. Place Lid back and return to Z.
11. Press the resume button on the microscope.
12. Image the plate for 2 hours to allow enough time for SGs to appear **(Figure 1)**

SG Disassembly Assay

1. After the appearance of SGs, pause the experiment on the scope.
2. Use the PVac with a 200 µL tip to remove all media from cells.
3. Add 200 µL Fluorobrite with 2% FBS into the cells using a multichannel pipette.
4. Then resume the experiment to follow the disassembly assay **(Figure 1)**

Data Storage

1. Do not forget to obtain your images after the experiment before you erase your data from the microscope.
2. Use Google drive for long term storage of any videos you collect and you can also use GitHub for any data analysis. https://github.com/

Characterization of Flp-In T-REx Cell Line

To characterize this cell line, I wanted to determine the rate of induced expression over time. To this end, I used fluorescent microscopy and western blotting. See the protocol below for more details:

Tetracycline Inducible Cell Line using Fluorescent Microscopy

1. I seed cells in a 96 well plate at $0.01x10^6$ and allow them to grow for a total of 48 hours.
2. I change the media for each well using 200 uL of Fluorobrite that is supplemented with 2% FBS.
3. Follow the protocol above to turn on the **Microscope and NIS Elements Software.**
4. Pipette in 0.1 µg/mL of tetracycline, mix gently using a P1000, and leave the scope on for 36 hours
5. When collecting data, be sure to collect every 5 mins. Please see **(Figure 2)** for results.

Cell Scape and Lysis for preparation of Western Blot Samples

- Cell Scraper (Sigma Aldrich, Cat # 229306)

- 2 Ice Buckets
- PBS (Cold) (Thermofisher, Cat #10010049)
- 1.5 mL Safe Lock Eppendorf Tubes
- 100 mm dish
- Prepare Lysis Buffer:

Hepes 7.5	20 mM
KCl	10 mM
DTT	1 mM
NP40	1%
Mg Acetate	5 mM
Protease Inhibitor	1X
H2O	Fill up to

1. Plate 2.2x10^6 cells using a 100 mm dish.
2. Induce cells 24 hours later by pipetting in 0.1 µg/mL of tetracycline.

3. Harvest cells on the 3rd day.
4. Move cells on an ice box to cool them.
5. Remove Media from cells pipetting using a pipette aide.
6. Wash cells one time with 3 mL of PBS
7. Remove PBS by pipetting using a pipette aide.
8. Add 750 µL of PBS to plate
9. Scrape Cells in clockwise fashion.
10. Uptake 750 µL of cells in a safe lock 1.5mL Eppendorf tube
11. Pellet Cells in 4 °C centrifuge (2.5 mins @ 0.5 RCF)
12. Remove Supernatant
13. Add 100 µL of Lysis Buffer and resuspend cells by pipetting.
14. To lyse cells, vortex @ 8 setting for 30 secs and then place on ice for 1 min. Repeat this process a total of 6 times.
15. 4 °Ccentrifuge 5 mins @14,000 RCF
16. Transfer supernatant and place in a new 1.5 mL Safe Lock Eppendorf tube
17. Flash freeze cell lysate in liquid nitrogen and store in -80C

Western Blot Protocol

SDS PAGE

1. Pour 8% SDS Page gels (1mm thick) using a 10 well comb.
2. Assemble SDS PAGE equipment.

3. Load between 50–100 µg of sample per well.
4. Heat samples at 90 °C for 3 mins in a 1.5 mL safe lock Eppendorf lock tube. Load in wells.
5. Run samples at 120V.

Overnight Transfer

1. Prepare a 10X stock of the transfer buffer. (This will last for 24 months at 4°C)

Transfer Buffer	10X
Tris Base	30.3 g
Glycine	144 g
Methanol	-
H_2O	Up to 1 L

1. Assemble the transfer buffer for your western: 100 mL of 10X stock Transfer Buffer, 200 mL methanol, and 700 mL of water. Place the transfer buffer in 4 °C before you use it.

2. Set up the transfer box. Need 2 sponges, 4 pieces of 3 mm filter paper, PVDF membrane, and your gel.

3. Pre-wet PVDF membrane in methanol for 30 seconds, then equilibrate in the transfer buffer for 2 minutes.

4. Assemble the western blot cassette in a small dish or plastic container to keep everything wet with transfer buffer *** Be sure not to dry your membrane so that you could prevent a bad background stain:

Orientation of Western Blot Cassette

- Positive electrode side (clear side)
- Sponge
- 2 pieces filter paper
- PVDF membrane
- Gel
- 2 pieces filter paper
- Sponge
- Negative electrode side (black)

5. Place the western blot cassette in the holder, and place the holder in the transfer box with a small stir bar. Take the transfer box to a 4 °C room for

overnight transfer.

6. Place the transfer box on a stir plate to keep the buffer circulating and cold while running.
7. Fill the transfer box with ~1L buffer. Can reuse the buffer used to assemble cassette and equilibrate membrane.
8. Run transfer at ~75 V for 1.5-2 hours, or ~35 V overnight. All transfers should be done at 4 °C.

Blocking

1. Use a 5% nonfat dry milk solution in 1X TBST (1 g milk per 20 mL TBST).
2. Place western blot protein side up in the blocking solution for 1 hour rocking at room temperature.
3. Do 2 rinses in TBST to remove the milk.

Antibody Incubations

1. Add primary antibody:
    - eIF4B primary antibody (Santa Cruz Biotechnology Lot #B2322 1:1000 dilution in TBST)
    - GAPDH primary antibody (Santa Cruz Biotechnology Lot #L0204 1:3000 dilution in TBST)
2. Incubate primary antibodies overnight at 4 °C. You can often reuse the two

antibodies for at least 3 blots (until titer is too low). Pour into 15 mL conical and store 4 °C short term for two weeks.

3. Rinse the blot to remove any residual primary antibody, then wash 3X 10 mins in TBST.
4. Add fluorescent anti-Mouse or anti-Goat secondary antibody at 1:10,000 dilution.
    - GADPH Secondary antibody (Anti-Goat) Alexa Fluor 647 (Life Technologies Lot# 1301819)
    - eIF4B Secondary antibody (Anti-Mouse) DyLight 680 (Invitrogen Lot# XL362195)
5. Incubate in secondary antibodies for 1 hour at room temperature while rocking. Be sure to cover the box with foil as the secondary antibodies are light sensitive.
6. Discard diluted secondary antibody (cannot be reused). Rinse blot briefly in TBST then wash 1X for 10 mins in TBST.

Azure Scanner for Western Blot

1. Ready to scan western blot using Azure Scanner. Settings I have used:
    a. To image 4B- Dylight 680 intensity 7
    b. To image GAPDH- Dylight 680 intensity 5

IF Protocol

- 16 % Paraformaldehyde

- PBS
- PBS-Tween
- Methanol
- Odyssey blocking buffer (LiCor Bio, Intercept Blocking Buffer Cat# 927-40000)
- Primary Antibody (Refer to Page 79 Materials List)
- Secondary Antibody (Refer to Page 79 Materials List)

1. Once you have completed Days 1-3 in the SG assay, take the cells into the chemical hood and directly add 16 % of Paraformaldehyde (PFA) to fix the cells with a final concentration of 4 % PFA and wait 10 mins. (If there was 150 µL of media then add 50 µL of the PFA.
2. Remove the media and wash the cells with 1X PBS-T, leave in the PBS for 10 mins on a plate rocker.
3. Remove the PBS-T and add 200 µL of Methanol for each well (This is to permeabilize the cells) and then wait for 10 mins.
4. Wash 1X with PBS *** Be sure to remove all PBS quickly or you could increase background.
5. Add 50 µL of Odyssey blocking buffer per well and incubate at room temperature for 60 mins.
6. Add Primary antibody: G3BP1 1:250 directly into the Odyssey blocking buffer, seal and incubate at 4 °C overnight on a rocking plate.

7. Wash cells 3X with PBS-T for 5 minutes in between washes on a rocking plate at room temperature.
8. For a 96-well plate, each well holds 200 µL. Prepare the following components to your 20mL blocking buffer: Add Secondary antibody Dylight 680 1:250 dilution into the blocking buffer, Add DAPI 1:10,000 to blocking buffer. Mix and Dispense 200 µL into each well. Seal, cover with foil and incubate for 2 hours at room temperature.
9. Wash 4X with PBS-T for 5 mins
10. Add 200 µL of PBS, seal the plate, and image on the microscope **(Figure 4)**.
11. Follow the imaging protocol in SG assay.

Imaging Pipeline Protocol (Cell Profiler)

In a collaboration with Nick Decuzzi from the Albeck Lab, we created an imaging pipeline to measure SG dynamics using a custom built pipeline for two software programs to talk to each other (Cell Pose and Cell Profiler). The section that I specifically worked on was optimizing the Cell Profiler package.

Cell Profiler is a cell image analysis software that can process all of your images automatically and summarize the data in an excel spreadsheet. Below is a step by step protocol on how to use the software:

1. Download the software package here: https://cellprofiler.org/releases
2. Be sure to export all of your images and save them in a separate folder.
3. Once you added the images to your pipeline, then you will click on the meta data

section and input the following steps below:

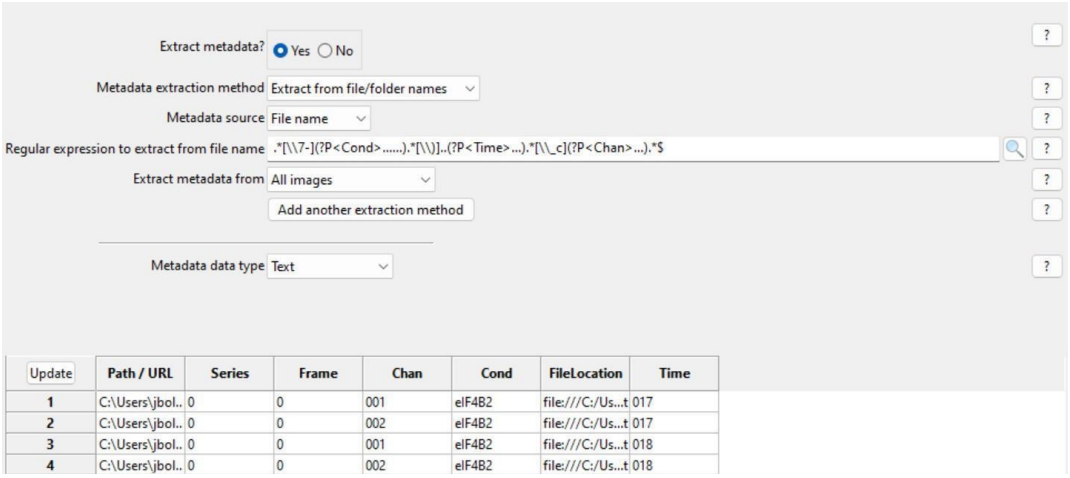

4. Click on the Names and Types section and be sure to add the following parameters, depending on how many colors you want to analyze. For example, to add two channels: GFP (OrigGreen), and Dapi (OrigReds). Be sure to input the following parameters below:

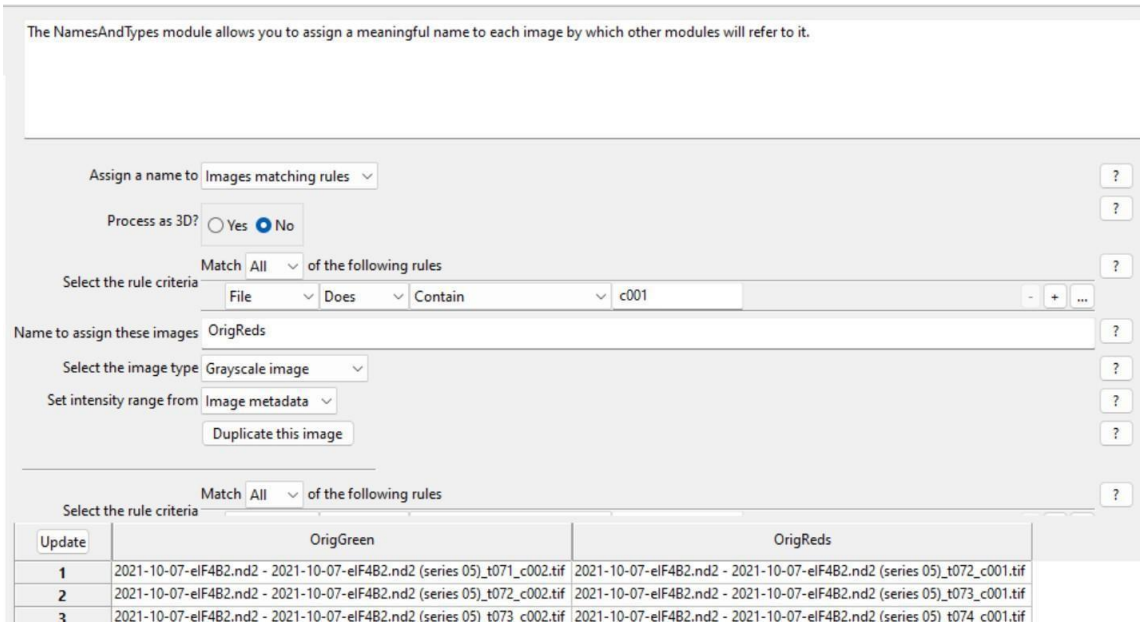

5. Once you have added the following: Images, Metadata, NamesandTypes, you

can start building your imaging pipeline.

6. Images were aligned using NIS Software.

7. Elijah Kofke (Albeck lab) trained a neural net in Cell Pose to track individual SGs and Nick built a program for Cell Pose to be added in the Cell Profiler pipeline called “RunCellPose”.

8. Next, we added a Track Objects to the pipeline, using follow neighbors and the object to track was the nucleus.

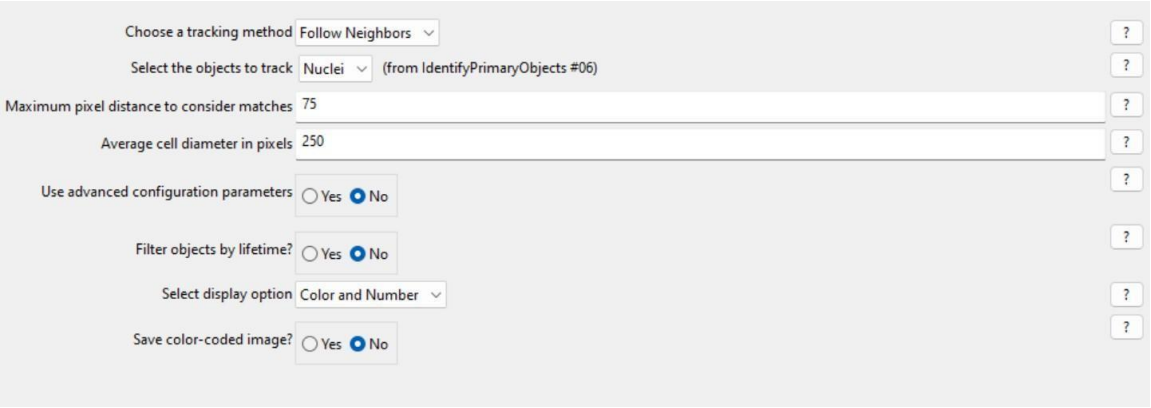

9. Next, we added an Identify Secondary Objects to the pipeline, using the following parameters below. This is to ensure that every SG is aligned with every cell (Cytoplasm).

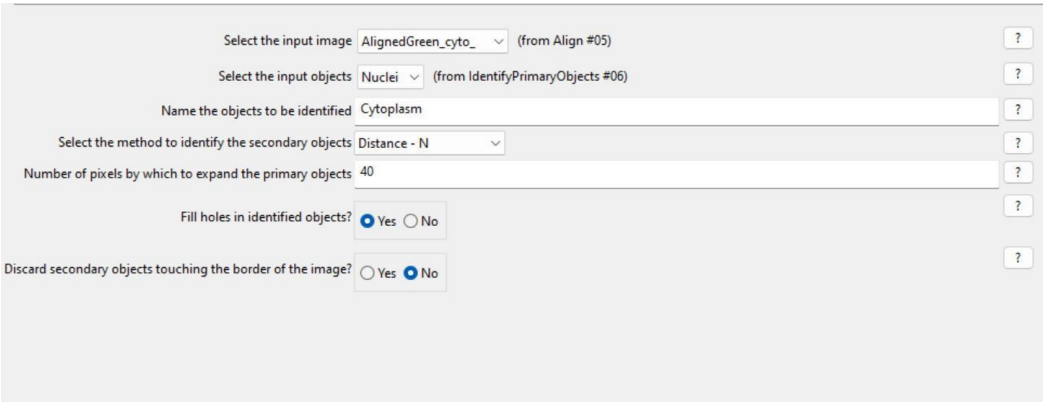

10. Next, we added Measure Object Intensity, MeasureSizeandShape, for the "RunCellPose Module" and then Exported to Excel Spreadsheet.

11. Once we exported all of the data, we used MatLab (SG Data Handler) to obtain curve fitting, run statistical analysis, and make other various graphs.

Future Directions

In this chapter, I discussed the development of protocols to measure stress granule (SGs) dynamics in real time. Leveraging the Flp-In T-REx inducible cell line, I optimized the induction duration, imaging, and characterization of SGs. This system is an excellent tool for modeling and characterizing the rate, number, and size of SGs. It allows us to model and track SGs over time, enabling the comparison of different protein mutants to determine their roles in SG dynamics.

One limitation of this assay is it currently relies on the use of an overexpression cell line.

To address this and to avoid potential artifacts, the next step would be to generate a cell line whereby GFP-tagged eIF4B is not overexpressed. We have on hand in the lab a knockout eIF4B HeLa cell line **(Figure 5)**. It would be exciting to engineer this cell line so that it can expressGFP-tagged eIF4B (using the Flp-In T-REx system). Essentially, this would enable the replacement of endogenous eIF4B with a GFP-tagged eIF4B or GFP-tagged eIF4B mutants. This approach will provide a more accurate representation of SG dynamics without the possibility of introducing artifacts from overexpression. Additionally, comparing different translation initiation factors and their effects on SG assembly dynamics will be an intriguing direction for future research.

Figures and Legends

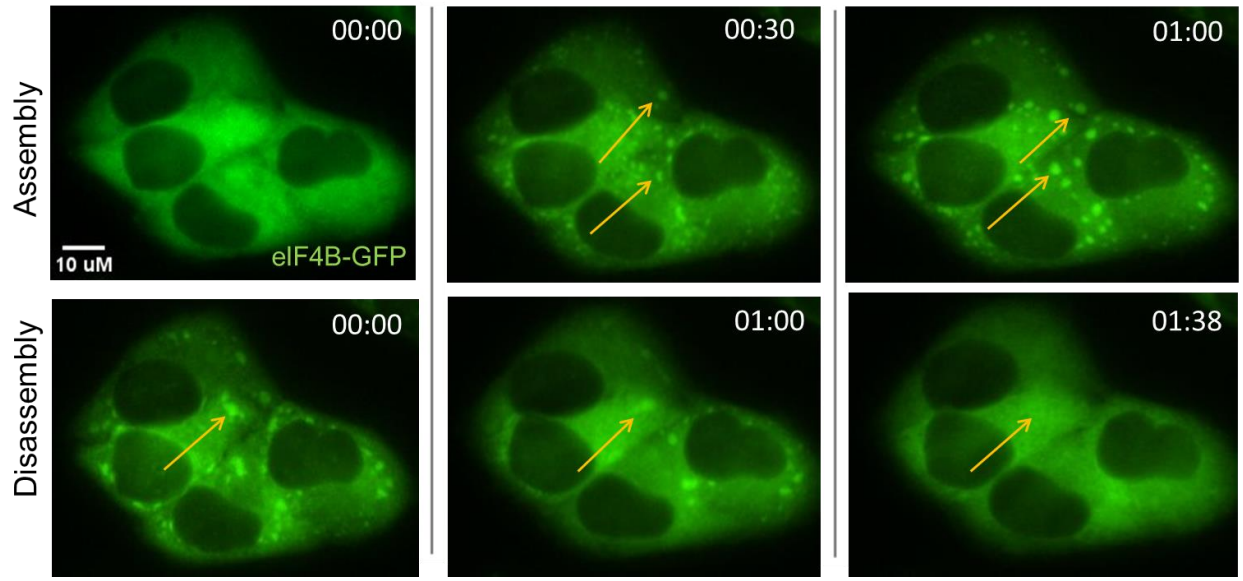

Figure 1. Measure stress granule dynamics overtime. *Images from left to right, top to bottom.* Time-lapse imaging of stress granule formation in HeLa Cells expressing WT-GFP-eIF4B following treatment with 125 μM sodium arsenite. The yellow arrows identify an example of a SG formed during the time course (shown in hours). Cells were washed twice to follow disappearance of stress granules. The yellow arrow indicates the disappearance of the stress granule. The dark holes in the cells indicate the nuclei (for this experiment the nuclei were not stained). Scale bar is 10μm.

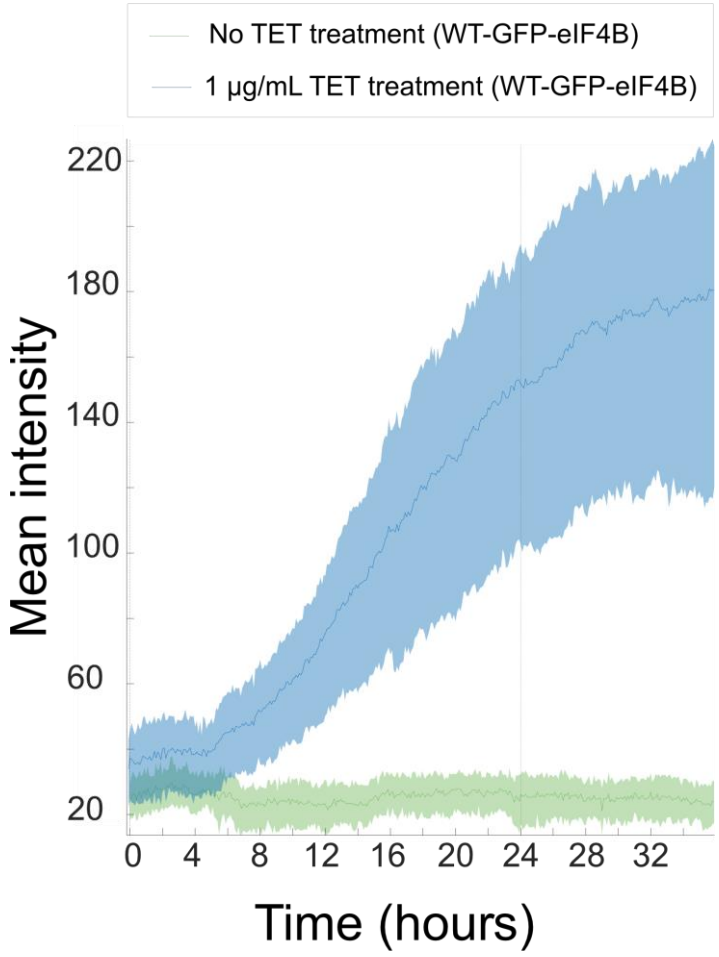

Figure 2. Measuring mean intensity of WT-GFP-eIF4B Flp-In T-REx tetracycline inducible cells over time. Dark lines represent the mean and the shaded regions are 25th/75th quartiles of data for tetracycline induced (blue) or uninduced (green) cells. All experiments moving forward used a 24-hour induction time to express GFP-eIF4B, which is indicated at the dotted line. Signal was offset at earliest time points due to some tetracycline background.

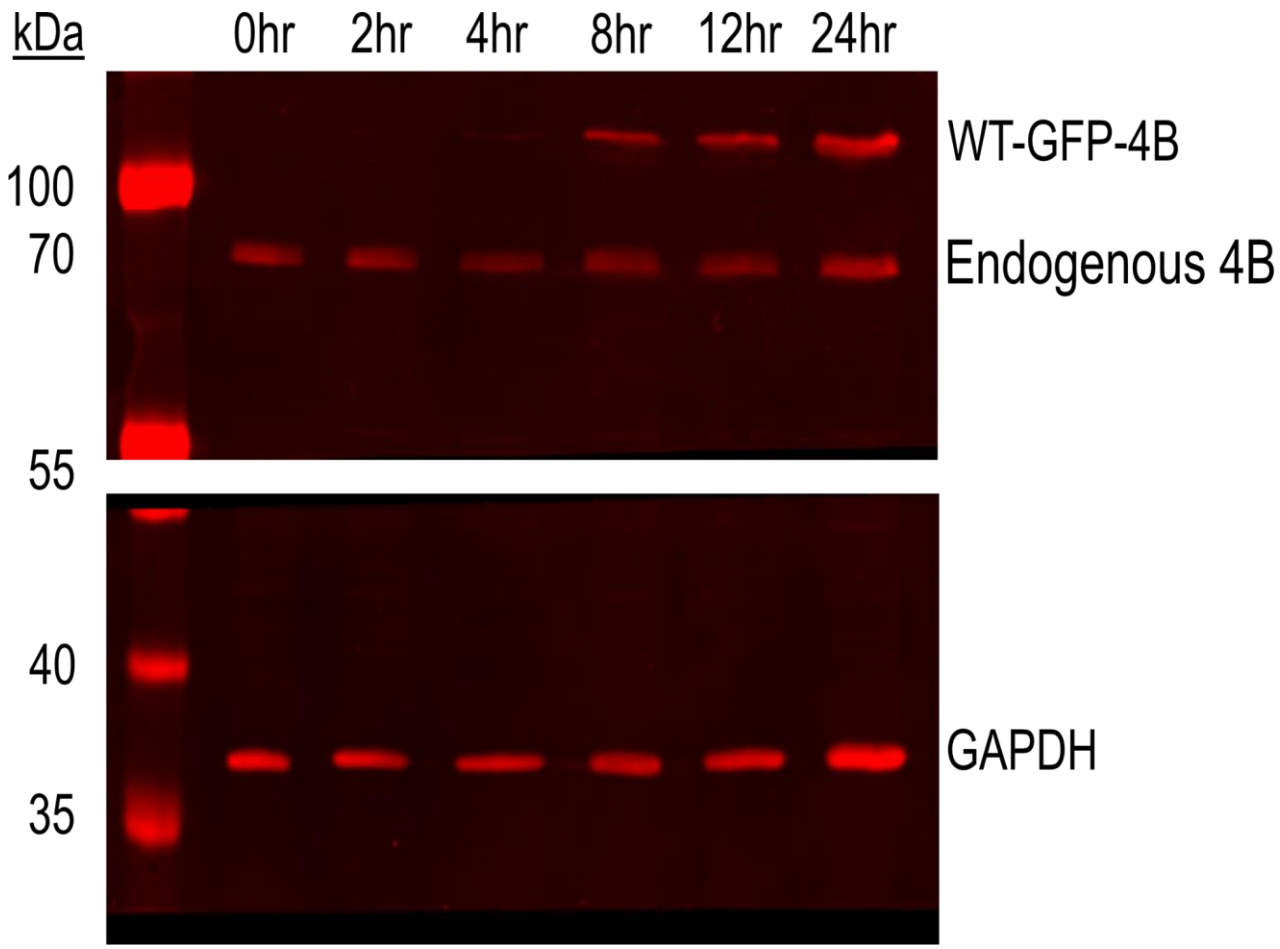

Figure 3. Measure protein expression of GFP-eIF4B in Flp-In T-REx

tetracycline inducible system over time. Western blot was performed at different induction times to measure the difference between endogenous eIF4B and overexpressed WT-GFP-eIF4B. GAPDH is used as a loading control. The gel was cut in two because the primaries were in two different hosts eIF4B (mouse) and GAPDH (goat). From left to right is the time of induction 0-24 hours. In total, 30 ug of total lysate protein was loaded and separated on an 8% SDS page gel.

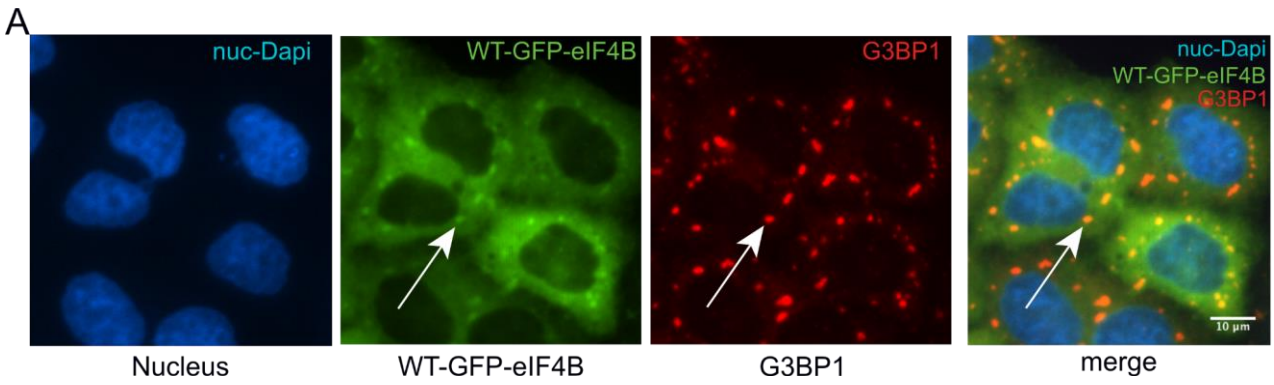

Figure 4. GFP-eIF4B colocalizes with G3BP1 in SGs. HeLa cells expressing GFP-eIF4B were induced for 24 hours and next day treated with 125 µM arsenite for one hour. Cells were subjected to immunofluorescence stain to visualize the stress granule nucleator G3BP1 using an anti-G3BP1 antibody (Alexa 647 Red), eIF4B-GFP (green), and the nucleus with Hoescht stain (blue).

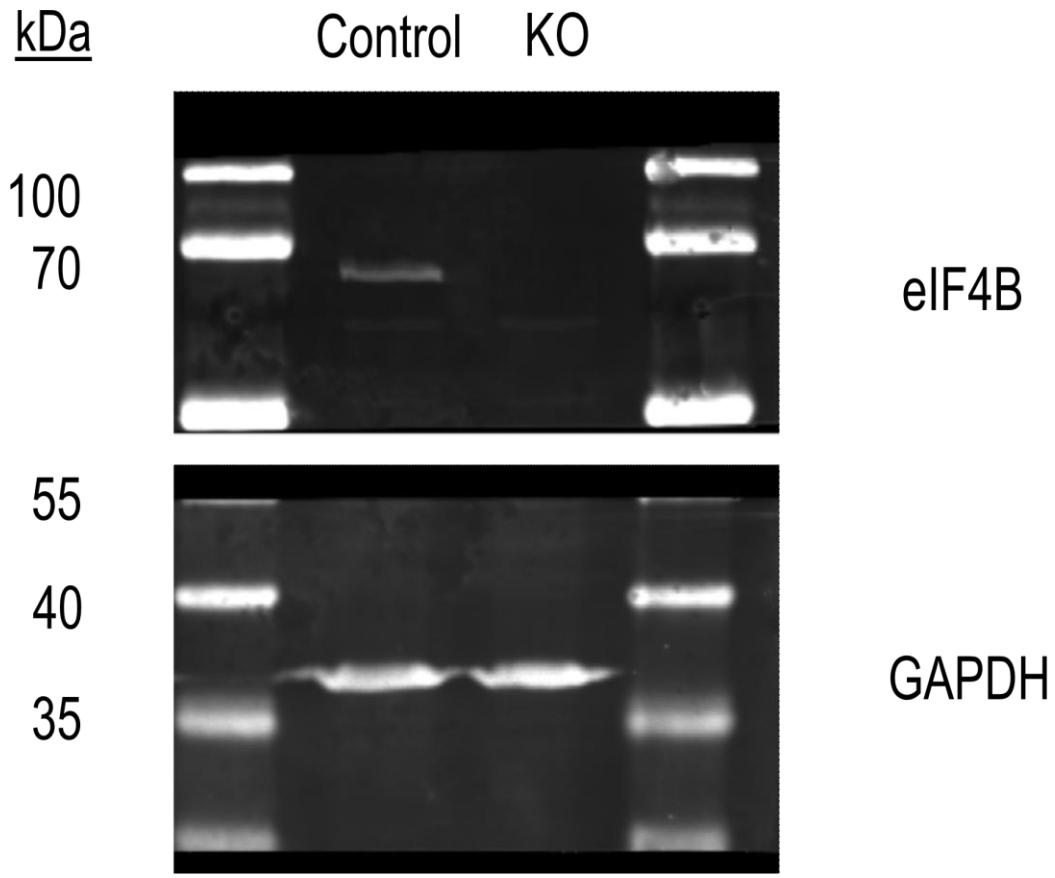

Figure 5. Western blot confirming eIF4B knockout in HeLa cell lines compared to Control. GAPDH is used as a loading control. The gel was cut in two because the primaries were in two different hosts eIF4B (mouse) and GAPDH (goat). 30 µg of protein was loaded that was extracted from cells on a 8% SDS page gel.

References

Kedersha, Nancy, Sarah Tisdale, Tyler Hickman, and Paul Anderson. 2008. “Chapter 26 Real-Time and Quantitative Imaging of Mammalian Stress Granules and Processing Bodies.” In *Methods in Enzymology*, 448:521–52. Academic Press.

Niewidok, Benedikt, Maxim Igaev, Abel Pereira da Graca, Andre Strassner, Christine Lenzen, Christian P. Richter, Jacob Piehler, Rainer Kurre, and Roland Brandt. 2018. “Single-Molecule Imaging Reveals Dynamic Biphasic Partition of RNA-Binding Proteins in Stress Granules.” *The Journal of Cell Biology* 217 (4): 1303–18.

Streit, Lisa, Timo Kuhn, Thomas Vomhof, Verena Bopp, Albert C. Ludolph, Jochen H. Weishaupt, J. Christof M. Gebhardt, Jens Michaelis, and Karin M. Danzer. 2022. “Stress Induced TDP-43 Mobility Loss Independent of Stress Granules.” *Nature Communications* 13 (1): 5480.

Vonaesch, Pascale, Philippe J. Sansonetti, and Pamela Schnupf. 2017. “Immunofluorescence Analysis of Stress Granule Formation After Bacterial Challenge of Mammalian Cells.” *Journal of Visualized Experiments: JoVE*, no. 125 (July). https://doi.org/10.3791/55536.

Chapter Three

RNA Recognition Motif of eukaryotic translation initiation factor 4B regulates stress granule assembly

Jessica Bolivar[1,2], Nicholaus L. DeCuzzi[1,2], Elijah Kofke[1], Masaaki Sokabe[1], Katherine Beglinger[1], John G Albeck[1]*, and Christopher S. Fraser[1,3]**

1 Department of Molecular and Cellular Biology, University of California, Davis, CA 95616, USA

2 These authors contributed equally.

3 Lead contact.

*Correspondence: jgalbeck@ucdavis.edu

**Correspondence: csfraser@ucdavis.edu

This chapter is currently under review for publication. J.B. and C.S.F. conceived and designed the experiments and led the project. NLD conceived live-cell and OPP assay experiments, developed the image analysis/data processing pipelines, performed analysis and model fitting on all live-cell and immunofluorescent data. JB, NLD, EK, and MS carried out experiments. KB created the GFP-eIF4B cell line. JB and NLD wrote and edited the manuscript with input from the other authors. JB and NLD made figures 1-3, and sup figures 1-4. MS made figure 4. JGA provided guidance on experiments and helped edit the manuscript

Graphical Abstract

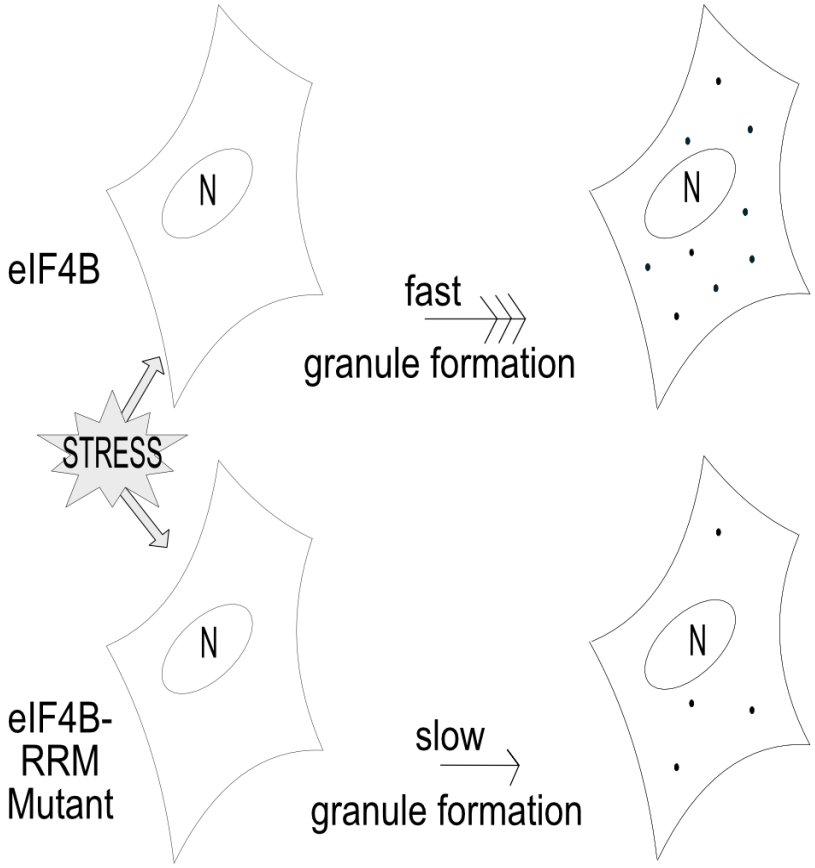

Summary

Cells respond to environmental stress to ensure survival and recovery, in part through the formation of cytoplasmic structures known as stress granules (SGs). Stress granules are non-membrane bound organelles composed of mRNA transcripts, RNA-binding proteins, 40S ribosomal subunits, and eukaryotic initiation factors (eIFs). It remains unclear, however, whether mRNA translation machinery actively regulates SG formation. Human eIF4B has been identified as an initiation factor that plays an active role in controlling cell growth by promoting the translation of growth-promoting mRNAs including c-myc and Cdc25C. Notably, eIF4B has been discovered as a component of SGs, raising the question of its role in SGs. To address this question, we used single-cell live-imaging to monitor the assembly of GFP-tagged human eIF4B in response to oxidative stress. By developing a single-cell imaging analysis pipeline, we quantified the kinetics of SG formation in real-time. Overexpression of GFP-tagged eIF4B with a point mutant in the RNA recognition motif (RRM) domain resulted in decreased rate of SG formation, fewer SGs formed, and a delayed response to treatment, compared to wild type eIF4B. To understand the mechanism by which eIF4B regulates SG formation, we used recombinant purified components to show that eIF4B directly binds to G3BP1, a known SG nucleator. Taken together, our findings suggest that the RRM of eIF4B affects SG assembly via its direct binding to G3BP1 and mRNA, which could be targeted as a therapeutic approach in future cancer studies.

Keywords

Live-Cell Imaging, eIF4B, Stress granules, G3BP1, translation, oxidative stress, stress response

Introduction

In response to certain types of environmental stress, such as heat shock and oxidative stress, eukaryotic cells can increase survival by triaging mRNAs within stress granules (SGs).(Campos-Melo et al., 2021) SGs are non-membrane bound organelles composed of mRNA transcripts, RNA-binding proteins, 40S ribosomal subunits, and eukaryotic initiation factors (eIFs).(Ivanov et al., 2019; N. Kedersha et al., 2002) These granules are formed by sequestration of translation initiation machinery stalled on mRNAs, leading to a liquid-liquid phase separation.(Buchan & Parker, 2009) This phase separation is caused by RNAs that are recruited to and self-organize on RNA condensate surfaces.(Tauber et al., 2020) Due to this process, the RNA condensate leads to enhanced interaction between trans RNA-RNA interactions and the formation of an RNA shell, which stabilizes the condensates.(Tauber et al., 2020) Formation of SGs regulates the protection or degradation of mRNAs and the translation machinery.(Ivanov et al., 2019)

Dysregulation of SG formation has been linked to poor cancer prognosis.(Asadi et al., 2021) For example, *in vitro* studies have linked SGs to cancer cell chemotherapy resistance.(Asadi et al., 2021; T. Hu et al., 2022) A model whereby increased SG

formation can protect cancer cells from stress and promote survival has therefore emerged.(Zhou et al., 2023) Understanding the molecular mechanism of SG assembly can therefore help identify targets to increase effectiveness of chemotherapeutic treatments.(Gao et al., 2019)

While components of SGs vary depending on the type of stress, there are only a few RNA-binding proteins that are considered to be essential to SG nucleation: ataxin-2, T-cell internal antigen-1 (TIA1), TIA-1 related (TIAR), and the Ras GTPase-activating protein-binding proteins 1/2 (G3BP1/2).(Anderson & Kedersha, 2002; Gilks et al., 2004; N. Kedersha et al., 2000; Tourrière et al., 2001; P. Yang et al., 2020)(N. L. Kedersha et al., 1999) The importance of these proteins is based on observations that their expression regulates the appearance of SGs. For example, G3BP1 overexpression can induce SG-like structures in the absence of stress, and its knockdown hinders SGs formation.(Matsuki et al., 2013)

The regulation of the translation initiation machinery actively contributes to SG assembly. One of the best characterized pathways leading to SG formation is the integrated stress response (ISR) pathway, which results in an increase in the phosphorylation of eIF2α at serine 51, preventing proper formation of eIF2·GTP·Met-tRNA^{Met} ternary complexes (TCs) and inhibiting translation initiation.(N. Kedersha et al., 2002) Nevertheless, SGs can form in the absence of eIF2α phosphorylation, implying that there is an eIF2α-independent mechanism of SG formation.(Mokas et al., 2009) Consistently, the SG nucleation factor G3BP1 has been shown to interact with the eIF4G component of the eIF4F complex to promote SG formation during viral infection.(X. Yang et al., 2019) The helicase activity of the eIF4A

component of eIF4F has also been shown to act as a novel RNA chaperone that limits mRNA recruitment into SGs.(Tauber et al., 2020) The eIF4F complex interacts physically and functionally with additional accessory factors including eIF4B, eIF4H, and polyA-binding protein (PABP). Reduction in any of these accessory factors triggers SG formation.(Andreou et al., 2017; Mokas et al., 2009; Özeş et al., 2014) eIF4B specifically functions as an accessory protein that enhances the duplex unwinding activity of eIF4A alone or in the eIF4F complex.(Özeş et al., 2011; Rogers et al., 1999, 2001; Rozen et al., 1990) Human eIF4B converts the eIF4A helicase into a processive helicase in the presence of eIF4G, thereby providing a mechanism to explain how this protein promotes the translation of growth promoting mRNAs.(Shahbazian et al., 2010) Based on these findings, we hypothesized that eIF4B may play an active role in SG assembly.

In this study, we investigated the role of eIF4B in the kinetics of SG assembly in human cells. Using a real-time live cell assay, we have characterized the rate of assembly of GFP-tagged eIF4B into SGs in response to oxidative ($NaAsO_2$) stress. Unexpectedly, our assay reveals that mutation of the N-terminal RRM domain in eIF4B limits the total number of SGs that assemble and reduces the rate of SG formation in response to oxidative stress. By monitoring protein synthesis at the single-cell level, our data show that hindered SG formation caused by the eIF4B-RRM mutant correlates with a partial suppression of translation activity in response to oxidative stress when compared to wild type GFP-tagged eIF4B. Finally, our work has identified a direct interaction between eIF4B and G3BP1, providing a possible mechanism to explain how eIF4B can regulate SG formation.

Results

Human eIF4B assembly into SGs is dose dependent following oxidative stress

Human eIF4B was previously found to be a component in the SG proteome,(Jain et al., 2016) so we first sought to verify that GFP tagged eIF4B is localized into SGs. We created a stable HeLa cell line with an N-terminally GFP-tagged wild-type eIF4B under a tetracycline (TET) inducible promoter (referred to as WT-GFP-eIF4B). Cells were treated with tetracycline for 24 hours to induce the expression of WT-GFP-eIF4B, as described in Materials and Methods. We noted that this induction time resulted in the over-expression of a roughly equivalent amount of WT-GFP-eIF4B compared to endogenous eIF4B (Figure S1E). The WT-GFP-eIF4B signal was initially found to be diffuse throughout the cytoplasm but became concentrated into punctae within 30 minutes of sodium arsenite treatment **(Figure 1A)**. In addition, we measured colocalization of WT-GFP-eIF4B with G3BP1, a well-established marker for SGs, using immunofluorescence at the end of the time course of the live-cell experiments (Figure S1A). Mander's overlap correlation between WT-GFP-eIF4B and G3BP1 was 0.81, indicating they are both similarly sequestered into SGs (Figure S1B).

To rigorously characterize the assembly of WT-GFP-eIF4B into SGs, we developed a live-cell time-lapse imaging assay using a custom image analysis pipeline. The imaging pipeline consists of NIS Elements, Cell Profiler, CellPose, and MatLab, and is used to detect, quantify features, and track granules over time (outlined in Figure 1B). To model the kinetics of granule formation, we modified an equation previously used to describe

the cleavage of caspase substrates in individual cells.(Albeck et al., 2008)

$$SG(t) = f - f1 + e(t-Td)(Ts/4) \quad (1)$$

This equation (1) assumes a sigmoid shaped increase in SG number over time (SG(*t*)) up to a maximal value. We iteratively fit this equation to each cell's observed SG number over time, as described in detail in the Materials and Methods. The resulting parameter values fitted for each cell describe the maximum number of granules formed (f), the time from first SG nucleation to max number of granules formed (Ts), and time from treatment to half max number of granules (Td). From these parameters we then calculate the rate of granule nucleation (f/Ts), and nucleation delay in SG from treatment (Td-(Ts/2)) (Figure 1C).

Using this approach we measured WT-GFP-eIF4B SG formation over time at varying concentrations of sodium arsenite, ranging from 0–250 μM, and fit models for the 62.5 μM, 125 μM, and 250 μM sodium arsenite doses. We found that higher doses of sodium arsenite increased the rate of SG formation (f/Ts), increased the maximum number of SGs (f), and decreased SG nucleation time (Td-(Ts/2)) (Figure 1D-F). When the rates of SG formation were compared, we found a significant rate increase between 62.5 μM and 125 μM (214% increase), but no significant rate increase between 125 μM and 250 μM (9% increase) (Figure 1D). This suggests that 125 μM is sufficient to cause a saturating rate of SG formation in these cells. Interestingly, we observe a significant increase in the max number of SGs (f) formed with each increase in sodium arsenite dose (62.5 μM -> 125 μM = 46% increase; 125 μM -> 250 μM = 13% increase) (Figure

1E). The increase in max SGs formed despite similar rates of SG formation can be explained by the fact that cells treated with 250 μM sodium arsenite have a faster nucleation relative to both 62.5 μM and 125 μM (250 μM is 43% faster at nucleating than 125 μM; 125 μM is 38% faster than 62.5 μM) (Figure 1F).

RNA Recognition Motif (RRM) mutants of eIF4B inhibit SG formation

Because SGs form through RNA-protein interactions,(Marcelo et al., 2021) we wanted to determine if the interaction between eIF4B and RNA is important for its assembly into SGs. Human eIF4B is composed of four domains: a canonical RNA Recognition Motif (RRM), a DRYG domain (eIF3 binding domain), a non-canonical RNA binding domain, and an eIF4A binding domain (Figure 2A). The RRM is the most conserved domain between species. Thus, we created cells with TET inducible GFP-eIF4B containing mutations in the RRM (F139A (M1), F99A/N102A/R135A, (M2), and R135A/K137A/F139A (M3)) (Figure 2A).

Following treatment with 125 μM sodium arsenite for 1 hour, formation of GFP-eIF4B punctae was impaired for all mutants, when compared to cells expressing WT-GFP-eIF4B (Figure S2A). The M1-GFP-eIF4B cell line was selected for further experiments as it contained a single point mutation that was designed to prevent RNA binding (F139A; referred to as M1-GFP-eIF4B). The decreased number of punctae formed by M1-GFP-eIF4B raised the question as to whether overall SG formation is affected by the mutant or if only the assembly of M1-GFP-eIF4B into SGs is impaired. Immunofluorescent staining for G3BP1 also indicated a significant decrease in SGs in

M1-GFP-eIF4B expressing cells treated with 125 μM sodium arsenite for 2 hours compared to WT-GFP-eIF4B (13.6% decrease in G3BP1 granules; P = 0.0016). The reduction of G3BP1 punctae, an essential SG component of SGs, indicates that the over-expression of M1-GFP-eIF4B impairs SG formation rather than only affecting M1-GFP-eIF4B assembly into SGs (Figure S2B). Consistent with this model, the colocalization of M1-GFP-eIF4B and G3BP1 is similar to that for WT-GFP-eIF4B, (Mander's overlap 0.82, compared to 0.81 for WT) arguing against specific exclusion of the mutant eIF4B from SGs (Figure 2B).

Importantly, we performed a western blot analysis to determine the relative amounts of endogenous eIF4B and M1-GFP-eIF4B at various times following TET induction. After 24 hours of TET induction, M1-GFP-eIF4B was found to be expressed at ~1:1 ratio to the endogenous eIF4B protein **(Figure S2C)**. This is very similar to that found for WT-GFP-eIF4B (Figure S1D). At this level of expression, it is reasonable to conclude that incorporation of M1-GFP-eIF4B acts in a dominant negative manner to slow the overall formation of SGs.

After establishing that M1-GFP-eIF4B is assembled into SGs and can be used to accurately measure SG formation, we applied the modeling approach described above to rigorously compare M1-GFP-eIF4B SG kinetic parameters to that of WT-GFP-eIF4B expressing cells (max SGs (f), rate (f/Ts), nucleation delay in SG from treatment (Td-(Ts/2)). Our data show that the modest overexpression of M1-GFP-eIF4B caused a decrease in the rate of SG formation (f/Ts) at all sodium arsenite concentrations tested (Figure 2C). This decrease varied with sodium arsenite concentration and was generally in a range of a 15-60% decrease.

We also observed a decrease in the maximum number of SGs formed (f) at all sodium arsenite doses tested, with the decrease generally in a range of 8-30% when compared to WT-GFP-eIF4B cells (Figure 2D). We observed an appreciable delay in SG nucleation delay (Td-(Ts/2)) at both 62.5 μM and 125 μM sodium arsenite compared to the WT-GFP-eIF4B cells (Figure 2E). No significant change in SG nucleation delay was observed at the 250 μM sodium arsenite concentration, which may indicate that 250 μM sodium arsenite is saturating to cause rapid SG nucleation in both cell lines. We then investigated if the size of SGs formed in the M1-GFP-eIF4B cells were different from their WT counterpart. Generally, across all sodium arsenite doses and cell lines, the average SG area at f ranged from 3.1 - 3.5 μm^2 (Figure 2F). As this variation is approximately a 1 pixel difference in the images collected, the variation in SG size is negligible. Furthermore, we compared conditions where SGs are nucleating at a similar rate (i.e. WT-GFP-eIF4B cells treated with 125 μM sodium arsenite and M1-GFP-eIF4B cells treated with 250 μM sodium arsenite). Between these conditions that possess similar intrinsic SG formation rates and the maximum number of SGs formed, the area of SGs are not significantly different (Figure 2F). Together these data suggest the M1-GFP-eIF4B mutant negatively influences the cell's ability to form stress granules under arsenite-treated conditions.

Stress induced suppression of global translation is impaired by eIF4B RRM Mutant

Because SG formation can inhibit translation under stress(Mokas et al., 2009), impaired

SG formation potentially affects the cell's ability to adapt to stress conditions. We therefore hypothesized that impaired SG formation in M1-GFP-eIF4B cells limits their capacity to suppress translation under sodium arsenite treatment, compared to WT-GFP-eIF4B cells. To test this hypothesis, we compared global translation activity in the presence of over-expressed WT-GFP-eIF4B or M1-GFP-eIF4B in the absence or presence of sodium arsenite using an O-propargyl-puromycin (OPP) assay (Click Chemistry Tools #1407). We interpreted OPP intensity as the total incorporation of a label during the last 30 minutes of the experiment, and therefore an indication of the cell's average protein synthesis during that time. Under vehicle conditions, M1-GFP-eIF4B cells have significantly reduced protein synthesis relative to WT-GFP-eIF4B (~50% reduction; Figure 3A), indicating that over-expression of the RRM-mutant eIF4B reduces protein synthesis in the absence of stress. Under treatment with 125 μM sodium arsenite, protein synthesis was strongly reduced in both cell lines. Surprisingly, however, M1-GFP-eIF4B cells showed a smaller arsenite-induced suppression compared to WT-GFP-eIF4B cells (Figure 3A). Specifically, 125 μM sodium arsenite treatment caused a ~93% reduction in protein synthesis in WT-GFP-eIF4B cells and a ~74% reduction in M1-GFP-eIF4B cells compared to their vehicle-treated counterparts. This trend was consistent across all sodium arsenite doses tested, with M1-GFP-eIF4B cells forming fewer SGs and more weakly suppressing protein synthesis, compared to WT-GFP-eIF4B cells (Figure 3B).

We next wanted to determine if the kinetics of SG formation and the type of GFP-eIF4B expressed (WT or M1) is predictive of a cell's protein synthesis ($\log_2$ OPP intensity) following treatment with sodium arsenite. To accomplish this, we performed a partial

least squares regression (PLSR) with the single-cell SG kinetic parameters (f, rate, and nucleation delay in SG), eIF4B expression (WT or M1) and concentration of sodium arsenite as the input components. Together these inputs are able to explain 54% of the cell-to-cell variance in protein synthesis (the output vector; Figure 3C). When the sodium arsenite concentration parameter is removed, the % variance explained is 48%, suggesting SG kinetics and cell line information alone are predictive of the cell-to-cell variance in protein synthesis. When analyzing which individual input component was most predictive of the cell-to-cell variance in protein synthesis, we found SG nucleation delay (nd) was the most predictive of protein synthesis (26.3% variance explained). The sodium arsenite dose, cell line information, or f were also highly predictive of protein synthesis (26%, 23.5%, & 21.5% variance explained); however, rate was not as predictive (9.6% variance explained). Because this study is focused on single-cell behavior, we examined the PLSR model which included the SG kinetics and cell line information, excluding the sodium arsenite dose. When analyzing which input components are most predictive of protein synthesis across all principal components (PCs), we found that the max SGs formed (f) had a negative weighting, whereas cell line and nucleation delay had positive weights (Figure 3D). Similar trends were observed in the first principal component, which accounted for nearly all of the model's predictive capacity (Figure 3E). These weights indicated that an increased f value is correlated with a lower protein synthesis, whereas a higher nucleation delay and the expression of the M1-GFP-eIF4B protein were correlated with higher protein synthesis. Overall, these models are consistent with the interpretation that the SGs are strong regulators of protein synthesis rate in each cell.

eIF4B binds directly to the SG nucleator protein G3BP1

Because eIF4B is colocalized with G3BP1 in SGs and significantly contributes to SG formation, we wondered if these proteins may directly interact with each other. To this end, we use a native gel shift assay using a fluorescent-labeled purified human G3BP1 to test its interaction with purified human WT-eIF4B, M1-eIF4B, or eIF4H. The migration of G3BP1 is diffusive on its own in the native gel, but becomes appreciably shifted by the addition of eIF4B (Figure 4A, lanes 1 and 2). In contrast, eIF4H, which is an accessory protein that possesses similar eIF4A helicase stimulating activity, fails to cause any shift in labeled G3BP1 (Figure 4A, lane 4). We note that eIF4H also possesses a similar RRM domain as eIF4B. Interestingly, M1-eIF4B possesses a similar G3BP1 binding property to that found for the wild type protein (Figure 4A, lane 3). While these data cannot determine if the thermodynamic and/or kinetic parameters for the interaction between M1-eIF4B with G3BP1 are different to the wild type protein, they do show that both proteins are able to bind to G3BP1. Taken together, these results show that eIF4B directly and specifically interacts with G3BP1 at a physiological concentration (1 μM).

To determine if M1-eIF4B possesses any defect in eIF4Bs characterized *in vitro* activities, we determined if M1-eIF4B is able to stimulate the helicase activity of eIF4A using an established fluorescence helicase assay.(Özeş et al., 2014) For this assay, the ATP-dependent unwinding of a synthetic RNA duplex is monitored in real-time in the presence of purified eIF4A and eIF4G in the absence or presence of eIF4B.

Determining the initial rate of duplex unwinding in the presence of WT-eIF4B or M1-eIF4B reveals that they promote the duplex unwinding activity of eIF4A-eIF4G by the same extent (0.22 ± 0.02 fraction/min for WT-eIF4B and 0.21 ± 0.01 fraction/min for M1-eIF4B) (Figure 4B). Thus, the RRM domain in eIF4B does not appear to function in the ability of eIF4B to stimulate the helicase activity of eIF4A.

Human eIF4B can be crosslinked to the 40S subunit.(Eliseev et al., 2018) Residue 223, which is located immediately after the RRM domain, is crosslinked to the uS3 ribosomal protein at the mRNA entry site. We confirmed a direct interaction between human eIF4B and the 40S subunit using a fluorescence anisotropy binding assay similar to that used in our previous 40S subunit binding assays.(Sokabe & Fraser, 2014) In this assay, A fixed amount of fluorescently labeled WT-eIF4B shows an appreciable anisotropy increase upon titration of an increasing concentration of the 40S subunit. Converting anisotropy values into the fraction of fluorescently labeled eIF4B bound at each 40S subunit concentration yields an equilibrium dissociation constant (K_d) below the detection limit of ~10 nM **(Figure 4C)**. When a fixed amount of fluorescently labeled M1-eIF4B was incubated in the presence of increasing concentrations of the 40S subunit the Kd was found to be essentially the same as that found for WT-eIF4B (Figure 4C). Thus, we conclude that the RRM domain mutant does not alter the direct interaction between eIF4B and the 40S subunit, at least in the absence of any other initiation components.

Mammalian eIF4B can bind to RNA by virtue of its RRM domain and a separate RNA binding domain located in its C-terminus (Figure 2A). To determine if the RRM plays an important role in the interaction between eIF4B and RNA, we first generated a

fluorescently labeled 42-nt long unstructured RNA (CAA-FL).(Izidoro et al., 2022; Sokabe & Fraser, 2014) To establish a fluorescence anisotropy-binding assay, we monitored the binding of CAA-FL to WT-eIF4B or M1-eIF4B by titrating each eIF4B protein into a fixed amount of CAA-FL RNA. The change in fluorescence anisotropy was measured and converted into the fraction of CAA-FL bound at each eIF4B concentration. Using this assay, the K_d of CAA-FL binding to WT-eIF4B is 118 ± 17 nM while the K_d of CAA-FL binding to M1-eIF4B is 107 ± 19 nM (Figure 4D). Thus, the affinity of RNA for eIF4B using this anisotropy assay is not dependent on the RRM domain. Interestingly, we do observe an appreciable difference in maximum anisotropy changes at a saturating amount of protein (0.109 ± 005 with WT-eIF4B, and 0.079 ± 0.006 with M1-eIF4B). This likely suggests an altered RNA binding conformation between these two proteins, with an increase in flexibility of RNA binding to M1-eIF4B compared with WT-eIF4B.

Discussion

In this study, we have used a real-time live cell assay to quantitatively monitor the kinetics of SG formation in response to oxidative stress. We have shown that modest overexpression of GFP-tagged eIF4B in Hela cells forms discrete puncta that we determined to be SGs by virtue of the colocalization of G3BP1. This assay has enabled us to successfully generate a model with parameter values for individual cells describing the maximum number of granules formed (f), the time from first SG nucleation to max number of granules formed (Ts), and time from treatment to half max number of

granules (Td) (Figure 1C). These parameters also enable one to calculate the rate of granule nucleation (f/Ts) and nucleation delay in SG from treatment (Td-(Ts/2)), thereby providing a more complete analysis of SG formation in live cells (Figure 1C). We anticipate that this modeling approach will enable others to model the real-time appearance of puncta in many different cell types and organisms.

Changes in the availability and activity of eIFs and their function in controlling translation initiation has been identified as a key regulator of SG formation.(Buchan & Parker, 2009; Ivanov et al., 2019; N. Kedersha et al., 2002) Translation initiation on almost all cellular mRNAs is dependent on the ATP-dependent helicase activity of eIF4A and its regulation has implications for the translation of specific mRNAs during growth and stress.(Parsyan et al., 2011) Recently, it was shown that the eIF4A helicase also functions independently of the translation machinery as an RNA chaperone that limits the condensation of RNA that otherwise can form SGs.(Tauber et al., 2020) Human eIF4B strongly promotes the helicase activity of eIF4A by converting it to a processive helicase in the presence of eIF4G.(García-García et al., 2015) We therefore used our real-time single-cell assay to determine if the RNA binding property of eIF4B is important in regulating SG formation in response to oxidative stress. To this end, we created a point mutant in the RNA Recognition Motif (RRM), named eIF4B-M1, to prevent this domain binding to RNA. Our data showed that the modest overexpression of eIF4B-M1 appreciably reduced the overall rate of SG nucleation and the number of SGs in individual cells (Figure 2). This surprising result is observed despite roughly 50% of eIF4B in the cell (the endogenous protein) being wild type. Thus, eIF4B-M1 functions as a dominant negative regulator of SG nucleation, which appears to limit the number of

SGs that can form in response to oxidative stress.

To gain mechanistic insight into how M1-eIF4B can negatively regulate SG formation, we directly compared the ability of WT-eIF4B and M1-eIF4B in their eIF4A helicase promoting activity using a real-time fluorescent helicase assay (Figure 4B). The WT-eIF4B and M1-eIF4B proteins possess the same ability to promote the helicase activity of an eIF4A-eIF4G complex in this assay, suggesting that SG dysregulation by M1-eIF4B is not due to an inhibition of the eIF4A helicase. Consistent with this, one would expect the inhibition of eIF4A helicase activity would result in an increase in SG formation in light of its RNA chaperone activity.(Tauber et al., 2020) We note, however, that a previous study did show that a double mutation in the RRM domain of eIF4B results in a roughly 80% inhibition of the helicase activity of eIF4A in the absence of eIF4G.(Méthot et al., 1994) The reason for this apparent discrepancy with our data is not clear, but it is possible that the RRM domain of eIF4B may be more important in promoting the helicase activity of eIF4A in the absence of eIF4G.

We used purified components to reveal a direct high affinity interaction between eIF4B and the 40S subunit. Similar to the helicase activating property of eIF4B, the interaction with the 40S subunit was not found to be altered by the RRM mutant eIF4B protein (Figure 4C). Nevertheless, this interaction may be important for a later step in the initiation pathway since the RRM domain of eIF4B has been proposed to interact with the mRNA entry channel of the 40S subunit.(Eliseev et al., 2018)

Using a fluorescence anisotropy binding assay, we show that M1-eIF4B has a similar overall binding affinity to WT-eIF4B when using a short RNA (Figure 4D). This is

perhaps surprising given the fact that M1-eIF4B possesses one less functional RNA binding domain than the wild-type protein. We do note, however, that the change in anisotropy of M1-eIF4B compared to WT-eIF4B is appreciably different, which is consistent with these two proteins possessing a different conformation when bound to RNA.

Unexpectedly, we discovered that eIF4B possesses a direct binding interaction with the SG nucleating factor G3BP1 in the absence of any other components (Figure 4A). This interaction appears to be specific for eIF4B since the related protein eIF4H was not found to bind to G3BP1 using the same native gel shift assay. We did not detect any large change in binding between eIF4B and G3BP1 when the RRM domain is mutated, but a future thermodynamic and kinetic analysis will be needed to more rigorously characterize this novel interaction. Interestingly, a recent study showed that the intrinsically disordered regions (IDRs) of human eIF4B can promote the self-association of the protein into a condensed phase in vitro.(Swain et al., 2024) This physical property of eIF4B is consistent with it playing a role in regulating SG formation.

Taken together, it is tempting to speculate that there may be an important cooperativity provided by the interaction of the eIF4B RRM with mRNA together with the interaction between eIF4B and G3BP1 that is important for enabling G3BP1 to nucleate SGs. It will be important in future to test this potential model and determine whether this also applies to other stresses beyond oxidative stress. It is noteworthy to recognize that eIF4B has been shown to promote cell proliferation by stimulating the translation of mRNAs needed for cell cycle progression (e.g. cdc25 and c-myc).(Shahbazian et al., 2010) Thus, eIF4B potentially provides the cell with an important molecular switch that

can control both cell growth through its interaction with the translation machinery and the stress response through its interaction with G3BP1.

In this study, we used an O-propargyl-puromycin (OPP) assay to monitor the amount of protein synthesis at the single cell level following treatment of cells with sodium arsenite. This powerful approach enabled us to directly compare the amount of protein synthesis in individual cells to the parameters of SG formation from our real-time SG formation assay in precisely the same cells **(Figure 3)**. Using this approach, our data revealed that treatment of cells with increased sodium arsenite concentration increased the maximum SGs formed, leading to reduced protein synthesis within the cell. Importantly, we observe an appreciable reduction in the nucleation delay in SG formation in response to sodium arsenite in cells expressing the mutant eIF4B, which corresponded to a greater amount of protein synthesis in those cells compared to cells expressing wild type eIF4B. Essentially, the M1-eIF4B mutant somehow protects cells from full translation inhibition in response to oxidative stress by preventing the nucleation of SG formation.

We note that previous studies have shown that the transient overexpression of eIF4B inhibited global rates of translation.(Holz et al., 2005; Milburn et al., 1990) In contrast, we now show that the modest induction of eIF4B overexpression using a Hela stable cell line doesn't result in translation inhibition. Global translation activity, however, is inhibited by roughly 50% upon the modest overexpression (by 50%) of the RRM mutant eIF4B (Figure 3A). While we do not understand the mechanism by which M1-eIF4B functions as a dominant negative protein for translation initiation, it is entirely possible that its RRM domain promotes initiation by virtue of its likely position at the mRNA entry

channel of the 40S subunit.(Eliseev et al., 2018) Nevertheless, as stated above, a dominant negative protein for translation initiation would be expected to result in the increase in SG formation based on our understanding of the activity of the translation apparatus and SG formation in response to stress. The fact that M1-eIF4B inhibits global translation but prevents the full inhibition of translation in response to oxidative stress is consistent with the RRM domain mutant containing eIF4B functioning as an SG nucleation regulator.

In conclusion, we have developed a single cell assay that is able to follow real-time kinetics of SG formation. Using a custom analysis pipeline, we can successfully identify, track, and model GFP-eIF4B granule assembly in real-time. Together with monitoring protein synthesis in individual cells, we can now compare SG formation parameters with the total amount of protein synthesis at the single cell level. Our data verify that human eIF4B is a component of SGs and show that a mutation in its RRM domain that prevents RNA binding strongly inhibits SG nucleation in live cells. Thus, eIF4B likely provides the cell with a molecular switch that controls both cell growth and the stress response through its interaction with the 40S subunit and G3BP1 respectively. In the future, it will be important to identify the precise mechanism by which the RRM domain in eIF4B regulates SG formation and the stress response.

Acknowledgements

We wish to thank Masa Sokabe and Nancy Villa from the Fraser laboratory for many insightful comments and critical reading of the manuscript. We also wish to thank

Michael Pargett for his discussions on PLSR. We like to thank Drs. Elena Dobrikova and Matthias Gromeier from Duke University Medical Center for the gift of the HeLa Flp-In T-Rex host cell line.

Author Contributions

J.B. and C.S.F. conceived and designed the experiments and led the project. NLD conceived live-cell and OPP assay experiments, developed the image analysis/data processing pipelines, performed analysis and model fitting on all live-cell and immunofluorescent data. JB, NLD, EK, and MS carried out experiments. KB created the GFP-eIF4B cell line. JB and NLD wrote and edited the manuscript with input from the other authors. JB and NLD made figures 1-3, and sup figures 1-4. MS made figure 4. JGA provided guidance on experiments and helped edit the manuscript.

Declaration of Interests

J.G.A. has received research funding from Kirin Corporation. The other authors declare that they have no conflicts of interest with the contents of this article.

Figure 1: Measurement of GFP labeled eIF4B granule formation kinetics

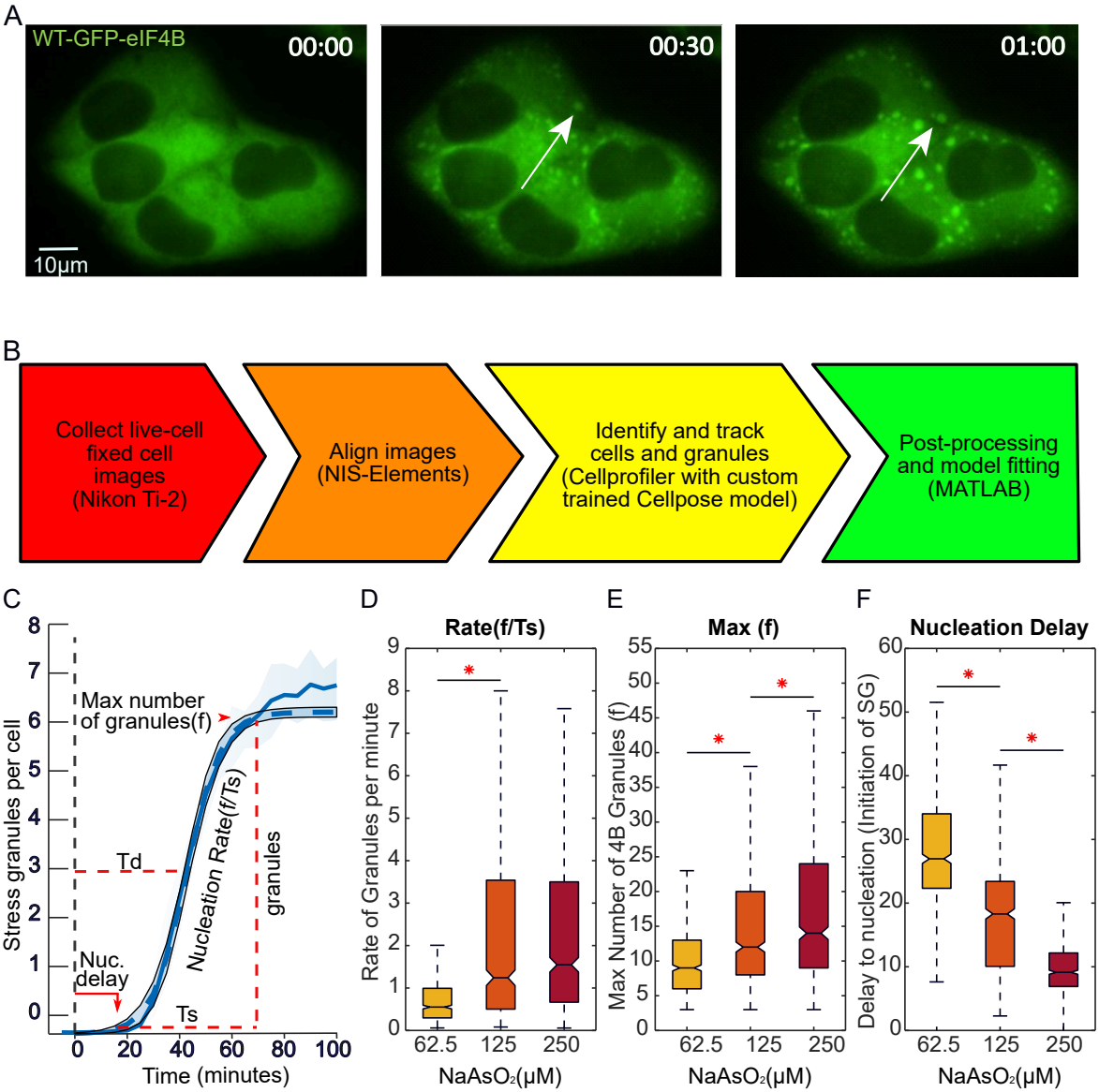

Figure 1. Measurement of GFP labeled eIF4B granule formation kinetics

(A) Time-lapse imaging of stress granule formation in HeLa Cells expressing WT-GFP-eIF4B following treatment with 125 μM sodium arsenite. The white arrow identifies an example of a SG formed during the time course (shown in hours). Scale bar is 10μm.

(B) Outline of custom pipeline for SG identification and modeling, as described in the Materials and Methods. Live-cell and immunofluorescent (fixed) images were acquired, shifts in the images are corrected, images are analyzed by a Cell Profiler pipeline that uses a custom Cellpose neural net trained to identify SGs; and the tracked SG data are imported into MATLAB where it is filtered for erroneous data and used to make plots and fit a model to determine the rate of SG assembly.

(C) SG kinetics are extracted from live-cell data using a modified equation.(Albeck et al., 2008) This equation is fit to the single cell SG data to determine: Max number of SGs per cell (f), Rate of SG formation (f/Ts), and SG nucleation delay (Td – (1/2)Ts). Graph shows the average number of SGs per cell over time. The dark blue line is the mean of SGs and the shaded light blue area includes the 75 and 25 quantiles of mean. Dashed line is model fit to live-cell data with 95% confidence intervals.

(D-F) Box and whisker plots showing single-cell WT-GFP-eIF4B rate, max number, and initiation of SGs per cell. Colors indicate treatment with either 62.5 μM (Yellow), 125 μM (Orange), or 250 μM (Red) sodium arsenite (NaAsO2). Asterisk indicates $P<0.005$ between groups. Significance was determined via One-Way ANOVA comparison to compare the difference between each treatment group with a Dunnett multi-comparison

protocol to account for false discovery rate. n>660 cells per condition pooled from 3 experimental replicates with at least 2 technical replicates each.

See also Figure S1.

Figure 2. RNA Recognition Motif (RRM) mutants of eIF4B inhibit SG formation

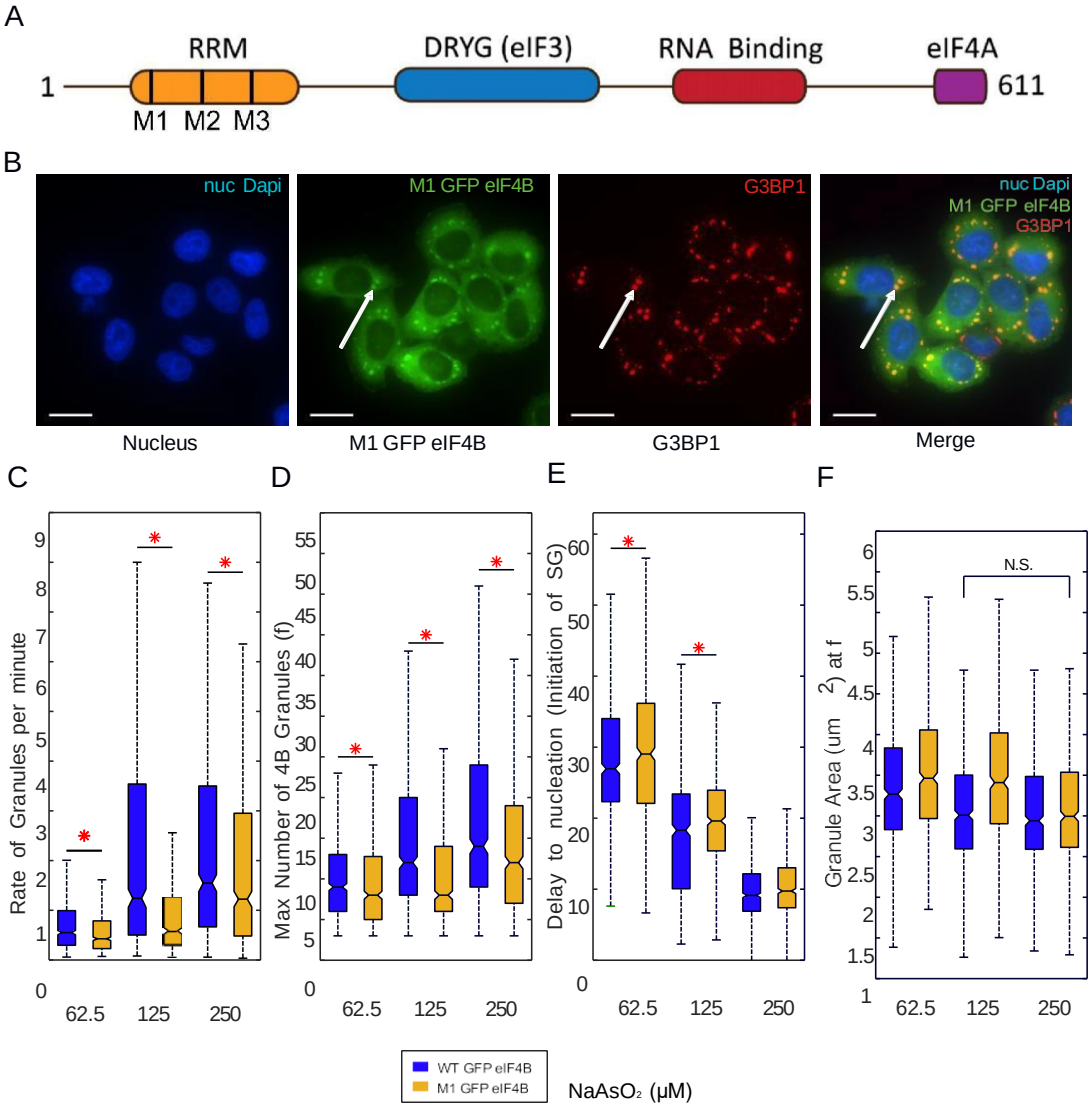

Figure 2. RNA Recognition Motif (RRM) mutants of eIF4B inhibit SG formation

(A) Domain map of the human eIF4B protein: The human eIF4B comprises an RRM spanning amino acids 96 to 173, followed by a region rich in DRYG domain repeats from amino acids 214 to 327. The C-terminus of the protein contains an arginine-rich motif (ARM) RNA binding domain spanning amino acids 367 to 423. Additionally, eIF4B contains a putative eIF4A binding region spanning from amino acids 423 to 611. Mutants were created in the RRM to disrupt the protein's ability to bind to RNA. Three different RRM mutants were generated: M1 (F139A), M2 (F99A/N102A/R135A), and M3 (R135A/K137A/F139A).

(B) Fixed cell images of HeLa cells expressing M1-GFP-eIF4B treated with 125 μM sodium arsenite for two hours. Images from left to right are stained with DAPI to identify the nucleus, GFP-eIF4B, the SG nucleator, G3BP1, and a merged image from all three images to verify GFP-eIF4B in SGs. Scale bars are 25 μm.

(C-F) Box and whisker plots showing single-cell WT-GFP-eIF4B and M1-GFP-eIF4B SG kinetics, including (C) of rate of formation, (D) max number of SGs, (E) initiation of SGs, and (F) SG area. The following treatment with 62.5 μM, 125 μM, or 250 μM sodium arsenite. Asterisk indicates $P<0.005$ between groups. Significance was determined via One-Way ANOVA comparison to compare the difference between each treatment group with a Dunnett multi-comparison protocol to account for false discovery rate. n =269 WT and n = 349 M1. Cells per condition pooled from 3 experimental replicates with at least 2 technical replicates in each experiment.

See also Figure S2.

Figure 3: Stress induced suppression of global translation is impaired by eIF4B RRM Mutant

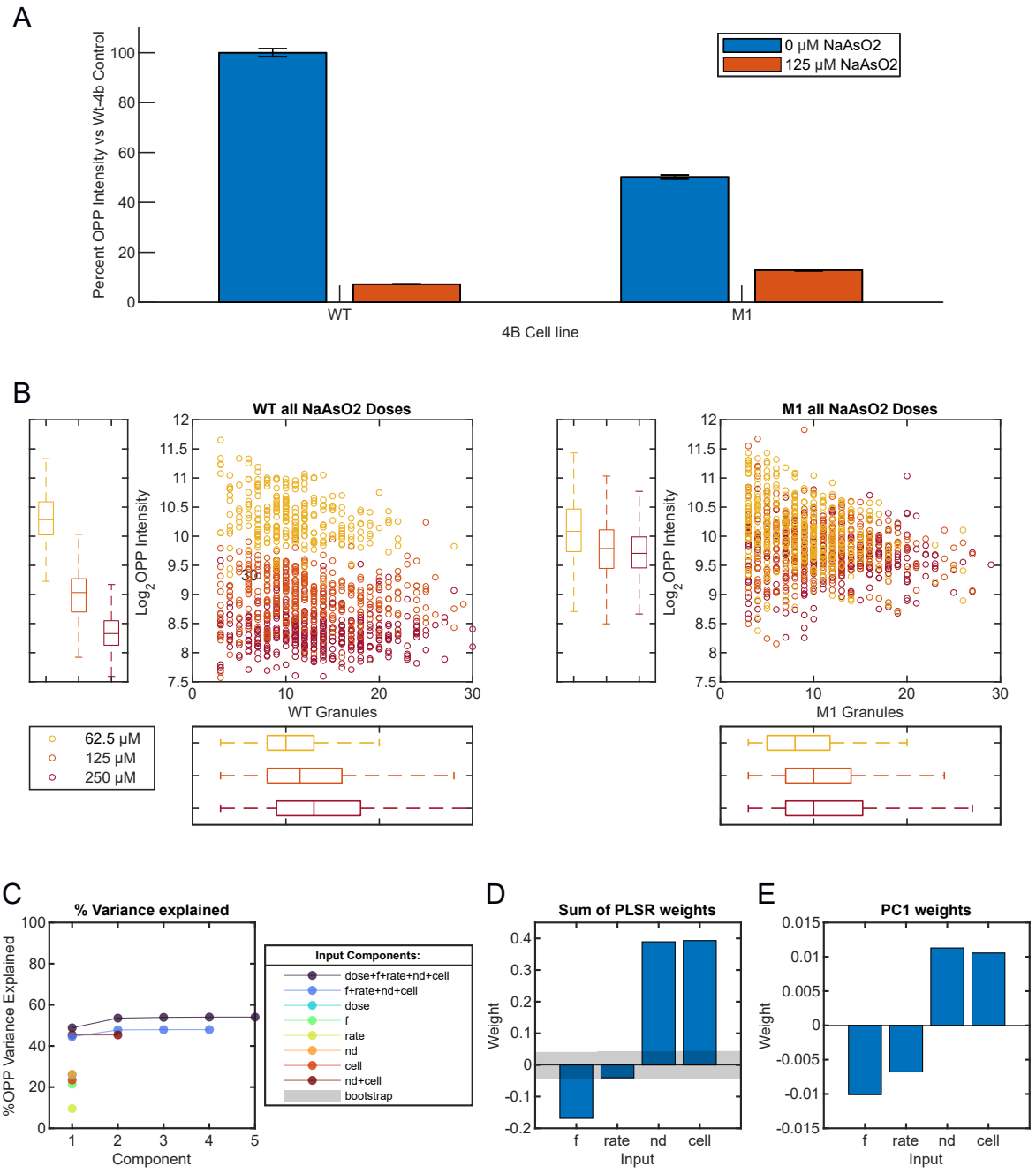

Figure 3. Stress induced suppression of global translation is impaired by eIF4B RRM Mutant

(A) Bar graph with standard error of the mean (SEM) showing the relative % O-propargyl-puromycin (OPP) signal intensity of WT-eIF4B and M1-eIF4B expressing cells treated with vehicle control (blue) or 125 μM Sodium Arsenite (orange) for 2 hours. The p value between the two treatment groups (orange) $P<0.005$.

(B) Box, whisker, and scatter plots showing single-cell Log_2 OPP intensity (y-axis) versus number of SGs (x-axis) at varying sodium arsenite concentrations. Colors used represent arsenite concentration: yellow (62.5 μM), orange (125 μM), and red (250 μM). *Left Half* is data from WT-GFP-eIF4B expressing HeLa cells, *Right half* is data from M1-GFP-eIF4B expressing HeLa cells. For all doses, in the WT cell line the OPP activity there is a lower trend on the Y-axis, on the X-axis, there is a higher amount of stress granules.

(C) Percent of Log_2 OPP variance explained, as determined by partial least squares regression (PLSR). Differently colored series represent models generated using different combinations of input parameters (indicated in legend to the right of C), including arsenite concentration (dose), max number of granules (f), rate of SG formation (rate), nucleation delay (nd) and cell line (cell). For models generated with multiple input variables, lines represent the cumulative variance explained as additional principal components (PCs) are added. Single-variable models have only one component (by definition) and are shown as points. The combined variables of the percent variance explained is 54% (purple). The combined variables (minus dose) of the

percent variance explained is 48% (blue). The nucleation delay and cell line percent variance is 45%.

(D) Comparison of input variable weights in predicting Log_2 OPP % variance. Bars indicate the sum of the weights for each input variable over four principal components for the (F+rate+nd+cell) mode (blue series in (C)). Bars outside of the gray shaded region indicate input components with significant predictive contribution to output (OPP) as determined by 5,000 iterations of bootstrapping with scrambled input values. Positive input component weights correspond to positive correlation with the output variable (OPP), and negative weights to negative correlations.

(E) Weights of input parameters in the first principal component (PC1) of the (f+rate+nd+cell) PLSR model.

See also Figure S3.

Figure 4: eIF4B binds directly to the SG nucleator protein G3BP1

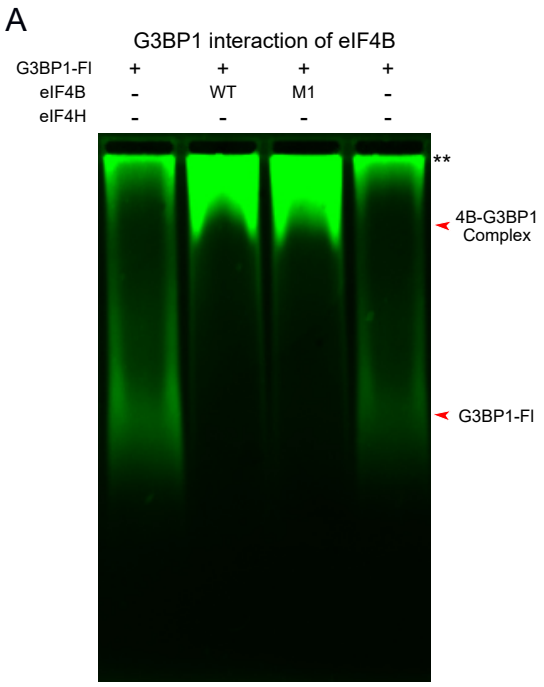

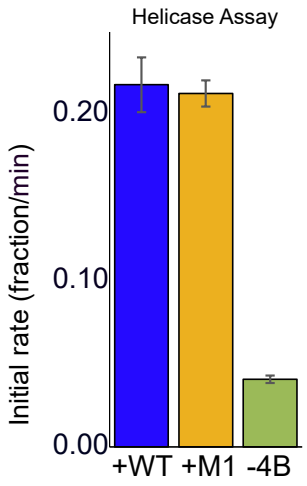

	Initial rate (frac./min)
+WT	0.22 ± 0.02
+M1	0.21 ± 0.01
-4B	0.04 ± 0.002

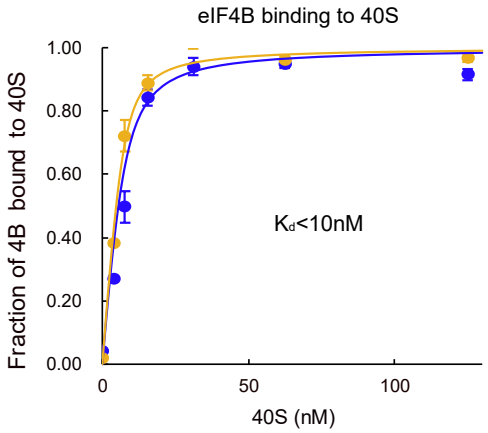

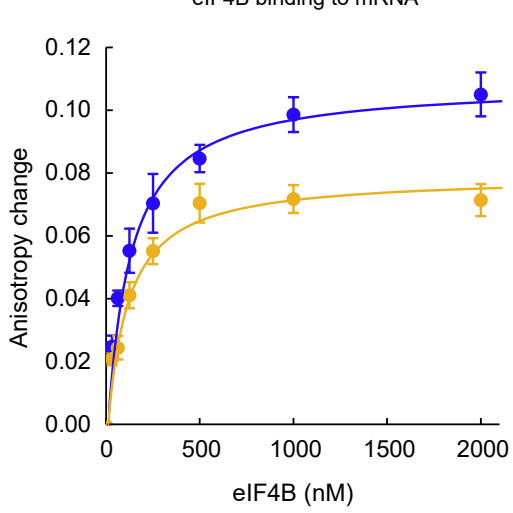

	Kd (nM)	Anisotropy Change
WT	118 ± 17	0.109 ± 0.005
M1	107 ± 19	0.079 ± 0.006

Figure 4. eIF4B binds directly to the SG nucleator protein G3BP1

(A) A native gel analysis of fluorescently labeled G3BP1 (G3BP1-Fl) in the absence or presence of 1 μM WT-eIF4B (WT), M1-eIF4B (M1), or eIF4H (4H) as indicated. WT and M1 cause an upward shift in G3BP1-Fl, which is otherwise diffusive as indicated in the figure. eIF4H does not cause any shift in G3BP1-Fl. ** Denotes aggregation in the well.

(B) Real-time fluorescent helicase assay where the ATP-dependent unwinding of a synthetic RNA duplex is monitored in the presence of purified eIF4A helicase, eIF4G, and eIF4B as indicated. The initial rates of unwinding are estimated by linear regression of the early part of the curves as described in the Materials and Methods.

(C) Equilibrium binding of fluorescently labeled WT (blue line) or M1 (orange line) eIF4B proteins to the 40S subunit, as measured by an anisotropy assay. The fraction of eIF4B bound at different concentrations of the 40S subunit is shown. The data are the average of at least three trials and error bars indicate the SEM. Equilibrium binding data were fit to determine the equilibrium dissociation constant (K_d) of eIF4B binding to the 40S subunit, as detailed in the Materials and Methods.

(D) Equilibrium binding of fluorescently labeled 42 nt RNA to WT (blue line) or M1 (orange line) eIF4B proteins, as measured by an anisotropy assay. The fraction of eIF4B bound at different concentrations of the 42 nt RNA is shown. The data are the average of at least three trials and error bars indicate the SEM. Equilibrium binding data were fit to determine the equilibrium dissociation constant (Kd) of eIF4B binding to the 42 nt RNA, as detailed in the Materials and Methods.See also Figure S4.

Funding and additional information—This work was supported by the NIH grant R35GM152137 to CSF, and R01HL151983 and R35GM139621 to JGA. NLD was supported by the UC Davis Lung Center T32 - NIH HL007013. The content is solely the responsibility of the authors and does not necessarily represent the official views of the National Institutes of Health.

STAR Methods

REAGENT or RESOURCE	SOURCE	IDENTIFIER
Chemicals, Peptides, and Recombinant Proteins		
FluoroBrite™ DMEM	Gibco	Cat# A1896701
Sodium (meta) Arsenite	Sigma Aldrich	Cat# 7784-46-5
Corning™Dulbecco's Modification of Eagle's Medium (DMEM)	Thermofisher Scientific	Cat# MT15017CV

Fetal Bovine Serum	Gibco	Cat# 16000069
Tetracycline	Sigma-Aldrich	Cat# T7660
X-tremeGENE™ 9 DNA Transfection Reagent	Sigma Aldrich	Cat# 06365779001
Opti-MEM™ I Reduced Serum Medium	Gibco	Cat# 31985062
Hoescht Stain	Invitrogen	Cat# 33342
Click-iT™ Plus OPP Alexa Fluor™ 647 Protein Synthesis Assay Kit	Invitrogen	Cat# C10458
Nterm-His-TEV-eIF4B-F139A,C457S and S183C	This report	NA

Nterm-His-TEV eIF4B-C457S and S183C	This report	NA
G3BP1	This report	NA
Odyssey Blocking Buffer	Li-Cor	Cat# 927-40000
Bacterial and virus strains		
E Coli DH5α competent cells	NA	NA
Antibodies		
eIF4B (D-4)	Santa Cruz Biotechnologies	sc-376062
GAPDH (V-18)	Santa Cruz Biotechnologies	sc-365062

G3BP	BD Biosciences	Cat#611126
Donkey anti-Goat IgG (H+L) Cross-Adsorbed Secondary Antibody, Alexa Fluor™ 647	Invitrogen	Cat# A21447
Goat Anti-Mouse IgG (H+L) Secondary Antibody, Dylight™ 680	Invitrogen	Cat# 35518
Experimental Models: Cell Lines		
eIF4B-GFP	This report	NA
eIF4B-F139A-GFP	This report	N/A
eIF4B-F99A/N102A/R135A-GFP	This report	N/A
eIF4B-R135A/K137A/F139A-GFP	This report	N/A

Recombinant DNA		
eIF4B-GFP	This report	N/A
eIF4B Mutants	This report	N/A
Software and Algorithms		
NIS-Elements AR ver. 4.20	Nikon	RRID: SCR_014329
MATLAB	Mathworks	RRID: SCR_001622
Bio-Formats	OME	RRID: SCR_000450
Cellprofiler	www.cellprofiler.org	RRID: SCR_007358

Cellpose	www.cellpose.org	RRID: SCR_021716
Other		
Glass bottom plates, #1.5H high performance cover glass	Cellvis	Cat# P96-1.5H-N, P06-1.5H-N

Resource availability / Lead contact

For further information and any requests for resources and regents, please contact Dr. Chris Fraser (csfraser@ucdavis.edu) or John Albeck (jgalbeck@ucdavis.edu).

Materials availability

Plasmids and cell lines generated in this study are available from lead contacts.

Data and Code availability

Raw NIS elements image data can be made available upon request, but were not uploaded to the submission portal due to their large size.

All code used to import cellprofiler data into Matlab, filter and process live-cell or IF

data, pool experimental replicates, align live-cell to IF data, fit data models, produce figures, and perform statistical analysis are available on github at: https://github.com/Albeck-Lab/SG_4B

Figures 1-3 have html output files which can be read on any device, showing all code used for each figure at: https://github.com/Albeck-Lab/SG_4B/tree/main/Paper_Figures/html

Plasmid Construction

To create stable inducible cell lines, wild-type human eIF4B with a N-terminal EGFP tag was subcloned into the pcDNA5/FRT/TO vector (Invitrogen) using BamHI and XhoI restriction sites. Point mutations in the eIF4B RRM were synthesized by Genscript and subcloned into the above plasmid using ClaI and BstBI restriction sites, as described in the following vectors: M1 (F139A), M2 (F99A, N102A, R135A), M3 (R135A, K137A, F139A). For *in vitro* experiments, eIF4B with an N terminal His-TEV tag was expressed from a derivative of the pET28c vector, as described previously.(Feoktistova et al., 2013) To fluorescently label eIF4B, the single native cysteine residue was mutated to serine (C457S) and a new cysteine was introduced (S183C) using site-directed mutagenesis with the following primers:

C457S F primer GAAGATTCCCACTCACCGACGTCGAAACCG

C457S R primer TGAGTGGGAATCTTCTTCTTTATTCAGGGT

S183C F primer ACGATCGTTGCTTTGGTCGCGATCGTAACCG

S183C R primer CAAAGCAACGATCGTCGCGGTCTTTATCTTGG

To test the M1 mutant in fluorescence assays this mutation was also added using site-directed mutagenesis with the following primers:

4B RRM F139A F primer TGAAAGGTGCAGGCTATGCAGAATTCGAAG

4B RRM F139A R primer AGCCTGCACCTTTCAGACGTTCCGGATTAG

All primers were purchased from Integrated DNA Technologies. All plasmid sequences were confirmed by Sanger sequencing (Azenta Life Sciences and Quintara Biosciences).

Cell Culture and Imaging Medium

The HeLa Flp-in TRex cell line was a generous gift from Drs. Elena Dobrikova and Matthias Gromeier (Duke University Medical Center). All HeLa cell lines were maintained in DMEM supplemented with 10% fetal bovine serum (FBS) and grown at 37°C in 5% CO_2. For all imaging experiments, media was replaced with Gibco FluoroBrite DMEM supplemented with 2% FBS for at least 1 hour prior to imaging (or first treatment) to minimize background fluorescence (referred to as ‘imaging medium’).

Creating stable cell lines

All transfections consisted of the gene of interest inserted into a pcDNA5/FRT/TO plasmid and the plasmid pOG44. All transfections are carried out in Opti-MEM Reduced Serum Media (Thermo Fisher) supplemented with 3% FBS according to manufacturer's guidelines with minor changes. For each transfection, 1.5–3.0 µg of pcDNA5/FRT/TO plasmid and 1 µg of POG44 is diluted into 100 µL of Opti-MEM media. For each transfection, 6 µL of X-tremeGENE9 DNA Transfection Reagent (Roche) was diluted in 100 µL of Opti-MEM media and incubated for 5 minutes at room temperature. The two incubations were then combined to create a DNA-lipid mixture that was incubated for 30 minutes at room temperature. The transfection was then added to the cell line and incubated for 5 hours. Stable cell lines were generated with Blasticidin Hygromycin selection using a 6- well plate according to manufacturer's guidelines.

Live-Cell imaging and Immunofluorescence Microscopy

For all live-cell, immunofluorescence, and OPP assays, GFP-eIF4B HeLa cells were seeded at 10,000 - 20,000 cells per well in a 96-well glass bottom imaging plate (CellVis - P96-1.5H-N) 48 hours prior to the experiment. Expression of GFP-eIF4B was induced by the addition of tetracycline at 0.1 µg/µL final concentration for 2–24 hours prior to the experiment start as indicated (24 hours induction for data in Figures 1-3, Sup Figure 1 A&B, Sup Figure 2 A&B; 0-24 hours of induction for data in Sup Figure 1C&D, Sup Figure 2C, and Sup Figure 3). Cells were washed once with 200 µL imaging medium per well, then incubated in 200 µL imaging media per well for 1 hour prior to the start of

experiments and maintained in this medium until the conclusion of the experiment. Sodium Arsenite was added to the cells via the addition of a 10 µL of a 21X stock (of the final concentration desired) solution in imaging medium.

Time-lapse wide-field microscopy was performed using a Nikon (Tokyo, Japan) 40X/0.95 NA Plan Apo objective on a Nikon Eclipse Ti-e or Ti2-e inverted microscope, equipped with a Lumencor SPECTRA X or SPECTRA iii light engine, and Andor Zyla 5.5 scMOS or Teledyne Photometrix Kinetix scMOS camera. Fluorescence filters used are: DAPI (Chroma filters: Excitation: ET395/25x, Mirror: T425lpxr Emission: ET460/50), GFP (49002, Chroma), Orange (Ex: ET546/22x, Mirror: T560lpxr, Em: ET572/23m), and Cy5 (49006, Chroma). Cells were imaged at 2–3 minute intervals with relative powers ranging from 5-35%, and exposure times ranging from 100–400 ms depending on expression and fluorescence. During Live-Cell experiments cells were imaged at 2-3 minute intervals and maintained at 37°C with 5% CO_2 on the microscope via OKO systems.

Immunofluorescence

After performing the SG assay, the cells were fixed and immunofluorescent staining was performed for G3BP1 via the following protocol. Cells were permeabilized and fixed by the addition of 16% PFA (for a final concentration of 2% PFA) directly to the media and incubated for 10 minutes at room temperature in a fume hood. The PFA/media solution was removed by pipetting, and cells were washed once with 150 µL of 1X PBS per well with gentle rocking for 10 minutes. The PBS was removed and 100 µL MeOH was

added per well and incubated for 10 minutes in the fume hood. MeOH was removed via pipetting and the cells were washed three more times by gentle rocking with 100 µL PBS per well for 5 minutes each wash. After the washes, the PBS was removed and 100 µL of Odyssey blocking buffer was added per well and incubated with gentle rocking at room temperature for 60 minutes. Then, the blocking buffer was removed and 100 µL of blocking buffer containing a 1:250 dilution of G3BP1 Primary Antibody was added to each well (G3BP1 Primary Antibody - BD Transduction mouse anti human G3BP1). The plate was wrapped in aluminum foil to reduce light exposure and incubated for 1 hour at room temperature on a rocking plate, then washed three times with 100 µL PBS-T (0.1% Tween-20 in PBS) for 5 minutes at room temperature. The PBS-T was removed via pipetting, then 100 µL of blocking buffer containing a 1:1000 dilution of Secondary Antibody and a 1:10000 dilution of Hoechst (for nuclear staining) was added to each well (Alexa Fluor 647). Still covered, the plate was incubated at room temperature for 1 hour on a rocking plate, then washed three times with 100 µL PBS-T (per well) for 5 minutes on a rocking plate. Finally, the PBS-T was aspirated and 200 µL PBS was added to each well and imaged as described above.

Single cell protein synthesis estimation by O-proparagly-puromycin (OPP)

To measure global protein synthesis, cells were labeled with the puromycin analog O-propargyl-puromycin (OPP) at 10 µM final concentration for 30 minutes before the end of live-cell imaging (1.5 hours after stress induction) experiments. Wells were fixed with 2% PFA solution, washed with PBS, methanol permeabilized, washed with PBS

twice (as described in detail above in live cell imaging section), then incubated with click chemistry reaction buffer (10 μM Azide dye, 4 mM CuSO4, 50 mM Ascorbic acid in 100 mM Tris Buffer pH 8.5 and Alexa 647 Azide dye) for 1 hour per the manufacturer's directions. Finally, cells were washed twice with PBS, then imaged.

Image Analysis, SG Modeling, and PLSR

To extract live-cell SG data, first the time lapse images are aligned over time using the NIS elements "align images" software package. This is done to eliminate any potential shifts in the image field that could be introduced during experimental treatment spikes which could cause breaks in cell/granule tracking in later processing steps. Once aligned, live-cell and IF data are fed into a custom cellprofiler 4 pipeline.(Stirling et al., 2021) This pipeline includes cell identification via the built-in cellpose model cyto2 and isolation of these identified cells. Stress granules were then identified in the cells using a custom cellpose model we trained to identify stress granules (called SGI_High_Contrast; available on our github.(Stringer et al., 2021; Stringer & Pachitariu, 2022) Where applicable (live-cell data), cells were tracked over time using the "follow neighbors'' track objects module, and verified proper cell and granule identification using the overlay outlines module. Cell and granule intensity, size, shape, location, and counts were exported to csv files placed into folders per image field (XY) for that experiment. For immunofluorescence (IF) images (i.e. G3BP1) a similar pipeline was used that did not track the objects over time.

Once the Cell Profiler pipeline extracted the SG data, the csv files were iteratively

opened in Matlab, where the metadata from that experiment (including which cell line and treatments were in each XY) are appended to the Live-Cell or IF data. Live-cell data was filtered to ensure quality by requiring a minimum amount of time the cells were tracked to be at least 1 hour. Where applicable, IF data was aligned to the Live-Cell data using the coordinates of the cells in the last frame of the movie and a KNN-search for cells within a given radius. This data was saved per experiment in a data object and performed via the function SG_Datahandler.

To extract SG kinetics from Live-Cell images, data was fed into a custom function called convertDatalocToModelFit. This function loops over the experimental datasets provided and for each cell uses nonlinear least squares to fit the following equation to the SG number of that cell using Matlab's built in 'fit' function. "f-f/(1+exp(((xdata-Td)/(Ts/4))))". Figures 1 and 2 used data aggregated from three experimental replicates that had at least two technical replicates each.

Because GFP-eIF4B granules first appear, reach a maximum number, then begin to aggregate over time, this can cause poor model fitting. To circumvent this, each cell's data was truncated to include the point of treatment until 1 time point (3 minutes) after reaching that cell's maximum SG count (f). To accomplish this a fixed f was fed into the model along with the SG count, and xdata is the timepoints (in minutes) of the data included. The fit function then used non-linear least squares regression to solve for Td (time from treatment to half max SGs) and Ts (time from first SG appearance to max SGs). Fit models with an R^2 of less than 0.8 were filtered out of the data.

Partial least squares regression (PLSR) was performed using previously published

methodology.(Gillies et al., 2017) Briefly, a PLSR model which could explain the variance in single-cell Log_2 OPP between cells expressing either WT- or M1-GFP-eIF4B was solved using the single-cell the metrics of SG kinetics (maximum number of SGs formed, rate of SG formation, SG nucleation delay), sodium arsenite concentration, and the type of GFP-eIF4B expressed. GFP-eIF4B expression was designated for PLSR input by assigning a 0 value to WT-GFP-eIF4B expressing cells and a 1 value to M1-eIF4B expressing cells. All inputs were z-score normalized within the parameter before being fed into the PLSR function. To validate that the PLSR model variance explained was significant, it was compared to a "scrambled" PLSR model. A scrambled PLSR model took the same data and randomly reassigned the cell's input data, then was solved. To ensure consistency, the scrambled PLSR model was performed 5,000 times. Due to the variability in relative intensity of OPP staining from run to run (e.g. OPP intensities for all cells are 20% higher in one experimental replicate compared to another), data in figure 3 is from one representative experiment (that was also used in figures 1 and 2), with the trends and significance indicated being found in replicate experiments as well. If experimental replicates are pooled by first z-score normalizing the Log_2 OPP intensities, the OPP data across experimental replicates follow similar trends and maintain statistical significance, suggesting reproducibility between experimental replicates.

Cell extracts and Western Blotting

Cells were seeded at $1.5x10^6$ in a 10cm dish. When cells reached 80% confluent, cells

were scraped and placed in a lysis buffer. Each cell pellet was lysed in 200 µL of lysis buffer containing 20 mM HEPES, pH 7.5, 10 mM KCl, 1 mM DTT, 1% NP40, 5 mM Mg Acetate and 7x protease inhibitor. Lysis was done using a vortex mixer, in which cells were vortexed for 30 seconds and rested on ice for 1 minute for a total of 10 times. SDS PAGE gels were transferred to Immobilon-FL polyvinylidene fluoride (PVDF) membrane. An overnight transfer was performed at 35V. PVDF membranes were incubated with primary antisera specific to eIF4B (Santa Cruz Biotechnology Lot #B2322) at 1:1000 in Tris-buffered saline with 0.1% Tween 20 (TBST) overnight at 4°C. PVDF was washed three times for 10 min in TBST, followed by 1 hour incubation at room temperature with goat anti-mouse secondary antibody DyLight 680 (Invitrogen/Thermo Fisher Scientific PI35518). Lastly, Western blots were scanned on an Azure Sapphire Biomolecular Imager (Azure Biosystems).

Mathematical Model for SG Kinetics

SG(t) = f - f1 + e(t-Td)(Ts/4)

The equation used to model the kinetics of granule formation was modified from the equation in Albeck *et. al.* which was used to describe the cleavage of caspase substrates in individual cells.(Albeck et al., 2008) Whereby, SG(*t*) is the number of stress granules at a given time (in minutes), *f* is the maximum number of granules formed in that cell, Ts is the time from first SG nucleation event to the time when the max number of granules formed (i.e. when the cell reaches it's *f*), and Td is the time from treatment (in our case, with sodium arsenite) to when the cell reaches half of the

max number of granules it will form (i.e. *f* / 2). From these parameters f/Ts which is the rate of granule nucleation (i.e. from first nucleation event until reaching the max number of granules), and Td-(Ts/2) which is the time from treatment to the first measured SG in the cell (also referred to as nucleation delay) was calculated.

Biochemical sample preparations

Human eIF4A1, eIF4G1 (residues 682-1599), and eIF4H isoform 2 were purified from overexpressing E. coli as described previously.(Feoktistova et al., 2013; Özeş et al., 2011) The 40S subunit was purified from HeLa cell extract as described previously.(Fraser et al., 2007) The 42-nt unstructured RNA with CAA repeat was transcribed and labeled with fluorescein at the 3'-end as described previously.(Sokabe & Fraser, 2017) N-terminal His_6-tagged WT- and M1-eIF4B were expressed in E. coli, with their sequence essentially identical to that previously expressed in insect cells(Özeş et al., 2011), but have C457S and S183C mutations for a labeling purpose in addition to F139A in M1-eIF4B. eIF4B was purified through Ni-NTA, Heparin, Mono S, and Superdex 200 prep grade columns, and labeled at C183 with fluorescein-5-maleimide as described previously.(Sokabe & Fraser, 2014) G3BP1 has a N-terminal His_6-MBP tag similar to eIF4A1, but also has a ybbR-tag after TEV cleavage site. G3BP1 is expressed in E.coli, and captured with Ni-NTA. After TEV protease cleavage, it was further purified through heparin and Mono S columns. The resulting ybbR-G3BP1 was labeled with fluorescein modified coenzyme A using SFP phosphopantetheinyl transferase as essentially described previously.(Yin et al., 2006)

Briefly, 10 μM ybbR-G3BP1 is incubated with 10 μM CoA-fluorescein and 4 μM SFP enzyme at 4°C overnight in buffer containing 50 mM Hepes-K pH 7.5, 100 mM KCl, 10 mM $MgCl_2$, and 1mM DTT. The labeled protein was purified through SP sepharose, yielding 60-70% labeling efficiency. Qualities of purified eIF4Bs and G3BP1, and their labeled forms were analyzed in SDS gels (Fig. S5A).

Helicase Assay

The helicase assay was done as essentially described previously.(Feoktistova et al., 2013) The reaction contained 50 nM RNA duplex substrate, 0.5 μM eIF4A1 and eIF4G1 (residues 682-1599), either with or without 0.5 μM WT-eIF4B, M1-eIF4B, or eIF4H, in buffer containing 20 mM tris-acetate pH 7.5, 100 mM potassium acetate, 2 mM Mg acetate, 10% glycerol, 2 mM ATP-Mg^{2+}, and 1 mM DTT. The results shown are averages of three independent experiments with SEM.

Fluorescence Anisotropy Assay

The anisotropy binding assay was done as essentially described previously.(Sokabe & Fraser, 2014) The reaction contained 10 nM labeled WT- or M1-eIF4B with 0-125 nM 40S subunit, or 20 nM labeled RNA with 0-2000 nM WT- or M1-eIF4B, in buffer containing 20 mM tris-acetate pH 7.5, 70 mM KCl, 2 mM $MgCl_2$, 0.1 mM spermidine, 0.1 mg/ml BSA, 10% glycerol, and 1 mM DTT. Fitting with a quadratic equation suggests a tight dissociation constant below the lower limit (< 10 nM) for both eIF4Bs. The results

shown are averages of three independent experiments with SEM

Gel Shift Assay

A 10 µl reaction containing 50 nM labeled G3BP1, and 1 µM WT-eIF4B, M1-eIF4B, or eIF4H in the same buffer used for the anisotropy assay was incubated at 37°C for 10 min, and placed on ice for ~ 5 min before loading to a gel. Samples were then analyzed in 1% agarose gel in buffer containing 34 mM Tris Base, 57 mM Hepes, 0.1 mM EDTA, 2 mM $MgCl_2$ run at 100V for ~90 min at 4°C, and imaged with Azure Sapphire Biomolecular Imager (Azure Biosystems).

Supplementary Figure 1: Characterizing eIF4B overexpression cell line

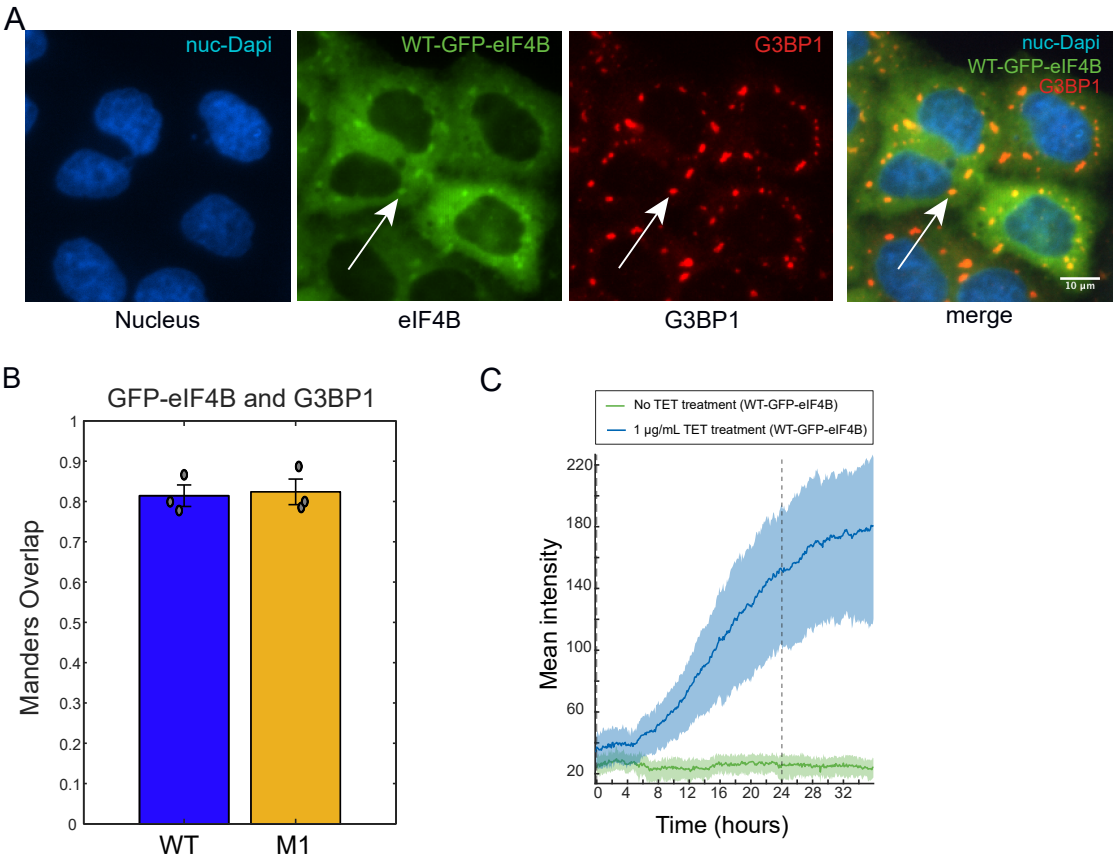

Supplementary Figure 1. Characterizing eIF4B overexpression cell line

(A) WT-GFP-eIF4B cells were subjected to immunofluorescence (IF) to visualize the stress granule nucleator G3BP1 using an anti-G3BP1 antibody, in order to verify GFP-eIF4B localization in stress granules. The images, from left to right, are as follows: DAPI (nucleus), WT-GFP-eIF4B, G3BP1 (SG marker), and the merged image (both eIF4B and G3BP1).

(B) Immunofluorescence data were analyzed using Mander's overlap of WT-GFP-eIF4B (blue) and M1-GFP-eIF4B (orange) granule signals with G3BP1 (SG marker) after cells were treated with 125 μM arsenite for 2 hours. There is no significant difference between the WT and M1. The mean and SEM of 3 replicates are shown; gray dots represent each replicate.

(C) Measuring mean intensity of WT-GFP-eIF4B TReX Flip-In tetracycline inducible cells over a 36 hour time frame. Dark lines represent the mean and the shaded regions are 25th/75th quartiles of data for cells in the respective condition. All experiments moving forward used a 24-hour induction time to express GFP-eIF4B which is indicated at the dotted line.

(D) Western blot was performed at different induction times to measure the difference between endogenous eIF4B and overexpressed WT-GFP-eIF4B. GAPDH is used as a loading control. The gel was cut in two because the primaries were in two different hosts eIF4B (mouse) and GAPDH (goat). From left to right is the time of induction 0-24 hours. In total, 30 ug of protein was loaded that was extracted from cells on a 8% SDS page gel.

Supplementary Figure 2: Characterizing RRM of eIF4B overexpression cell line

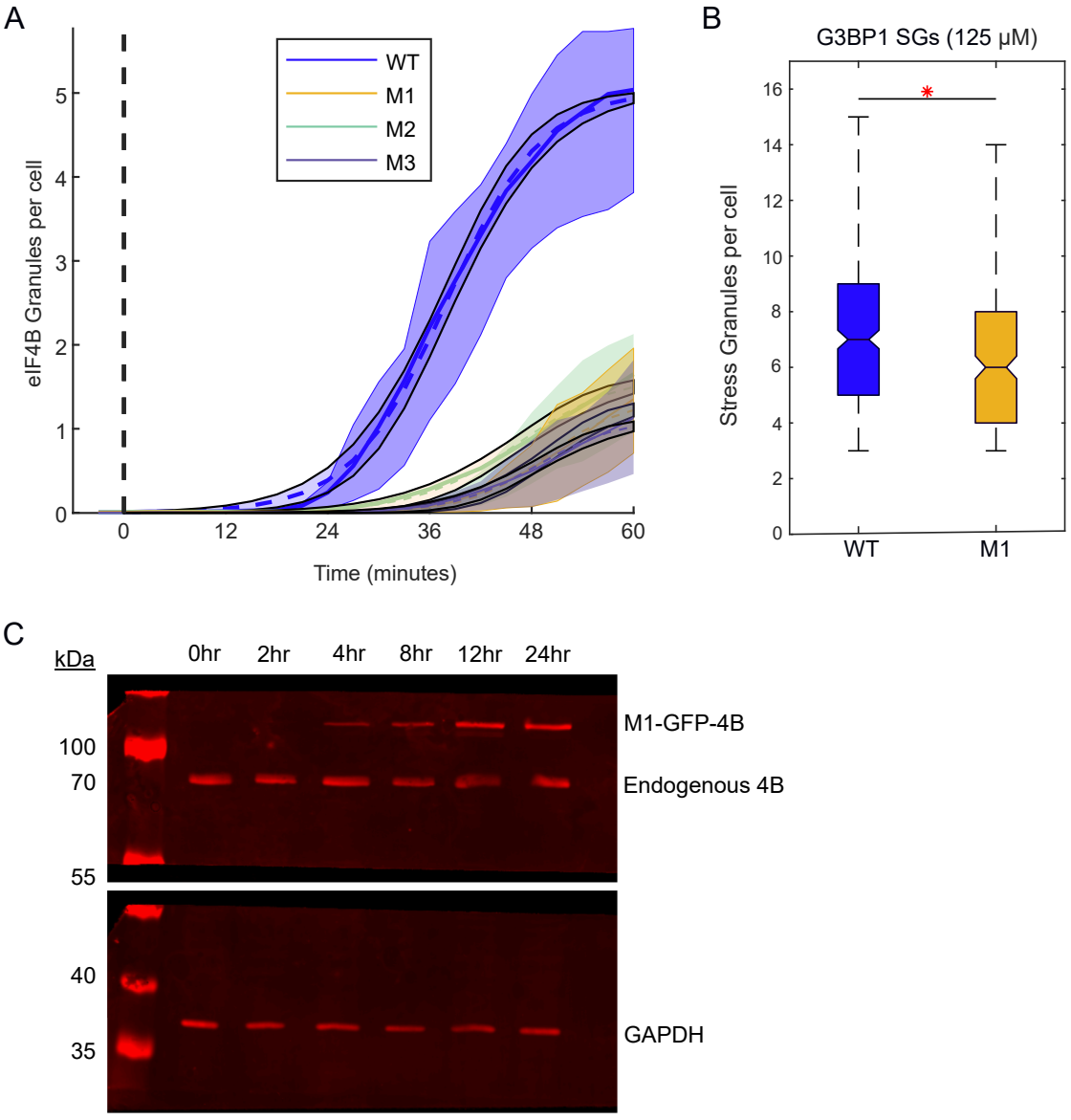

Supplementary Figure 2. Characterizing RRM of eIF4B

(A) Granule formation equations were fit to measure the f max as each cell line approaches 1 hour. Mean (dark line) and 25th/75th quartiles (shaded regions) of granules formed per cell line over time following treatment with 125 μM arsenite. WT-GFP-eIF4B in red, M1-GFP-eIF4B (F139A) in green, M2-GFP-eIF4B (F99A/N102A/R135A) in yellow, and M3-GFP-eIF4B (R135A/K137A/F139A) in blue. Arsenite treatment occurs at dashed line (hour 0). The number of SGs per cell for each cell line WT=5.04, M1 =1.35, M2 =1.65, and M3 =1.13.

(B) Box and whiskers plot showing G3BP1 granules in the WT and M1 cell lines following 2 hours of treatment with 125 μM arsenite. Black line with the red asterisk indicates a significant difference between the groups (P = 0.0016). Significance was determined via One-Way ANOVA comparison.

(C) Western blot was performed at different induction times to measure the difference between endogenous M1 and overexpressed M1-GFP-eIF4B. GAPDH is used as a loading control. The gel was cut in two because the primaries were in two different hosts eIF4B (mouse) and GAPDH (goat). From left to right is the time of induction 0-24 hours. In total, 30 ug of protein was loaded that was extracted from cells on a 8% SDS page gel.

Sup Figure 3. Measuring translation activity levels overtime in WT and M1

A

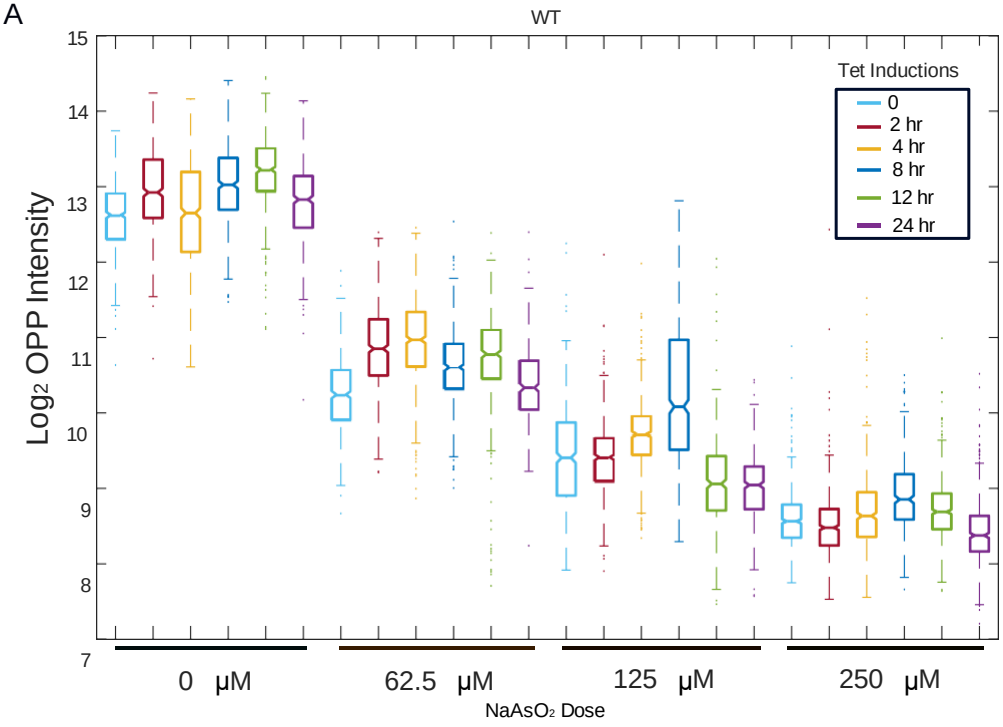

B

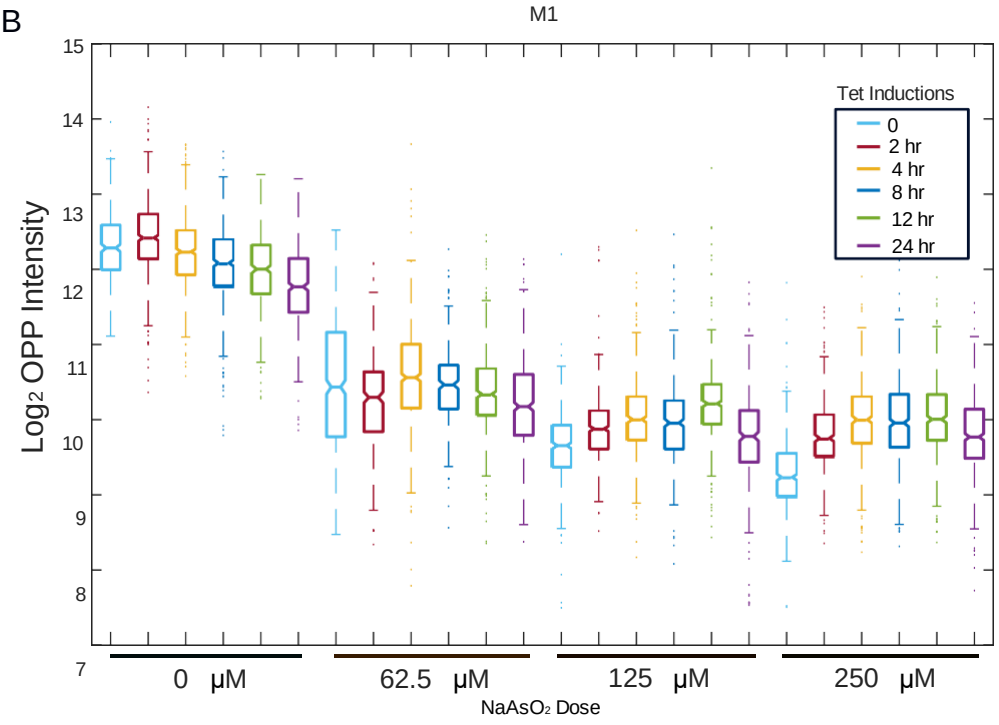

Sup Figure 3. Measuring translation activity levels overtime in WT and M1

(A) Box and Whisker plot of single-cell Log_2 O-propargyl-puromycin (OPP) signal intensity of WT-GFP-eIF4B (WT) HeLa cells at varying TET inductions (In colors from Blue to purple) and arsenite doses (grouped left to right). Colors indicate hours of TET induction with 0 hours being light blue, 2 hours being red, 4 hours blue, 12 hours green, and 24 hours purple. Plots are grouped by arsenite concentration as indicated on the x-axis and range from 62.5-250 μM. Measurements were made after one hour and 30 mins of sodium arsenite treatment and 30 minutes of OPP exposure.

(B) Box and Whisker plot of single-cell Log_2 O-propargyl-puromycin (OPP) signal intensity of M1-GFP-eIF4B (M1) HeLa cells at varying TET inductions (In colors from Blue to purple) and arsenite doses (grouped left to right). Colors indicate hours of TET induction with 0 hours being light blue, 2 hours being red, 4 hours blue, 12 hours green, and 24 hours purple. Plots are grouped by arsenite concentration as indicated on the x-axis and range from 62.5-250 μM. Measurements were made after one hour and 30 mins of sodium arsenite treatment and 30 minutes of OPP exposure.

Supplementary Figure 4: Protein purification and labeling

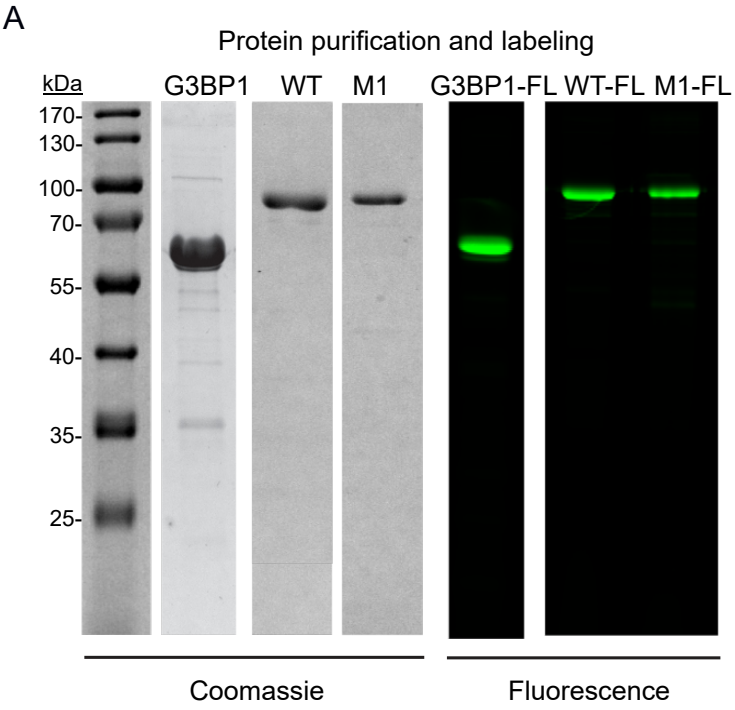

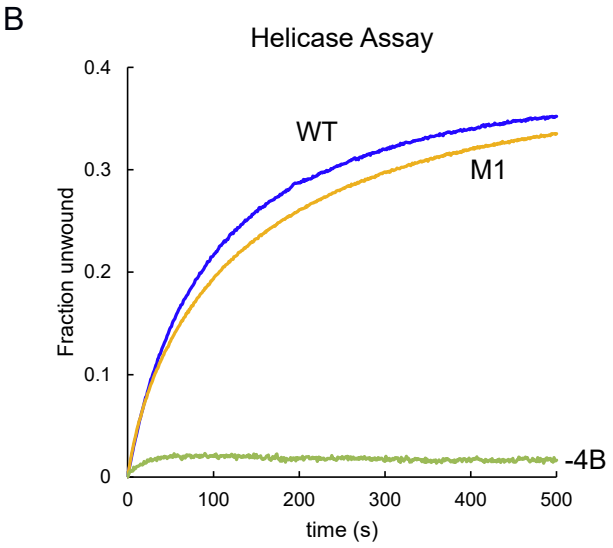

Supplementary Figure 4. Protein purification and Labeling

(A) Coomassie stained SDS gels of purified G3BP1, WT, and M1, and fluorescence gel images of labeled G3BP1, WT, and M1 used in Fig. 4.

(B) Real-time fluorescent helicase assay where the ATP-dependent unwinding of a synthetic RNA duplex is monitored in the presence of purified eIF4A helicase, eIF4G, and eIF4B as indicated.The initial rates are estimated by linear regression of the early part of the curves. See Fig. 4B for the plots.

References

Albeck, John G., John M. Burke, Sabrina L. Spencer, Douglas A. Lauffenburger, and Peter K. Sorger. 2008. “Modeling a Snap-Action, Variable-Delay Switch Controlling Extrinsic Cell Death.” *PLoS Biology* 6 (12): 2831–52.

Anderson, Paul, and Nancy Kedersha. 2002. “Stressful Initiations.” *Journal of Cell Science* 115 (Pt 16): 3227–34.

Andreou, Alexandra Zoi, Ulf Harms, and Dagmar Klostermeier. 2017. “eIF4B Stimulates eIF4A ATPase and Unwinding Activities by Direct Interaction through Its 7-Repeats Region.” *RNA Biology* 14 (1): 113–23.

Asadi, Mohammad Reza, Dara Rahmanpour, Marziyeh Sadat Moslehian, Hani Sabaie, Mehdi Hassani, Soudeh Ghafouri-Fard, Mohammad Taheri, and Maryam Rezazadeh. 2021. “Stress Granules Involved in Formation, Progression and Metastasis of Cancer: A Scoping Review.” *Frontiers in Cell and Developmental Biology* 9 (September): 745394.

Buchan, J. Ross, and Roy Parker. 2009. “Eukaryotic Stress Granules: The Ins and Outs of Translation.” *Molecular Cell* 36 (6): 932–41.

Campos-Melo, Danae, Zachary C. E. Hawley, Cristian A. Droppelmann, and Michael J. Strong. 2021. “The Integral Role of RNA in Stress Granule Formation and Function.” *Frontiers in Cell and Developmental Biology* 9 (May): 621779.

Eliseev, Boris, Lahari Yeramala, Alexander Leitner, Manikandan Karuppasamy, Etienne Raimondeau, Karine Huard, Elena Alkalaeva, Ruedi Aebersold, and Christiane Schaffitzel. 2018. “Structure of a Human Cap-Dependent 48S Translation Pre-Initiation Complex.” *Nucleic Acids Research* 46 (5): 2678–89.

Feoktistova, Kateryna, Enkhee Tuvshintogs, Angelie Do, and Christopher S. Fraser. 2013. “Human eIF4E Promotes mRNA Restructuring by Stimulating eIF4A Helicase Activity.” *Proceedings of the National Academy of Sciences of the United States of America* 110 (33): 13339–44.

Fraser, Christopher S., Katherine E. Berry, John W. B. Hershey, and Jennifer A. Doudna. 2007. “eIF3j Is Located in the Decoding Center of the Human 40S Ribosomal Subunit.” *Molecular Cell* 26 (6): 811–19.

Gao, Xiaomeng, Li Jiang, Yanling Gong, Xiaobing Chen, Meidan Ying, Hong Zhu, Qiaojun He, Bo Yang, and Ji Cao. 2019. “Stress Granule: A Promising Target for Cancer Treatment.” *British Journal of Pharmacology* 176 (23): 4421–33.

García-García, Cuauhtémoc, Kirsten L. Frieda, Kateryna Feoktistova, Christopher S. Fraser, and Steven M. Block. 2015. “RNA BIOCHEMISTRY. Factor-Dependent Processivity in Human eIF4A DEAD-Box Helicase.” *Science* 348 (6242): 1486–88.

Gilks, Natalie, Nancy Kedersha, Maranatha Ayodele, Lily Shen, Georg Stoecklin, Laura M. Dember, and Paul Anderson. 2004. “Stress Granule Assembly Is Mediated by Prion-like Aggregation of TIA-1.” *Molecular Biology of the Cell* 15 (12): 5383–98.

Gillies, Taryn E., Michael Pargett, Marta Minguet, Alex E. Davies, and John G. Albeck. 2017. “Linear Integration of ERK Activity Predominates over Persistence Detection in Fra-1 Regulation.” *Cell Systems* 5 (6): 549–63.e5.

Holz, Marina K., Bryan A. Ballif, Steven P. Gygi, and John Blenis. 2005. “mTOR and S6K1 Mediate Assembly of the Translation Preinitiation Complex through Dynamic Protein Interchange and Ordered Phosphorylation Events.” *Cell* 123 (4): 569–80.

Hu, Taobo, Wei Hou, Enhua Xiao, and Mengping Long. 2022. “Mechanism and Effect of Stress Granule Formation in Cancer and Its Potential Roles in Breast Cancer Therapy.” *Genes & Diseases* 9 (3): 659–67.

Ivanov, Pavel, Nancy Kedersha, and Paul Anderson. 2019. “Stress Granules and Processing Bodies in Translational Control.” *Cold Spring Harbor Perspectives in Biology* 11 (5). https://doi.org/10.1101/cshperspect.a032813.

Izidoro, Mario Servulo, Masaaki Sokabe, Nancy Villa, William C. Merrick, and Christopher S. Fraser. 2022. “Human Eukaryotic Initiation Factor 4E (eIF4E) and the Nucleotide-Bound State of eIF4A Regulate eIF4F Binding to RNA.” *The Journal of Biological Chemistry* 298 (10): 102368.

Jain, Saumya, Joshua R. Wheeler, Robert W. Walters, Anurag Agrawal, Anthony Barsic, and Roy Parker. 2016. “ATPase-Modulated Stress Granules Contain a Diverse Proteome and Substructure.” *Cell* 164 (3): 487–98.

Kedersha, Nancy, Samantha Chen, Natalie Gilks, Wei Li, Ira J. Miller, Joachim Stahl, and Paul Anderson. 2002. “Evidence That Ternary Complex (eIF2-GTP-tRNA(i)(Met))-Deficient Preinitiation Complexes Are Core Constituents of Mammalian Stress Granules.” *Molecular Biology of the Cell* 13 (1): 195–210.

Kedersha, N., M. R. Cho, W. Li, P. W. Yacono, S. Chen, N. Gilks, D. E. Golan, and P. Anderson. 2000. “Dynamic Shuttling of TIA-1 Accompanies the Recruitment of mRNA to Mammalian Stress Granules.” *The Journal of Cell Biology* 151 (6): 1257–68.

Kedersha, N. L., M. Gupta, W. Li, I. Miller, and P. Anderson. 1999. “RNA-Binding Proteins TIA-1 and TIAR Link the Phosphorylation of eIF-2 Alpha to the Assembly of Mammalian Stress Granules.” *The Journal of Cell Biology* 147 (7): 1431–42.

Marcelo, Adriana, Rebekah Koppenol, Luís Pereira de Almeida, Carlos A. Matos, and Clévio Nóbrega. 2021. “Stress Granules, RNA-Binding Proteins and Polyglutamine Diseases: Too Much Aggregation?” *Cell Death & Disease* 12 (6): 592.

Matsuki, Hideaki, Masahiko Takahashi, Masaya Higuchi, Grace N. Makokha, Masayasu Oie, and Masahiro Fujii. 2013. “Both G3BP1 and G3BP2 Contribute to Stress Granule Formation.” *Genes to Cells: Devoted to Molecular & Cellular Mechanisms* 18 (2): 135–46.

Méthot, N., A. Pause, J. W. Hershey, and N. Sonenberg. 1994. “The Translation Initiation Factor eIF-4B Contains an RNA-Binding Region That Is Distinct and Independent from Its Ribonucleoprotein Consensus Sequence.” *Molecular and Cellular Biology* 14 (4): 2307–16.

Milburn, S. C., J. W. Hershey, M. V. Davies, K. Kelleher, and R. J. Kaufman. 1990. “Cloning and Expression of Eukaryotic Initiation Factor 4B cDNA: Sequence Determination Identifies a Common RNA Recognition Motif.” *The EMBO Journal* 9 (9): 2783–90.

Mokas, Sophie, John R. Mills, Cristina Garreau, Marie-Josée Fournier, Francis Robert, Prabhat Arya, Randal J. Kaufman, Jerry Pelletier, and Rachid Mazroui. 2009. “Uncoupling Stress Granule Assembly and Translation Initiation Inhibition.” *Molecular Biology of the Cell* 20 (11): 2673–83.

Özeş, Ali R., Kateryna Feoktistova, Brian C. Avanzino, Enoch P. Baldwin, and Christopher S. Fraser. 2014. “Real-Time Fluorescence Assays to Monitor Duplex Unwinding and ATPase Activities of Helicases.” *Nature Protocols* 9 (7): 1645–61.

Özeş, Ali R., Kateryna Feoktistova, Brian C. Avanzino, and Christopher S. Fraser. 2011.

"Duplex Unwinding and ATPase Activities of the DEAD-Box Helicase eIF4A Are Coupled by eIF4G and eIF4B." *Journal of Molecular Biology* 412 (4): 674–87.
Parsyan, Armen, Yuri Svitkin, David Shahbazian, Christos Gkogkas, Paul Lasko, William C. Merrick, and Nahum Sonenberg. 2011. "mRNA Helicases: The Tacticians of Translational Control." *Nature Reviews. Molecular Cell Biology* 12 (4): 235–45.
Rogers, G. W., Jr, N. J. Richter, W. F. Lima, and W. C. Merrick. 2001. "Modulation of the Helicase Activity of eIF4A by eIF4B, eIF4H, and eIF4F." *The Journal of Biological Chemistry* 276 (33): 30914–22.
Rogers, G. W., Jr, N. J. Richter, and W. C. Merrick. 1999. "Biochemical and Kinetic Characterization of the RNA Helicase Activity of Eukaryotic Initiation Factor 4A." *The Journal of Biological Chemistry* 274 (18): 12236–44.
Rozen, F., I. Edery, K. Meerovitch, T. E. Dever, W. C. Merrick, and N. Sonenberg. 1990. "Bidirectional RNA Helicase Activity of Eucaryotic Translation Initiation Factors 4A and 4F." *Molecular and Cellular Biology* 10 (3): 1134–44.
Shahbazian, David, Armen Parsyan, Emmanuel Petroulakis, Ivan Topisirovic, Yvan Martineau, Bernard F. Gibbs, Yuri Svitkin, and Nahum Sonenberg. 2010. "Control of Cell Survival and Proliferation by Mammalian Eukaryotic Initiation Factor 4B." *Molecular and Cellular Biology* 30 (6): 1478–85.
Sokabe, Masaaki, and Christopher S. Fraser. 2014. "Human Eukaryotic Initiation Factor 2 (eIF2)-GTP-Met-tRNAi Ternary Complex and eIF3 Stabilize the 43 S Preinitiation Complex." *The Journal of Biological Chemistry* 289 (46): 31827–36.
———. 2017. "A Helicase-Independent Activity of eIF4A in Promoting mRNA Recruitment to the Human Ribosome." *Proceedings of the National Academy of Sciences of the United States of America* 114 (24): 6304–9.
Stirling, David R., Madison J. Swain-Bowden, Alice M. Lucas, Anne E. Carpenter, Beth A. Cimini, and Allen Goodman. 2021. "CellProfiler 4: Improvements in Speed, Utility and Usability." *BMC Bioinformatics* 22 (1): 433.
Stringer, Carsen, and Marius Pachitariu. 2022. "Cellpose 2.0: How to Train Your Own Model." *bioRxiv*. https://doi.org/10.1101/2022.04.01.486764.
Stringer, Carsen, Tim Wang, Michalis Michaelos, and Marius Pachitariu. 2021. "Cellpose: A Generalist Algorithm for Cellular Segmentation." *Nature Methods* 18 (1): 100–106.
Swain, Bikash Chandra, Pascale Sarkis, Vanessa Ung, Sabrina Rousseau, Laurent Fernandez, Ani Meltonyan, V. Esperance Aho, Davide Mercadante, Cameron D. Mackereth, and Mikayel Aznauryan. 2024. "Disordered Regions of Human eIF4B Orchestrate a Dynamic Self-Association Landscape." *bioRxiv*. https://doi.org/10.1101/2024.06.21.600094.
Tauber, Devin, Gabriel Tauber, Anthony Khong, Briana Van Treeck, Jerry Pelletier, and Roy Parker. 2020. "Modulation of RNA Condensation by the DEAD-Box Protein eIF4A." *Cell* 180 (3): 411–26.e16.
Tourrière, H., I. E. Gallouzi, K. Chebli, J. P. Capony, J. Mouaikel, P. van der Geer, and J. Tazi. 2001. "RasGAP-Associated Endoribonuclease G3Bp: Selective RNA Degradation and Phosphorylation-Dependent Localization." *Molecular and Cellular Biology* 21 (22): 7747–60.
Yang, Peiguo, Cécile Mathieu, Regina-Maria Kolaitis, Peipei Zhang, James Messing, Ugur Yurtsever, Zemin Yang, et al. 2020. "G3BP1 Is a Tunable Switch That Triggers

Phase Separation to Assemble Stress Granules." *Cell* 181 (2): 325–45.e28.
Yang, Xiaodan, Zhulong Hu, Qiang Zhang, Shanshan Fan, Yi Zhong, Dong Guo, Yali Qin, and Mingzhou Chen. 2019. "SG Formation Relies on eIF4GI-G3BP Interaction Which Is Targeted by Picornavirus Stress Antagonists." *Cell Discovery* 5 (January): 1.
Yin, Jun, Alison J. Lin, David E. Golan, and Christopher T. Walsh. 2006. "Site-Specific Protein Labeling by Sfp Phosphopantetheinyl Transferase." *Nature Protocols* 1 (1): 280–85.
Zhou, Huan, Jing Luo, Kelin Mou, Lin Peng, Xiaoyue Li, Yulin Lei, Jianmei Wang, Sheng Lin, Yuhao Luo, and Li Xiang. 2023. "Stress Granules: Functions and Mechanisms in Cancer." *Cell & Bioscience* 13 (1): 86.

Chapter Four

Characterizing eIF4B stress granule disassembly and adaptation

This chapter is unpublished and was written by me and edited by Dr. Christopher Fraser.

The equation and fitting was done by Nick DeCuzzi.

ABSTRACT

The mechanisms of SG disassembly and adaptation to stress are poorly understood. Studies have linked neurodegenerative disorders to SGs since the inability to disassemble these granules leaves cells in a constant state of stress. Here, I have developed a method to accurately measure the rate of SG disassembly. My analysis has revealed that focal drift, the gradual loss of focus in time-lapse imaging, significantly disrupts the accuracy of fluorescence measurements, posing a challenge that will need to be overcome. In future directions, I believe the problem of focal drift can be overcome by using a microfluidics device or microscope within an environmental chamber.

INTRODUCTION

There have been limited studies to investigate the process of SG disassembly. The proposed mechanism of SG disassembly includes a stepwise process in which the mature SG will remove its outer shell to release translating mRNPs, followed by SG core clearance by autophagy, which removes many different RNA binding proteins (Wheeler et al., 2016). The dysregulation of SG disassembly can contribute to neurodegenerative diseases such as Amyotrophic Lateral Sclerosis (ALS) where it was found that the SG nucleator, TDP-43, was present in these aggregates that was specific to ALS (Jo et al., 2020).

A current gap in knowledge in the field is how SG disassembly affects the restoration of mRNA translation and to what extent the translation machinery plays a role in the process. Translation elongation inhibitors like cycloheximide, which stabilize polysomes, can prompt the disassembly of stress granules (SGs) by preventing restructuring of these dynamic complexes (Hofmann et al. 2021). Additionally, ATPase chaperones such as eIF4A are known for their remodeling capabilities and can enhance the process of SG disassembly. (Baymiller & Moon, 2023; Jain et al., 2016; N. Kedersha et al., 2000,Tauber et al., 2020). To study these phenomena, I wanted to develop a system to follow SGs disassembly over time. Human eIF4B has been well established to promote the helicase activity of eIF4A, so I reasoned that it might have a role in SG disassembly. To this end, I tested point mutants in the RNA recognition motif of eIF4B, and discovered a difference in SG disassembly rates between mutant and wild-type eIF4B. In addition to SG disassembly, I have looked into a process of oxidative stress adaptation or hormesis. Hormesis is a process in which low doses of an oxidative

stressor can induce an effect whereas high doses of the stressor can prevent that effect of stress. There have not been extensive studies on SGs and cell adaptation; however, a few cancer studies have shown that the dose of oxidative stress can affect whether SGs either persist, dissolve, or change in composition (Redding and Grabocka 2023) To test the rate of hormesis, I left the stress on for a few hours to monitor the rate and number of SGs overtime.

RESULTS

Disassembly of SGs over time

To determine the rate of SG disassembly, cells were treated with 125 μM sodium arsenite for 2 hours, then washed twice with a media change and imaged as discussed in Chapter 2 for SG disassembly protocol. Once the images were processed and curve-fitted to determine the rate of stress granule disassembly, a pronounced dip (loss of signal) was evident after the cells were washed **(Figure 1)**. The curve fitting used is the following equation below:

$$SG(t) = f/(1 + e(t-Td)/(Ts/4))$$

The equation assumes a sigmoid shape where the f_{max} will decrease in SG number over time (SG(*t*)). We iteratively fit this equation to each cell's observed SG number over time, as described in detail in the Materials and Methods in Chapter 3. The resulting parameter values fitted for each cell describe the maximum number of granules formed (f), the time from first SG nucleation to max number of granules formed

(Ts), and time from treatment to half max number of granules (Td). Since we had a loss of fluorescence in the data, it was very difficult to fit the data. The curve fit measured the mean displacement between the dip and the f max (which is the maximum fluorescence and maximum number of SGs formed).

Troubleshooting the loss of fluorescence after wash off

I wanted to try and understand why there is a dramatic loss of fluorescence after the wash-off (the apparent dip from ~2-2.5 hours). To this end, I plated the HeLa GFP-eIF4B-WT cell line with the following conditions on a 24-well plate: 125 μM sodium arsenite followed by two brief media washes **(Figure 2, top)** and another experiment where 125 μM sodium arsenite was left on to see if the loss of fluorescence still occurred **(Figure 2, bottom)**. To wash the cells, I opened the chamber and left the plate on the microscope. Comparing Figure 1 and Figure 3, it is evident that the loss of fluorescence, or dip, only occurs after the cells were washed. For example, for Figure 1, the dip occurs after 2 hours (when I washed the cells) and Figure 3, the dip occurs after 1 hour. I initially believed that the dip occurred after one hour of stress. However, Figure 1 and Figure 3 clearly indicate that the rapid loss of fluorescence only occurred after the wash-off step while the chamber was open, which regulates the O_2 and Co_2, in the experiment. This observation is consistent with work by scientists at Nikon Instruments, who showed how the process of opening the chamber for more than one minute could result in an axial displacement of 3.4 micrometers (*Correcting Focus Drift in Live-Cell Microscopy*, n.d.). I realized that the average time I spent in this experiment performing the wash-off was approximately 10 minutes, and axial displacement could explain the loss of fluorescence I have observed.

Measuring Adaptation in Stress Granule Assembly

To determine whether the RRM domain in eIF4B is important for SG adaptation, I performed live-cell imaging to see how cells overexpressing wild type or mutant RRM containing eIF4B proteins would respond to extended exposure to oxidative stress. Cells were plated in a 24 well plate and treated with 125 μM sodium arsenite for 1 hour, then washed twice before being re-exposed to 125 μM sodium arsenite. We observed an increase in the number of SGs per cell to ~5 in the wild type GFP-eIF4B line (Figure 4D) within 1 hour, but only ~2-3 SGs per cell in the RRM mutant GFP-eIF4B cell lines in the same time frame (Figure 4A-C). As the SGs reach f max, the granules reach a plateau before decreasing in number over time **(Figure 4).** For this experiment, the reason for the apparent decrease is because the SGs merge with each other to form larger granules, thus decreasing the total number of stress granules per cell **(Figure 3)**. Because they form larger granules, they would lose approximately 1 SG per hour. Unfortunately, attempting to fit these data using a single exponential curve fit to model the process of adaptation was not successful, mostly due to the loss of fluorescence after SG merging and the presence of the dip in fluorescence following the opening of the microscope chamber discussed in the previous section. From this experiment, it is apparent that not enough time was provided to allow SGs to reach f max prior to the media change for the mutant cell lines (albeit with media containing an equal amount of sodium arsenite). Nevertheless, there does appear to be an appreciable difference between the mutant RRM containing proteins compared to the wild type eIF4B. Comparing all the RRM mutants to **(Figure 4A-C),** you can see that after 5 hours, they

almost reach zero granules. The WT is surprisingly taking more time to disassemble. Because stress was only left on for one hour, the point mutants did not allow enough time for them to reach steady state and it was cut off **(Figure 4A-C)**. Interestingly, it was apparent that as the sodium arsenite was reintroduced into the system, the peak increased 1.5 fold **(Figure 4A and 4C)**. We can also see that the curve fitting posed a challenge as it only accounts the mean intensity between the two signals **(Figure 4D)**. However, I would still need to optimize the assay to fix and ultimately determine the rate of adaptation. This is still preliminary data. Moving forward, it will be essential to optimize this assay to avoid sudden fluctuations of intensities during the experiment. This will make it possible to appropriately fit these data to obtain rate constants to quantify the process of stress adaptation.

DISCUSSION

In this chapter, I have presented my preliminary data toward the characterization of two cellular processes: (1) SG disassembly upon the rapid removal of oxidative stress; and (2) cellular adaptation when there is continued exposure to oxidative stress. To achieve this, I used the signal generated by the accumulation of GFP-tagged eIF4B into SGs during these processes to monitor how SGs change during prolonged stress or upon rapid removal of stress. From these data sets, I attempted to generate a model to determine the rate of SG dynamics (SG loss) for each process. The SG equation was used to measure the disassembly rate, but these data were difficult to fit due to the presence of an unexpected second process that included a dip followed by recovery of

SGs. Disrupting the cell's environment during imaging leads to a common problem in microscopy called focal drift. Focal drift is the inability for the microscope to select the plane for an extended period of time. For example, one needs to account for how much time the cells are exposed to disruption in temperature, or thermal drift (Kreft et al., 2005). The cells are especially sensitive to thermal drift, leading to one change in celsius per minute as the microscope chamber is open (*Correcting Focus Drift in Live-Cell Microscopy*, n.d.). This change can result in a second variable in addition to the process that is being measured (in this case SGs in response to stress). Thus, future studies will need to minimize or prevent focal drift so that only stress adaptation or SG disassembly is monitored. To overcome the focal drift problem, it may be possible to move the experiment to a microscope with an environment chamber to account for thermal drift or move the experiment to use a microfluidics device that is quick and avoids temperature fluctuations that promote loss of fluorescence during media changes.

It will be important in future to undertake a sodium arsenite dose curve and longer time course to precisely determine how long it takes for SGs to adapt and/or eventually disassemble due to prolonged exposure to stress. It will also be important to rigorously determine if the RRM mutants in eIF4B result in a change in a cell's ability to adapt to stress or disassemble when stress is removed**.** My preliminary data indicates that a modified pipeline will be needed to adjust for the process of SG merging that occurs in these experiments. It would be exciting to ultimately monitor the complete life cycle of SGs during the cellular response to stress and its ultimate adaptation or recovery from the removal of stress. This will enable a more complete understanding of these

processes and determine how eIF4B, or other components, regulate these important cellular responses.

Figures and Legends

Figure 1. Live- cell imaging of SG assembly and disassembly.

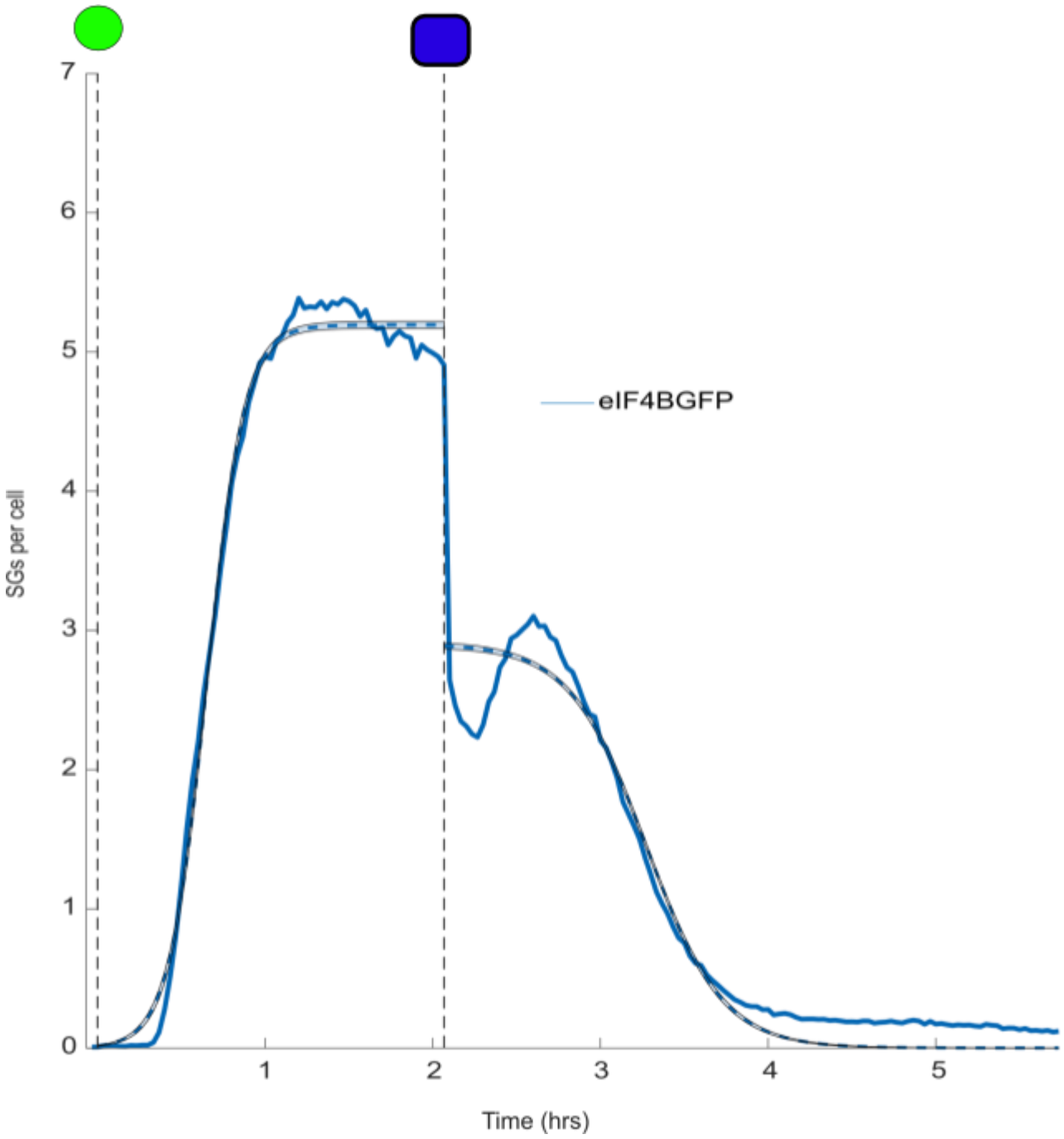

Figure 1. Live-cell imaging of SG assembly and disassembly. The green circle indicates that the GFP-eIF4B HeLa cells were exposed to 125 μM of sodium arsenite at time zero. The solid blue line is the mean for SGs per cell. The blue square indicates the cells were washed off 2x with Flurorobrite and filmed for a total of 5 hours.

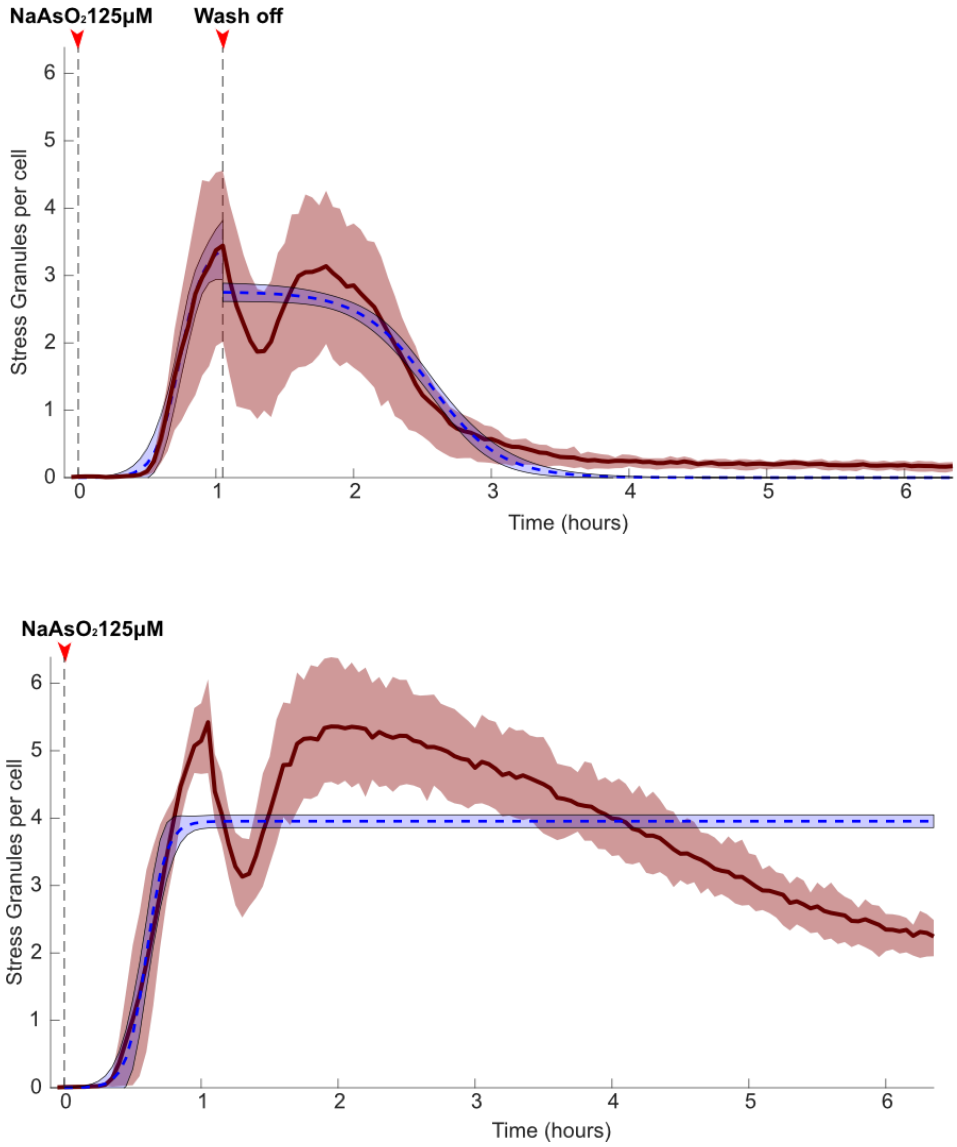

Figure 2. Troubleshooting the loss in fluorescence. Both Top and Bottom Panels were on the same plate during the experiment, however the cells had experienced different treatments: Top Panel, the sodium arsenite was washed off after 1 hour; and Bottom Panel, sodium arsenite was left on during the duration of the experiment. The potential reason for the loss in fluorescence (dip) was that this could be a result of temperature shock as described in the main text. The lapse imaging was 5 mins for the wash off.

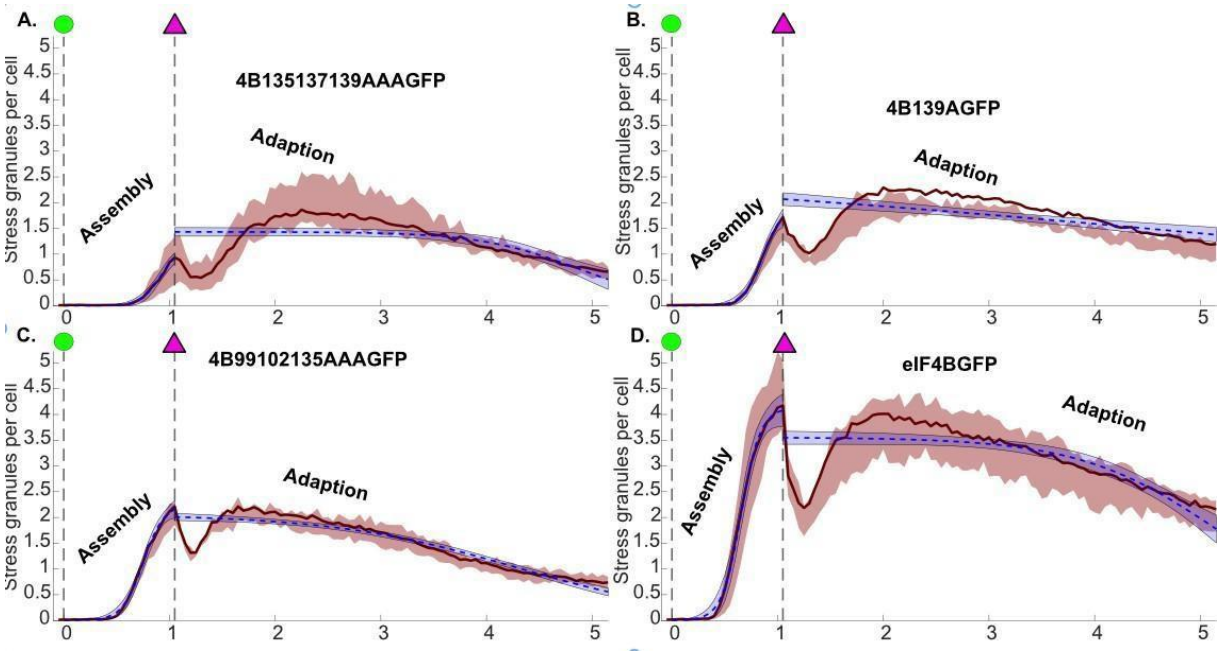

Figure 3. eIF4B RRM mutants compared to WT-eIF4B during stress adaptation. Live-cell imaging of SG assembly and adaptation to study stress adaptation between different point mutants in the eIF4B RRM domain. The green circle indicates the following RRM mutants were exposed to 125 μM of sodium arsenite, the purple triangle indicates at the 1 hour mark cells were washed off twice and then re-exposed to 125 μM of sodium arsenite with media. The cells were then imaged for 4 additional hours.

REFERENCES

Baymiller, Max, and Stephanie L. Moon. 2023. “Stress Granules as Causes and Consequences of Translation Suppression.” *Antioxidants & Redox Signaling* 39 (4-6): 390–409.

“Correcting Focus Drift in Live-Cell Microscopy.” n.d. Nikon’s MicroscopyU. Accessed July 23, 2024. https://www.microscopyu.com/applications/live-cell-imaging/correcting-focus-drift-in-live-cell-microscopy.

Jain, Saumya, Joshua R. Wheeler, Robert W. Walters, Anurag Agrawal, Anthony Barsic, and Roy Parker. 2016. “ATPase-Modulated Stress Granules Contain a Diverse Proteome and Substructure.” *Cell* 164 (3): 487–98.

Jo, Myungjin, Shinrye Lee, Yu-Mi Jeon, Seyeon Kim, Younghwi Kwon, and Hyung-Jun Kim. 2020. “The Role of TDP-43 Propagation in Neurodegenerative Diseases: Integrating Insights from Clinical and Experimental Studies.” *Experimental & Molecular Medicine* 52 (10): 1652–62.

Kedersha, N., M. R. Cho, W. Li, P. W. Yacono, S. Chen, N. Gilks, D. E. Golan, and P. Anderson. 2000. “Dynamic Shuttling of TIA-1 Accompanies the Recruitment of mRNA to Mammalian Stress Granules.” *The Journal of Cell Biology* 151 (6): 1257–68.

Kreft, Marko, Matjaz Stenovec, and Robert Zorec. 2005. “Focus-Drift Correction in Time-Lapse Confocal Imaging.” *Annals of the New York Academy of Sciences* 1048 (June): 321–30.

Redding, Alexandra, and Elda Grabocka. 2023. “Stress Granules and Hormetic Adaptation of Cancer.” *Trends in Cancer* 9 (12): 995–1005.

Tauber, Devin, Gabriel Tauber, Anthony Khong, Briana Van Treeck, Jerry Pelletier, and Roy Parker. 2020. “Modulation of RNA Condensation by the DEAD-Box Protein eIF4A.” *Cell* 180 (3): 411–26.e16.

Wheeler, Joshua R., Tyler Matheny, Saumya Jain, Robert Abrisch, and Roy Parker. 2016. “Distinct Stages in Stress Granule Assembly and Disassembly.” *eLife* 5 (September). https://doi.org/10.7554/eLife.18413.

Chapter Five

Characterizing Human Eukaryotic initiation factor 4G (eIF4G) in Stress Granules

This chapter is unpublished and was written by me and edited by Dr. Christopher Fraser.

Abstract

In this study, I investigated the interaction of GFP-tagged eIF4G with stress granules. Unexpectedly, I found that modest overexpression of eIF4G in HeLa cells results in an apparent hypersensitivity to oxidative stress even though SGs are still able to form. For the future, I have proposed several experiments to confirm and extend our understanding of this phenomenon.

Introduction

Stress granules (SGs) are dynamic cellular structures that form in response to various stress conditions, such as oxidative stress, heat shock, or viral infection. These granules contain stalled pre-initiation complexes, including several translation initiation factors. Among the translation initiation factors identified in SGs is eukaryotic initiation factor 4G (eIF4G) (Kedersha et al. 2002). eIF4G is a crucial component of the eIF4F complex, and plays a central role in the initiation of translation by acting as a scaffold protein that brings together other key components necessary for the recruitment of ribosomes to mRNA (Hinton et al. 2007). eIF4G is composed of 7 domains: PABP, eIF4E, RNA, eIF4A, eIF3, eIF4A, and MNK1.

A recent study revealed that eIF4G interacts with G3BP1, which is a core component of SGs (Yang et al. 2019). This research further demonstrated that knocking down or knocking out eIF4G disrupts the formation of SGs, highlighting the critical importance of eIF4G in this process. Thus, eIF4G plays a dual role in translation initiation and the cellular stress response. A possible mechanism to explain this is that eIF4G may somehow contribute to the sequestration of mRNA and translation factors into SGs, thereby temporarily halting translation and protecting the cell from stress.

To characterize the role of eIF4G in SG formation, I generated an inducible GFP-tagged eIF4G overexpression HeLa cell line using the Flp-In T-REx system. Surprisingly, I found that upon treatment with sodium arsenite and live-cell imaging as described previously, cells expressing either GFP-eIF4G$_{165\text{-}1599}$ or GFP-eIF4G$_{557\text{-}1599}$ shrunk appreciably in size over time, and I was unable to visualize GFP-tagged eIF4G

following treatment. Given these unexpected results, I also propose future experiments to investigate the underlying causes for this stress induced morphological change in cells expressing eIF4G.

Given these surprising results, it will be important in future to further investigate the underlying causes for this stress induced morphological change in cells expressing eIF4G. Thus, I propose the following approaches to confirm and extend these findings: confirm what is likely a programmed cell death pathway, rigorously characterize the growth rates of eIF4G expressing cells, and confirm this apparent morphological change in other cell types and stress conditions. Finally, it will be important to identify the domain in eIF4G that causes this apparent hypersensitivity to oxidative stress.

Results

Development of Fluorescently labeled Flp-in TRex Hela cell line

I subcloned eIF4G$_{165\text{-}1599}$ into a pcDNA5/FRT/TO plasmid with a N-term GFP reporter using restriction enzymes NdeI/XhoI and verified the plasmid by sequencing (Quintara Biosciences). I then transfected the cells with the above plasmid, JB1, and plasmid pOG44, which is to allow for the Flp recombinase to occur. All transfections are carried out in Opti-MEM Reduced Serum Media (Thermo Fisher) supplemented with 3% FBS according to manufacturer's guidelines with minor changes. For each transfection, 1.5–3.0 µg of pcDNA5/FRT/TO plasmid and 1 µg of POG44 is diluted into 100 µL of Opti-MEM media. For the transfection, I used 6 µL of X-tremeGENE9 HP DNA Transfection Reagent (Roche) diluted in 100 µL of Opti-MEM media and incubated for 5

minutes at room temperature. The two incubations were then combined to create a DNA-lipid mixture that was incubated for 30 minutes at room temperature. The transfection was then added to the cell line and incubated for 5 hours. Stable cell lines were generated with Blasticidin Hygromycin selection using a 6- well plate according to manufacturer's guidelines.

Overexpression of eIF4G leads to hypersensitivity to oxidative stress in HeLa cells

Two tetracycline inducible cell lines were generated for this work. We tested these two different regions specifically to see if SG assembly rates were different with and without the PABP domain, since it was shown to have an interaction with G3BP1 in this region (Yang et al. 2019). One of these possesses a GFP-tagged eIF4G$_{165\text{-}1599}$ protein while the other possesses a GFP-tagged eIF4G$_{557\text{-}1599}$ protein. Both cell lines were generated from the same parental HeLa cell line used to generate the eIF4B expressing cells. Similar to the GFP-tagged eIF4B experiments outlined in my previous chapters, I wanted to first determine if these GFP-tagged eIF4G proteins would accumulate in SGs in response to sodium arsenite. Each cell line was treated with tetracycline for 24 hours to induce expression of GFP-eIF4G prior to the addition of 250 μM sodium arsenite. Surprisingly, I noticed that in response to sodium arsenite the cells would detach from each other and the plate and appear to shrink. Initially, I thought that simply inducing the cell lines with tetracycline may be causing them to detach, but close analysis of cells in the absence of stress indicates that they possess a similar morphology to cells expressing eIF4B **(Figure 1A, 1C, and 1E)**. In contrast, following the addition of sodium arsenite for 2-2.5 hours, the GFP-eIF4G expressing cells appear to detach and shrink **(Figure 1B, 1D, and 1F)**. It was not apparent that GFP-tagged eIF4G proteins were

present in SGs in response to stress, although I note that the general background of GFP in the shrunken cells may complicate the detection of any eIF4G labeled SGs.

Overexpression of eIF4G forms SGs

Next, I wanted to confirm if G3BP1, a SG nucleator, was actively moving into SGs in response to stress in the GFP-eIF4G$_{165\text{-}1599}$ cell line. To this end, I performed an immunofluorescence assay using G3BP1 antiserum. Cells were treated for two hours with 250 μM of sodium arsenite and then imaged for the presence of GFP-eIF4G$_{165\text{-}1599}$. Cells were then fixed using the immunofluorescence protocol described in chapter 2. After imaging and fixing the cells, I successfully visualized GFP-eIF4G SGs in the green channel **(Figure 2A).** In addition, I was able to successfully detect clear SGs containing G3BP1 **(Figure 2B)**. Thus, despite the dramatic morphology change in response to sodium arsenite, these cells are indeed able to form SGs. Nevertheless, it is not clear whether the formation of SGs is dysregulated in some way since it is difficult to detect GFP-tagged eIF4G SGs using my live cell imaging method.

Discussion/Future Directions

Previous studies indicate that the overexpression of eIF4G1 promotes cellular transformation indicative of cancer cell growth, proliferation, and survival (Badura et al., 2012; Lu et al., 2021). However, this model has been largely based on observed levels of eIF4G1 in cancer cells rather than inducing its overexpression. The only study that

has claimed that overexpression of eIF4G can transform cells has never been repeated and used an eIF4G protein that was not in fact full-length (Fukuchi-Shimogori et al. 1997). Unexpectedly, my data indicates that eIF4G1 overexpression leads to a hypersensitivity to oxidative stress. To rigorously confirm this observation and move this project forward, below are the following experiments I would propose in the future.

Previous research has shown that G3BP1, a SG marker, binds to the PABP binding domain aa 182-203 of eIF4G (X. Yang et al., 2019). It is therefore possible that eIF4G1 overexpression dilutes G3BP1, or other SG components, so that they are unable to nucleate SG formation. However, my preliminary data using the overexpression of an eIF4G truncation that does not include the putative G3BP1 binding site (GFP-eIF4G$_{557-1599}$) indicates that stress hypersensitivity still occurs. Moreover, based on my preliminary data revealing that GFP-eIF4G still forms SGs, it will be important to determine if cell growth is inhibited in the absence or presence of stress. In addition, it would be interesting to use the OPP translation assay that I have described in chapter 3 to determine if the rate of translation is different in the absence or presence of oxidative stress.

It will also be important to confirm if the eIF4G overexpressing cells are in fact undergoing a specific programmed cell death pathway. To address this question, it would be possible to induce the cells and carry out a sodium arsenite dose curve for up to two days while counting cells and observing viability. Additionally, we can identify and study the pathway of how a cell can die; we can distinguish which pathway the cell might go through programmed cell death vs uncontrolled cell death. Additionally, we can identify and study the pathways of how a cell can die, distinguishing between

programmed cell death and uncontrolled cell death. To test this, we can use a Cell Death library that contains 152 compounds plated in 96-well format is available that will screen for the following cell death pathways: inducers and inhibitors of apoptosis, autophagy-dependent cell death, entotic cell death, ferroptosis, necroptosis, NETosis, and pyroptosis. The kit also includes inhibitors of lysosome-dependent cell death, oxeiptosis, and parthanatos (Cayman Chemicals, Cat #35093) (Peng et al., 2022).

Following the confirmation of a specific cell death pathway, one could next identify which domain of eIF4G1 is responsible for promoting stress hypersensitivity. This could be achieved by overexpressing different eIF4G1 truncations that are available in the Fraser lab and carrying out the SG assay. Once the minimum domain of eIF4G1 is identified, one could investigate if known SG components associate with it using immunoprecipitation and western blotting with the following SG nucleators: TIA-1/R,TDP-43 and FUS. Interestingly, it has previously been suggested that tRNA fragments that are generated in response to cellular stress bind to eIF4G and prevent the eIF4F complex from binding the m7G cap (Add ref: Mol Cell. 2011 Aug 19;43(4):613-23). It will therefore be interesting to determine if these tRNA fragments bind to a domain of eIF4G during stress.

It would be interesting to use proteomic cross linking/mass spectrometry approaches to identify candidate eIF4G binding partners during stress. Once candidate genes are identified, one can overexpress them, or knock them down, to determine if this can alter the eIF4G1-dependent hypersensitivity to stress.

It will be important to rigorously determine if eIF4G overexpressing HeLa cells are equally hypersensitive to different cellular stresses. Furthermore, it will be important to also determine if this same hypersensitivity is apparent in different cell types. To answer this question, one could use the following cell types that are commonly used to visualize stress granules:

- U2OS, human osteosarcoma cells used for large, flat morphology, easy to image (Gwon et al., 2021),
- MEF Cells (Mouse Embryonic Fibroblasts), flat (Buchan et al., 2013)
- 293T(Mazroui et al., 2006), human embryonic kidney cells
- COS, fibroblast-like cell line derived from monkey kidney tissue(Arimoto-Matsuzaki et al., 2016).

The different types of stressors listed below could also be used to determine hypersensitivity:

- Oxidative Stress- Hydrogen peroxide (H_2O_2) (Emara et al., 2012)
- Endoplasmic Reticulum (ER) Stress- Thapsigargin and Tunicamycin (Melo et al., 2022)
- Osmotic Stress-Sorbitol (Dewey et al., 2011)
- Heat Shock- 43 °C with 5% CO2 for 15 minutes (S. Hu et al., 2023)
- Nutrient Deprivation- Amino acid or glucose deprivation (Reineke et al., 2018)

Lastly, it will be important to determine the kinetics of G3BP1 and eIF4G1 entry into SGs by using the live cell SG assay I have developed. To answer this question, one could build a double reporter system that includes eIF4G1 and G3BP1. Importantly, it would

likely be necessary to attach a degron to G3BP1 to limit its overexpression when following SG kinetics overtime.

Even though this chapter contains only preliminary data, it is clear that multiple directions could be followed to understand how eIF4G overexpression causes hypersensitivity to oxidative stress. This hypersensitivity problem could help explain why it has been so difficult to overexpress eIF4G in eukaryotic cells to generate recombinant protein for purification.

Figures and Legends

Figure 1 Overexpression of eIF4G leads to cell death in response to stress

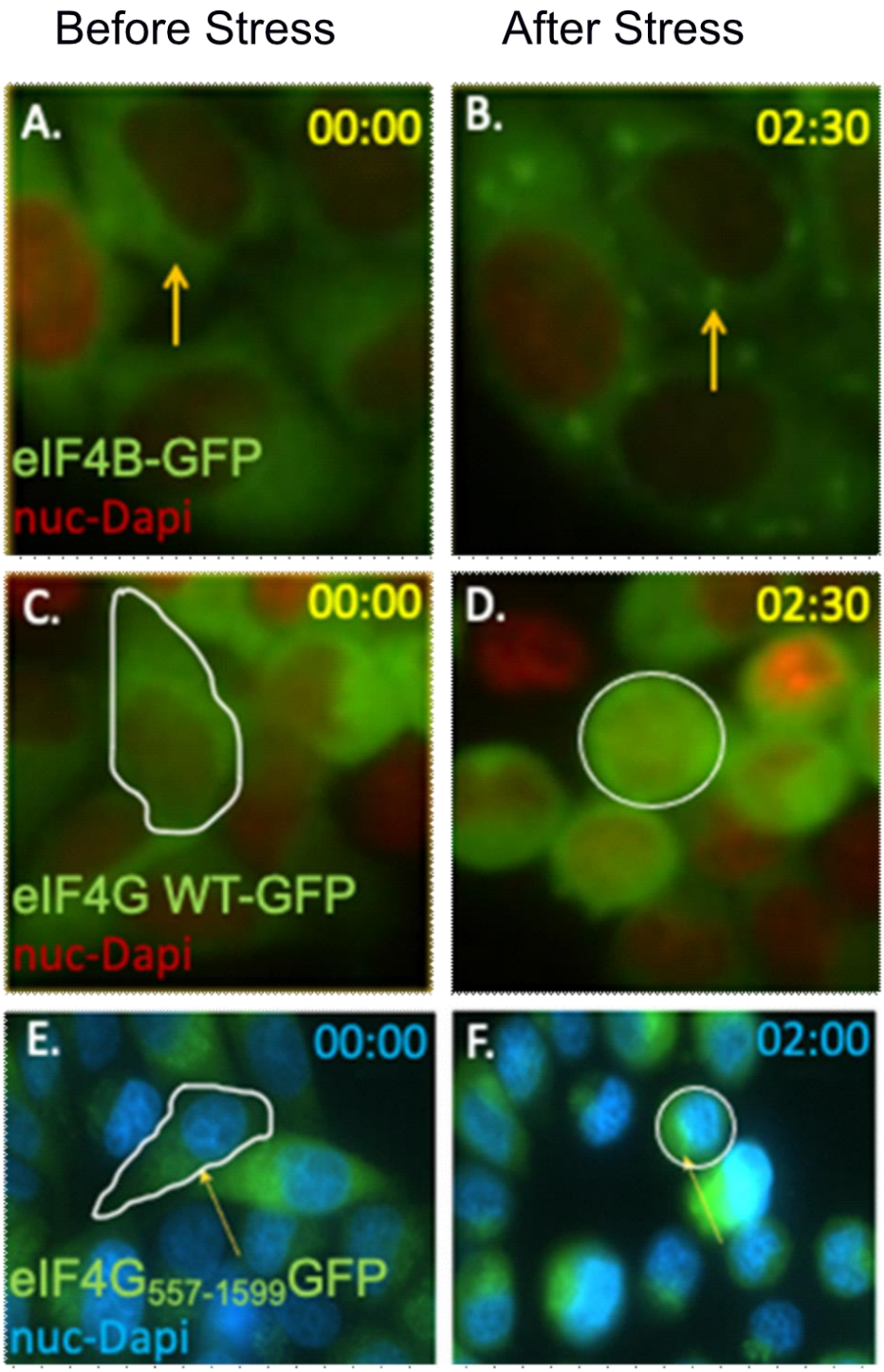

Figure 1 Overexpression of eIF4G leads to cell death in response to stress. *Left to Right, Top to Bottom* **(A-B)** Time lapse imaging of GFP-eIF4B. HeLa cells were treated with 250 μM of sodium arsenite for 2 hours and did not undergo cell death. **(C-D)** Time lapse imaging of GFP-eIF4G$_{165\text{-}1599}$. HeLa cells were treated with 250 μM of sodium arsenite for 2 hours. The arrow follows a cell shrinking and appearing to undergo cell death. The circles around the cell indicate the loss of volume before and after stress **(E-F)** Time lapse imaging of eIF4G$_{557\text{-}1599}$. HeLa cells were treated with 250 μM of sodium arsenite for 2 hours. The arrow follows a cell shrinking and appearing to undergo cell death, indicating that the N-terminal region of eIF4G is not responsible for promoting cell death in response to stress.

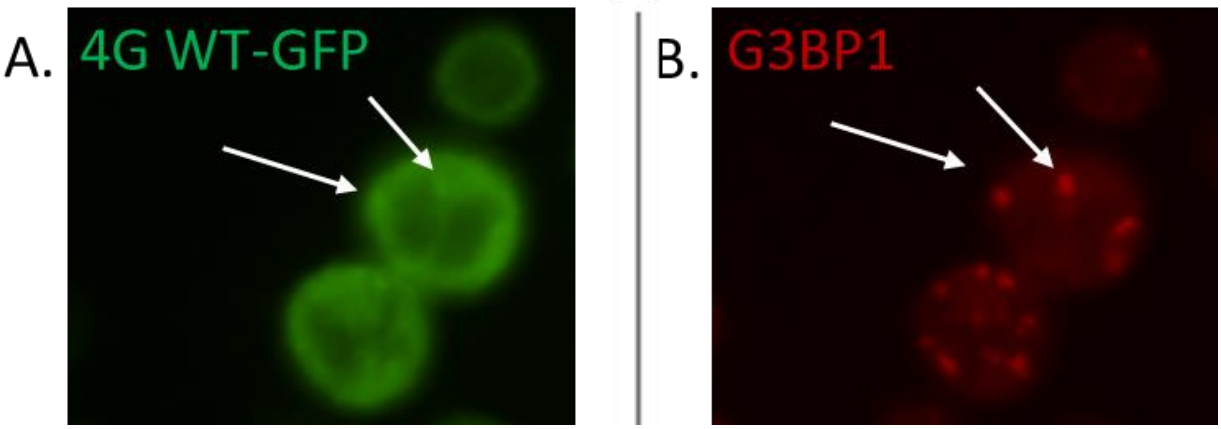

Figure 2 Overexpressed GFP-eIF4G$_{165\text{-}1599}$ forms stress granules.

Immunofluorescence was used to visualize stress granules in the eIF4G-GFP165-1599 cell line. The white arrows point to SGs in both the green and red channels. **A)** The GFP-eIF4G165-1599 cell morphology is shrinking and appears to be undergoing cell death. **B)** G3BP1 was used to visualize stress granules, which the white arrows are pointing to.

References

Arimoto-Matsuzaki, Kyoko, Haruo Saito, and Mutsuhiro Takekawa. 2016. “TIA1 Oxidation Inhibits Stress Granule Assembly and Sensitizes Cells to Stress-Induced Apoptosis.” *Nature Communications* 7 (January):10252.

Badura, Michelle, Steve Braunstein, Jiri Zavadil, and Robert J. Schneider. 2012. “DNA Damage and eIF4G1 in Breast Cancer Cells Reprogram Translation for Survival and DNA Repair mRNAs.” *Proceedings of the National Academy of Sciences of the United States of America* 109 (46): 18767–72.

Buchan, J. Ross, Regina-Maria Kolaitis, J. Paul Taylor, and Roy Parker. 2013. “Eukaryotic Stress Granules Are Cleared by Autophagy and Cdc48/VCP Function.” *Cell* 153 (7): 1461–74.

Dewey, Colleen M., Basar Cenik, Chantelle F. Sephton, Daniel R. Dries, Paul Mayer 3rd, Shannon K. Good, Brett A. Johnson, Joachim Herz, and Gang Yu. 2011. “TDP-43 Is Directed to Stress Granules by Sorbitol, a Novel Physiological Osmotic and Oxidative Stressor.” *Molecular and Cellular Biology* 31 (5): 1098–1108.

Emara, Mohamed M., Ken Fujimura, Daniele Sciaranghella, Victoria Ivanova, Pavel Ivanov, and Paul Anderson. 2012. “Hydrogen Peroxide Induces Stress Granule Formation Independent of eIF2α Phosphorylation.” *Biochemical and Biophysical Research Communications* 423 (4): 763–69.

Gwon, Youngdae, Brian A. Maxwell, Regina-Maria Kolaitis, Peipei Zhang, Hong Joo Kim, and J. Paul Taylor. 2021. “Ubiquitination of G3BP1 Mediates Stress Granule Disassembly in a Context-Specific Manner.” *Science* 372 (6549): eabf6548.

Hinton, Tracey M., Mark J. Coldwell, Gillian A. Carpenter, Simon J. Morley, and Virginia M. Pain. 2007. “Functional Analysis of Individual Binding Activities of the Scaffold Protein eIF4G.” *The Journal of Biological Chemistry* 282 (3): 1695–1708.

Hu, Shuyao, Yufeng Zhang, Qianqian Yi, Cuiwei Yang, Yanfen Liu, and Yun Bai. 2023. “Time-Resolved Proteomic Profiling Reveals Compositional and Functional Transitions across the Stress Granule Life Cycle.” *Nature Communications* 14 (1): 7782.

Kedersha, Nancy, Samantha Chen, Natalie Gilks, Wei Li, Ira J. Miller, Joachim Stahl, and Paul Anderson. 2002. “Evidence That Ternary Complex (eIF2-GTP-tRNA(i)(Met))-Deficient Preinitiation Complexes Are Core Constituents of Mammalian Stress Granules.” *Molecular Biology of the Cell* 13 (1): 195–210.

Lu, Ying, Shanshan Yu, Guangxue Wang, Zuan Ma, Xuelian Fu, Yueyu Cao, Qinchuan Li, and Zengguang Xu. 2021. “Elevation of EIF4G1 Promotes Non-Small Cell Lung Cancer Progression by Activating mTOR Signalling.” *Journal of Cellular and Molecular Medicine* 25 (6): 2994–3005.

Mazroui, Rachid, Rami Sukarieh, Marie-Eve Bordeleau, Randal J. Kaufman, Peter Northcote, Junichi Tanaka, Imed Gallouzi, and Jerry Pelletier. 2006. “Inhibition of Ribosome Recruitment Induces Stress Granule Formation Independently of Eukaryotic Initiation Factor 2alpha Phosphorylation.” *Molecular Biology of the Cell* 17 (10): 4212–19.

Melo, Eduardo Pinho, Tasuku Konno, Ilaria Farace, Mosab Ali Awadelkareem, Lise R. Skov, Fernando Teodoro, Teresa P. Sancho, et al. 2022. “Stress-Induced Protein Disaggregation in the Endoplasmic Reticulum Catalysed by BiP.” *Nature*

Communications 13 (1): 2501.
Peng, Fu, Minru Liao, Rui Qin, Shiou Zhu, Cheng Peng, Leilei Fu, Yi Chen, and Bo Han. 2022. “Regulated Cell Death (RCD) in Cancer: Key Pathways and Targeted Therapies.” *Signal Transduction and Targeted Therapy* 7 (1): 286.
Reineke, Lucas C., Shebna A. Cheema, Julien Dubrulle, and Joel R. Neilson. 2018. “Chronic Starvation Induces Noncanonical pro-Death Stress Granules.” *Journal of Cell Science* 131 (19). https://doi.org/10.1242/jcs.220244.
Yang, Xiaodan, Zhulong Hu, Qiang Zhang, Shanshan Fan, Yi Zhong, Dong Guo, Yali Qin, and Mingzhou Chen. 2019. “SG Formation Relies on eIF4GI-G3BP Interaction Which Is Targeted by Picornavirus Stress Antagonists.” *Cell Discovery* 5 (January):1.

Chapter Six

Concluding Remarks

This chapter is unpublished and was written by me and edited by Dr. Christopher Fraser.

CONCLUSION

Stress granules (SGs) are cytoplasmic structures formed in response to various stress stimuli, including heat shock, oxidative stress, osmotic shock, and proteasome inhibition. These non-membrane bound organelles consist of mRNA transcripts, RNA-binding proteins, and translation initiation factors, including the 40S ribosomal subunit. SG formation is primarily regulated by the phosphorylation of eIF2α, a key component of the integrative stress response (ISR) pathway, although recent research has identified an alternative, eIF2α-independent pathway for SG assembly through translation initiation machinery having an active role in this process.

Despite the known role of SGs in protecting mRNAs and translation machinery during stress, the precise mechanisms of SG assembly and disassembly remain poorly defined. Traditional studies have used fixed-time assays like immunofluorescence, but these methods do not capture real-time dynamics. To address this gap, I developed a system using a stable Flp-In™ T-REx™-HeLa cell line to monitor SG assembly and disassembly in real time.

Collaboration with the Albeck Lab, we have found that the Human eIF4B, a translation initiation factor, is a component of SGs and may regulate their formation. Through single-cell live imaging of GFP-tagged eIF4B under oxidative stress, I quantified SG formation kinetics and found that a point mutant of eIF4B in the RNA recognition motif (RRM) domain led to a reduced rate of SG formation and a delayed stress response. eIF4B directly binds to G3BP1, a known SG nucleator, suggesting that its RRM domain affects SG assembly.

Understanding SG disassembly is crucial, especially since impaired disassembly is linked to neurodegenerative disorders. I developed a method to measure SG disassembly rates but encountered challenges with focal drift in time-lapse imaging, which affects measurement accuracy. Future improvements could include using microfluidics devices or environmental chambers to mitigate this issue.

Additionally, I found that modest overexpression of eIF4G in HeLa cells results in hypersensitivity to oxidative stress while still allowing SG formation. Further experiments that are discussed in Chapter 5, could have the potential to address this result.

Overall, we have found that translation initiation machinery has an active role in stress granule assembly and disassembly. This body of work informs us that eIF4B has a role in SG assembly, eIF4G is known to interact with G3BP1, a stress granule marker, however, if you overexpress eIF4G it causes hypersensitivity which may lead to cell death. Moving the field forward, the next steps would be to undergo different modifications eIF4G to see if overexpression leads to cell death, optimizing SG disassembly assay which will inform us if there are any modifications that eIF4B may lead in a delay or rapid response in SG disassembly which may be crucial to know if eIF4B plays a role.